Erasmus MC
Universitair Medisch Centrum Rotterdam

Thoraxcentre

# The 16th European Symposium on Ultrasound Contrast Imaging

- An ICUS Conference -

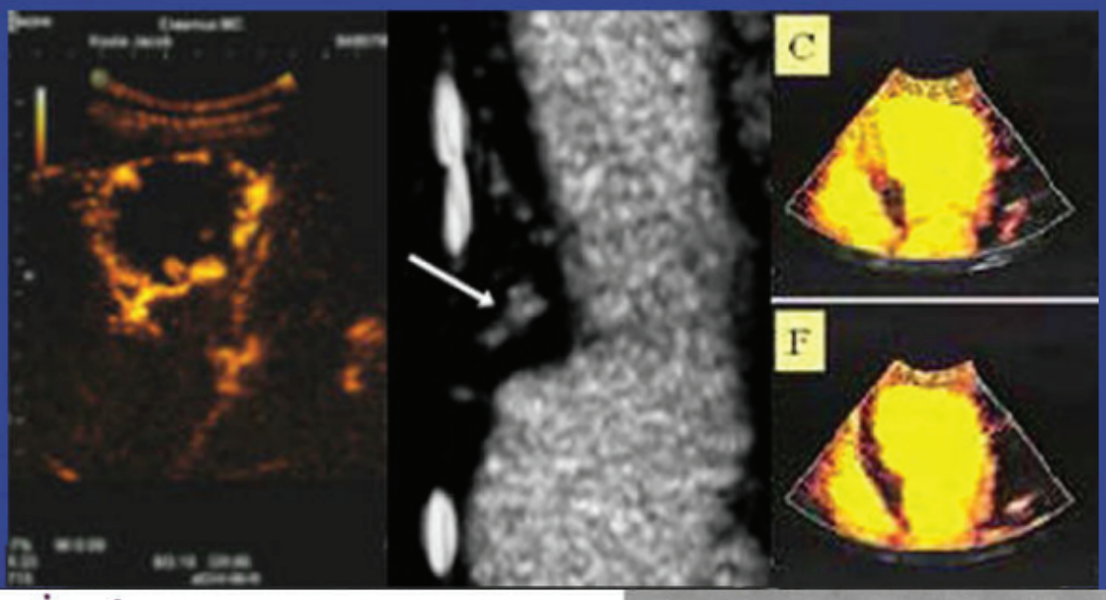


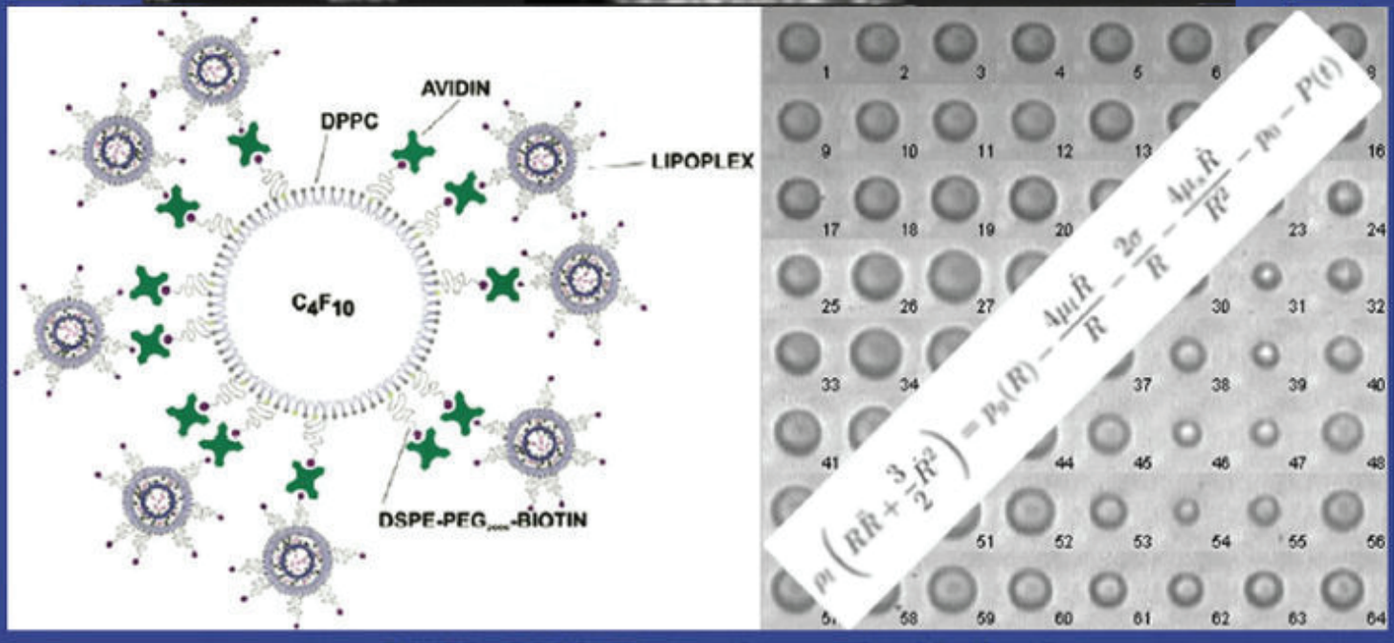


# Abstract book

January, 20-21 2011, Rotterdam, The Netherlands

Organized by Folkert ten Cate, Nico de Jong , Edward Leen

Erasmus MC Rotterdam - Imperial College London

16th EUROPEAN SYMPOSIUM ON ULTRASOUND CONTRAST IMAGING
20-21 JANUARY 2011, Rotterdam, The Netherlands

WEDNESDAY, 19 January 2011

15.30 Defense Klazina Kooiman (Arminius church – Museum Park)
Therapeutic bubbles

18.00 - 20.00 Registration - Welcome Drinks – Posters ..... Hilton Hotel

18.30 – 19.45 POSTER DISCUSSION A (for the youngest investigators) *Moderators: Folkert ten Cate/Nico de Jong*



THURSDAY, 20 January 2011

## Parallel HOW TO session

*Chairpersons: Edward Leen/Pavel Taimr*

13.45 – 14.10 Registration and coffee

14.10 – 14.20 Introduction and opening..... *Edward Leen/Pavel Taimr*

14.20 – 15.10 Session 1
Peter Burns — How do bubbles work with Ultrasound
Pavel Taimr — The diagnosis of liver tumors
Arend Schinkel — The use of contrast in vascular imaging

15.50-16.20 Intermission

16.20 – 17.20 Session 2
Edward Leen — Monitoring Radio Frequency Ablation (RFA)
Hans Peter Weskott — Economic evaluations in clinical practice

17.20 Closure & drinks

16th EUROPEAN SYMPOSIUM ON ULTRASOUND CONTRAST IMAGING
20-21 JANUARY 2011, Rotterdam, The Netherlands

THURSDAY, 20 January 2011

# Oral program

16th EUROPEAN SYMPOSIUM ON ULTRASOUND CONTRAST IMAGING
20-21 JANUARY 2011, Rotterdam, The Netherlands

FRIDAY, 21 January 2011

07.30 - 08.00 Registration

07.30 - 09.00 POSTER DISCUSSION B ..... *Moderator: Folkert ten Cate*



07.30 - 09.00 POSTER DISCUSSION C ..... *Moderator: Nico de Jong*

16th EUROPEAN SYMPOSIUM ON ULTRASOUND CONTRAST IMAGING
20-21 JANUARY 2011, Rotterdam, The Netherlands

FRIDAY, 21 January 2011

# Oral program

# Low-energy acoustic vaporizationof novel perfluorobutanenano and micrometer droplets

***Paul S. Sheeran[1], Vincent P. Wong[2], Lee B. Mullin[1], Samantha Luois[3], Terry O. Matsunaga[2,4],Paul A. Dayton[1]***

*[1]Joint Department of Biomedical Engineering –University of North Carolina and North Carolina State University, Chapel Hill, NC*
*[2]Biomedical Engineering Graduate Interdisciplinary Program, University of Arizona, Tucson, AZ*
*[3]Undergraduate Biology Research Program, University of Arizona, Tucson, AZ*
*[4]Department of Radiology Research, University of Arizona, Tucson, AZ*

**Introduction**

Progress in the field of ultrasound contrast agents has provided a robust set of tools for diagnostic and therapeutic applications. Designing agents based on the phenomenon of acoustic droplet vaporization (ADV) has allowed researchers to develop techniques that extend beyond those capable with standard microbubbles. ADV-based agents have been shown to vaporize as a function of droplet diameter, ambient temperature and pressure, ultrasound frequency and pressure, and pulse length. Agents designed to vaporize at reduced energies yield less possibility of inducing unwanted bioeffects. Encapsulation in a lipid or polymer shell exerts additional Laplace pressure on the liquid droplet, serving to keep them in solution at higher temperatures. Droplets with diameters in the low micron range have been proposed as temporary tissue occlusion agents and cavitation nuclei, while sub-micron droplets show potential for extravascular imaging and therapeutics. Studies to date have typically used compounds of the perfluorocarbon family (most commonly perfluoropentane) as the liquid-core component of ADV agents due to boiling points near body temperature, low toxicity, and stability of bubbles post-activation.

We report the ability to successfully generate stable lipid-encapsulated perfluorobutane droplets with diameters in the micron and sub-micron range. Perfluorobutane (PFB) - normally a gas at room temperature - has a significantly lower boiling point than alternative ADV compounds proposed to date. We present evidence of PFB droplet vaporization at micron sizes as a function of initial diameter, and demonstrate reduced activation energy when compared to perfluorocarbon compounds with boiling points above room temperature. Additionally, in-vitro persistence of micron-sized PFB droplets is demonstrated for periods greater than 4 hours at physiological temperature, indicating PFB-based agents have sufficient stability for applications that require longer circulation periods. Preliminary evidence of sub-micron droplet vaporization at clinically feasible frequencies and pressures is also reported, suggesting that a PFB-based ADV platform may provide advantages for a wide variety of applications.

## Methods

### *Micron-sized Droplets*

PFC-lipid emulsions were generated by membrane extrusion for PFB and alternative PFCs with higher boiling points using lipids composed of DPPC, LPC, and DPPE-PEG-2000. A dilute solution of droplets for each PFC was passed through a nearly optically and acoustically transparent cellulose tube in an acrylic-lined water bath heated to 37°C. The droplets were observed optically in the focal region of a 5MHz spherically-focused ultrasound transducer. Each droplet was exposed to a 2 μs pulse and pressure was increased in incremental steps until vaporization was observed. The peak negative pressure (PNP) that resulted in vaporization was recorded for correlation each droplet's initial diameter, which was measured using monochrome videos and still images.

### *PFB Droplet Viability*

Human prostate PC-3 cells were grown in a monolayer on glass cover slips until cells reached 80-90% confluence, after which they were incubated for four hours with media containing 5μL/mL of a PFB droplet solution. After incubation, the cover slips were washed with PBS and placed in a metal holder. A PBS filled fluid pocket was created with a gasket and Thermanox$^{TM}$ cover slip opposite the glass cover slip.Brightfield images were obtained before and after ultrasound exposure.Ultrasound imaging was performed using a Siemens Sequoia clinical ultrasound machine with a 15L8 linear transducer. The focal point of the transducer was set to the plane containing the cell sample holder in a degassed water bath. To gauge response of the droplets to mechanical indices of 1.5, 1.7, and 1.9, the transducer was translated linearly across the sample. After exposure to increasedMIs, the sample was rescanned for a comparison of contrast increase against baseline scans due to droplet vaporization.

### *Sub-micron Droplet Vaporization*

Modifyingdroplet emulsionification techniques with secondary filtering allowed for generation of strictly sub-micron populations of PFB droplets. Samples were sized initially using dynamic light scattering and exposed to 5 MHz ultrasound pressure as described earlier to determine the vaporization threshold. Resulting bubbles were measured for correlation to original droplet sizing using ideal gas law estimations.

## Results

Experiments on micron-sized droplets showed that for each PFC vaporization thresholdsincreased as droplet diameter decreased. Additionally, the observed vaporization threshold for a particular droplet was seen to decrease as PFC boiling point decreased.At sizes near 1 μm, PFB required over 30% less energy than the nearest candidate PFC. Viability studies showed a significant contrast increase in samples after exposure to ultrasound, suggesting a large portion of droplets remained viable after a 4 hour incubation period. Brightfield images before and after confirmed substantial regions of vaporized droplets present as a result of ultrasonic energy. Sub-micron droplets were successfully vaporized using clinically approved acoustic parameters – a mechanical index of 1.5 at 5 MHz produced bubbles that, when sized, correlated well with the measured peak droplet size using ideal gas law expansions of 5-6 times the original diameter. These results suggest that PFB may be a particularly well-suited platform for applications involving extravascular imaging, such as passive diffusion into solid tumors with 'leaky' vasculature.

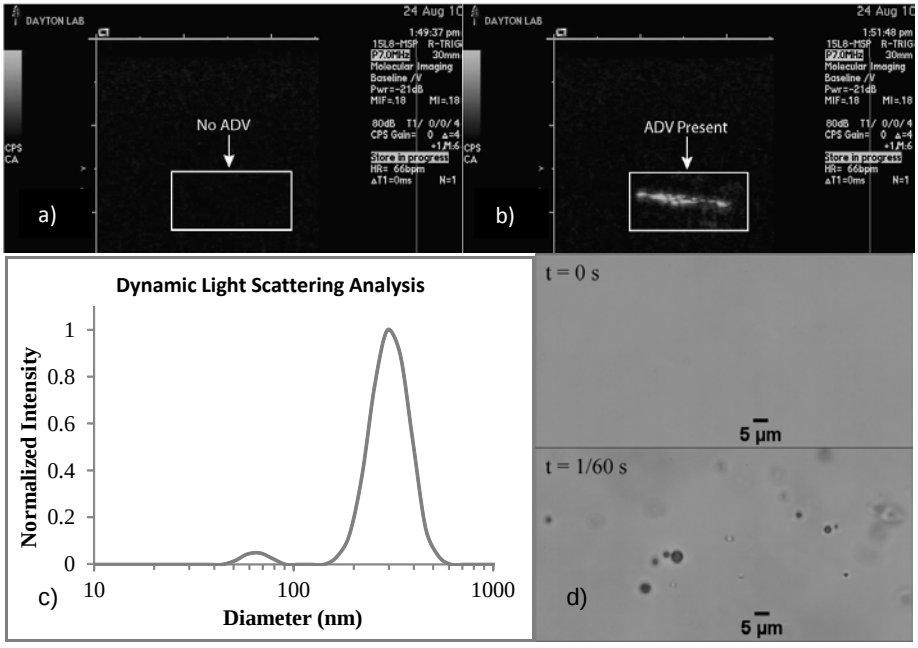


**Figure 1:A) Siemens Sequoia baseline scan of sample containing micrometer-sized PFB-droplets incubated for 4 hours. B) After exposure to a MI of 1.9, significant change in contrast indicates droplet activation. C) Particle sizing results for sub-micrometer sized PFB droplet sample. D) Droplet vaporization is observed optically for the previous sample at 5MHz, MI = 1.5, resulting in 1-5 micrometer bubbles.**

# Measuring blood pressure using microbubbles and ultrasound, revisited

***Charles Tremblay-Darveau, Peter N. Burns***

*Department of Medical Biophysics, University of Toronto, Toronto, Ontario Canada*

## Introduction

Microbubble behavior is very close to that of a harmonic oscillator while under the influence of low acoustic pressureand becomes resonant when driven at resonance frequency. Due to their high compressibility, microbubbles are sensitive to the fluid around them, which affects their scattering properties. It was suggested 30 years ago [1] that microbubbles could provide a direct way to measure blood pressure deep within the body by monitoring the change in their resonance frequency associated with quasi-static compression.In principle, this method, unlike subharmonic emission, is capable of measuring absolute ambient fluid pressure.Complications arise, however, when we consider a realistic setting:microbubbles are strong nonlinear oscillators even at low acoustic excitation (~30 kPa) and commercially available contrast agents are polydispersedin their size distribution, while coherent scattering introduces inherent statistical variation in the scatteredechoes. With the recent advances in microbubble modeling and microfluidic fabrication techniques (in particular the advent of almost monodispersedmicrofluidic microbubbles), we decided to revisit the idea of using microbubbles to measure blood pressureand assess its feasibility. The effects of static pressure in the nonlinear scattering regime were investigated through single microbubblesimulations using the Marmottant model and the statistical effects of microbubble populations were quantifiedboth theoretically and experimentally.

## Method

### *Static pressure dependent modeling of a single microbubble*

To understand the static pressure dependence of individual microbubbles, theacoustic response of a purely viscoelastic bubble (a linearized surface tension function) and a buckling phospholipid bubble were simulated numerically, using the Marmottant equation for a sequence of narrowband pulses to minimize frequency coupling. It was found that while a linear correction of the resonance frequency is sufficient to compensate for the nonlinear deviationsobserved in a simple viscoelastic bubble (Figure 1), the deviations intrinsic to buckling bubbles dependupon a complex relationship between static pressure and acoustic pressure.

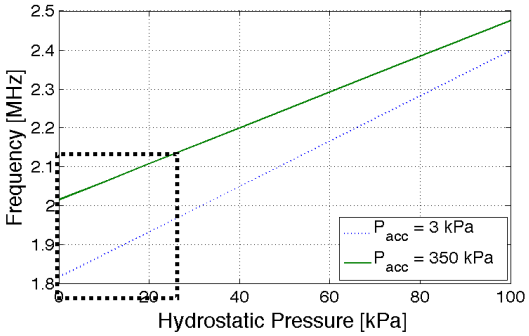


**Figure 1 :Simulation (Marmottant model) of the effect of the acoustic pressure on the resonance frequency for different static pressures (3 μm radiusmicrobubble). The dotted box indicates the clinical range of interest.**

***Fluctuation statistics of a microbubble population response***

Speckle causes dramatic fluctuations in the frequency space, which limits any estimation of the resonance frequency. Stochastic averaging over different bubble populations can be used to reduce speckle noise, at a cost of decreased temporal resolution. To estimate the number of required acquisitions, a statistical model based on existing theoryof the fundamental frequency scattering from red blood cells [2] was extended to all harmonics.It ispredicted that each harmonic component of the scattered pressure amplitude should follow Rayleigh statistics as a consequence of linear signal propagation within water. The scattered spectrum of phospholipid microbubbles was measured multiple times in a pulse-echo setup using a sequence of 17-cyclenarrowband pulses spanning 1 to 6 MHz on a 3.5 MHz (85% bandwidth) single element spherically focused transducer. The measured SNR agreed with Rayleigh statistics within the experimental error for both the fundamental and the second harmonic (figure 2).

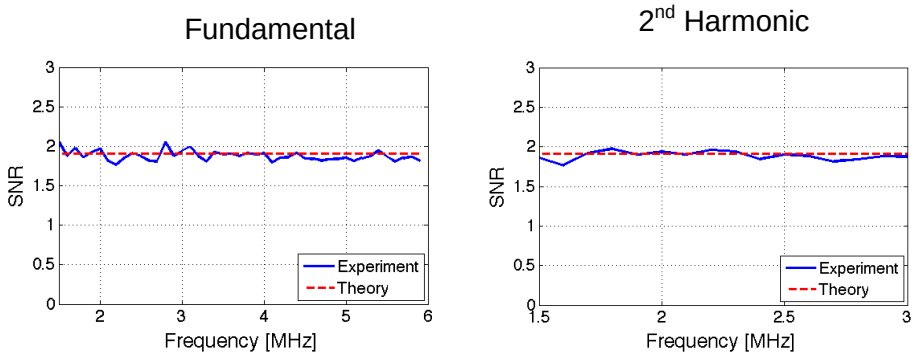


**Figure 2: Measured SNR ofDefinity microbubbles compared to Rayleigh-statistic predictions for both fundamental (left) and second harmonic (right).**

***The statistical effect of bubble size distribution***

The scattered spectrum of a native polydispersesolution of phospholipid microbubbles and a centrifuge-filtered population (2±1μm radius) were measured using the same apparatus.A noticeable shift and broadening of the resonance peak was observed for the polydisperse microbubbles (figure 3).These effects limit our accuracy in static pressure measurements and are undesired. Based on our statistical model, the final pressure amplitude spectrum will be proportional to the root mean square of the pressure response of individual bubbles. A 10% coefficient of variation (CV) of the microbubbleradius size distribution is required to avoid any frequency shift artifact and 3% CV is required to minimize peak broadening. Under such conditions, the scattered echo from a bubble population will be similar to the one of an individual bubble and statistical effects of size distribution can be safely neglected.Although such monodispersemicrobubble populations can't be achieved through usual sonication and centrifuge filtering techniques, such coefficients of variation are within reach usingmicrofluidic fabrication methods (CV of 1 to 2 % [3]).

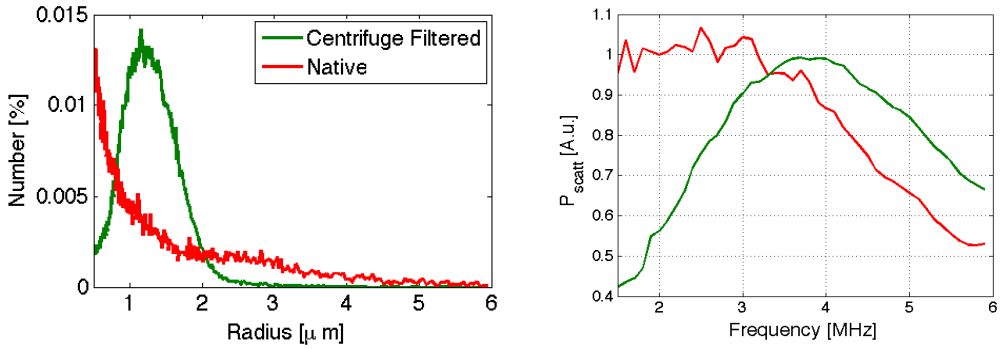


**Figure 3 : Experimental measurement of the effect of the microbubble population coefficient of variation on the scattered pressure amplitude spectrum**

## Conclusions

The static pressure-dependent response of nonlinear phospholipid microbubbles was simulated using the Marmottant model. It was found thatdeviations of the resonance frequency from linear theory can be compensated by first order corrections as long as buckling is negligible. The backscattered echo from a bubble is affected by both speckle and bubble size distribution. Speckle (dominated by Rayleigh statistics) can be compensated with stochastic averaging, but size distribution effects can be safelyneglectedonly by using a microbubble population with a CV < 3%.This criteria is satisfied by microfluidic microbubbles. The method for measuring absolute quasi-static blood pressure using such microbubbles is then, in principle, feasible.

## References

1. W. M. Fairbank, JR., M. Scully (1977) , BME -24 (2) : 107-110
2. R. S. C. Cobbold. Foundations of Biomedical Ultrasound. Oxford University Press, 2007
3. M. Seo, I. Gorelikov, R. Williams and N. Matsuura (2010) , Langmuir 26 (17) : 13855-13860

# Nonuniform oscillations of deflating bubbles - a pilot study

***J.Viti[1], R.Mori[1], F.Guidi[1] , P.Tortoli[1], N. de Jong[2]***

*[1]Electronics & Telecommunications Dept, Università di Firenze, Italy*
*[2]Erasmus MC, Erasmus Universiteit Rotterdam, The Netherlands*

The response originating from a bubble hit by ultrasound (US) pulses is linked to physical characteristics such as size, shell elasticity and viscosity. These characteristics are expected to change during extended exposure to US. The experiments described in this work aim at observing, both acoustically and optically, the changes in the bubble response due to prolonged US-induced stress.

Single Definity (Lantheus Medical Imaging, N. Billerica, MA) microbubbles are confined in a capillary tube and positioned in the focuses of two single-element wideband transducers. A programmable ultrasound system controls both transducers; 70 kPa peak-negative-pressure pulses in the range 2 – 4 MHz are generated by one transducer and the echo is received by the other one. This setup offers a sensitivity the order of 0.1Pa, allowing single bubble echo recording. The coherently digitized echo samples are saved in a large circular buffer, which can store several thousands of radiofrequency echoes. The Brandaris128 ultrafast framing camera is used to capture the full bubble oscillation; since the camera can store a limited number of movies in its internal memory, it was decided to record one movie every 26 US pulses transmitted at 250 Hz PRF.

In Fig.1, the radial oscillations captured for a bubble having a 4.2 μm initial diameter are sequentially shown; in this particular experiment, US excitation pulses at 2.0, 2.5, 3.0, 3.5 and 4.0 MHz were sequentially transmitted on consecutive intervals, in order to analyse the changes in the bubble behaviour at multiple frequencies. The bubble underwent an irreversible process of deflation while presenting different types of radial oscillations. Expansion-only, symmetric and compression-only radial oscillations were obtained even at a nearly constant resting radius; these different types of oscillation suggest that the elasticity of the bubble shell is changing non-monotonically in time. Remarkably, when bubbles pass from oscillations in which the compression phase is more pronounced than the expansion phase, to oscillations with opposite characteristics or to symmetric oscillations, a significant reduction of the resting size was always observed. These sequential changes suggest that, during prolonged US excitation, bubble deflation derives from a combination of gas diffusion and transformations in the bubble shell: gas diffusion would cause a reduction in shell elasticity and a compression-only behaviour; on the other hand, shell transformations, such as material shedding, would account for a reduction in the resting radius associated with an increase in shell elasticity, and could explain symmetric or expansion-only radial oscillation following a noticeable reduction in bubble radius.

Fig.2 shows the fundamental harmonic amplitude (top left) and phase lag (bottom left) of the received acoustic echo over time. The fundamental amplitude decreases monotonically for each of the excitation frequencies; however the decrease rate exhibits a frequency-dependent behaviour, as changes in the deflation rate occur at different times in the 2.0, 2.5 and 3.0 MHz traces. The monotonic amplitude decrease is consistent with the fact that the bubble is shrinking in size; furthermore, the different echo decreasing rates are consistent with an increasing bubble resonant frequency.

During most of the time, the phase lag monotonically increases for all frequencies; however, in the last part of the experiment, the 2.0 MHz and 2.5 MHz traces show a decreasing phase lag, while the higher frequency traces still exhibit a monotonic increase. It can be noted that for each excitation frequency, a maximum phase lag variation of at least $\pi/2$ is observed, which also suggests an increasing bubble natural frequency as the size decreases. Noticeably, the echo seems to be only dependant on the bubble size and resonant frequency, whereas no correlation between the echo and the types of oscillation shown by the bubble can be found.

Fig.2 shows the second harmonic echo amplitude (top right) and phase lag (bottom right) for 2.0 MHz and 2.5 MHz transmitted bursts; the amplitude shows a characteristic “bell” curve, where the maximum amplitude is achieved shortly before a rapid decrease occurs. The decline in second harmonic amplitude starts coincidentally with the decrease in fundamental harmonic amplitude. For completion purposes, the second harmonic phase lag is also shown.

In conclusion, these preliminary experiments, confirmed by further data obtained with other phospholipid-coated bubbles, demonstrate that interesting phenomena can be observed through combined acousto-optical experiments. Specifically, it seems that prolonged US-induced stress causes several transformations in a phospholipid-coated bubble, most notably in size. The deflation process is generally non-uniform, and several changes are seen in optical recordings concerning both the bubble resting radius and the type of radial oscillation. Acoustical recordings show changes in echo that appears to be mainly related to changes in bubble size and, consequently, in resonant frequency.

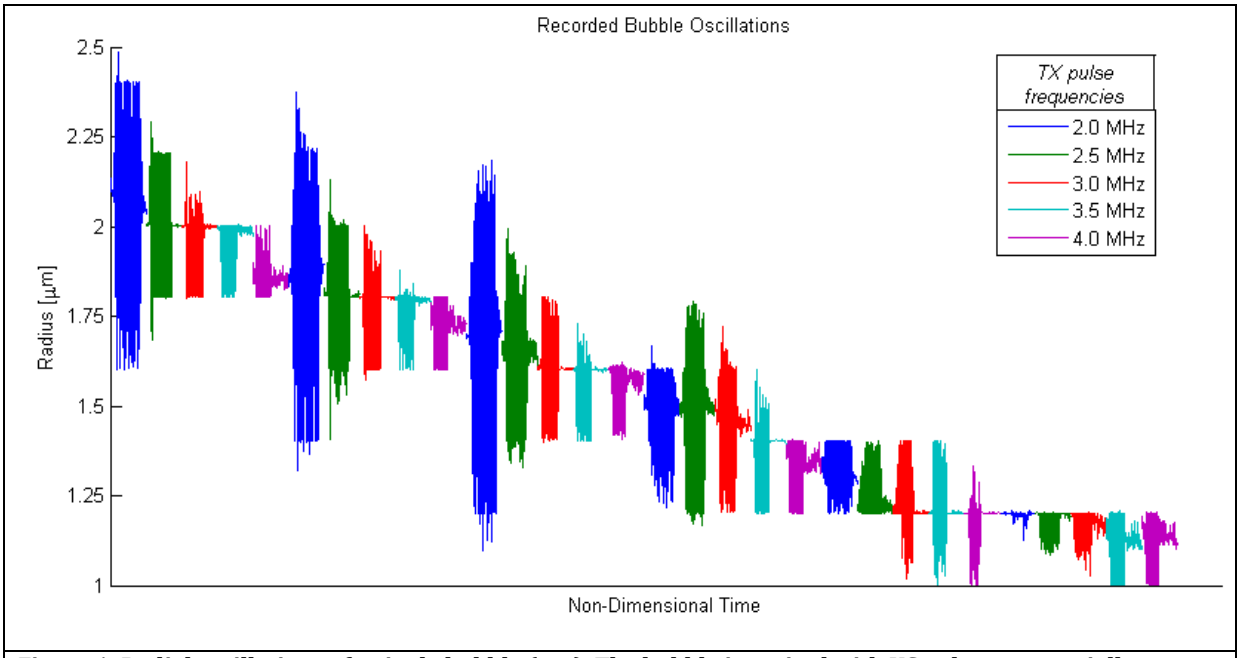


**Figure 1: Radial oscillations of a single bubble (top). The bubble is excited with US pulses sequentially transmitted at 2.0, 2.5, 3.0, 3.5 and 4.0 MHz. The sequence is repeated about 160 times. Consecutive optical recordings are spaced by 26 PRI (=104ms).**

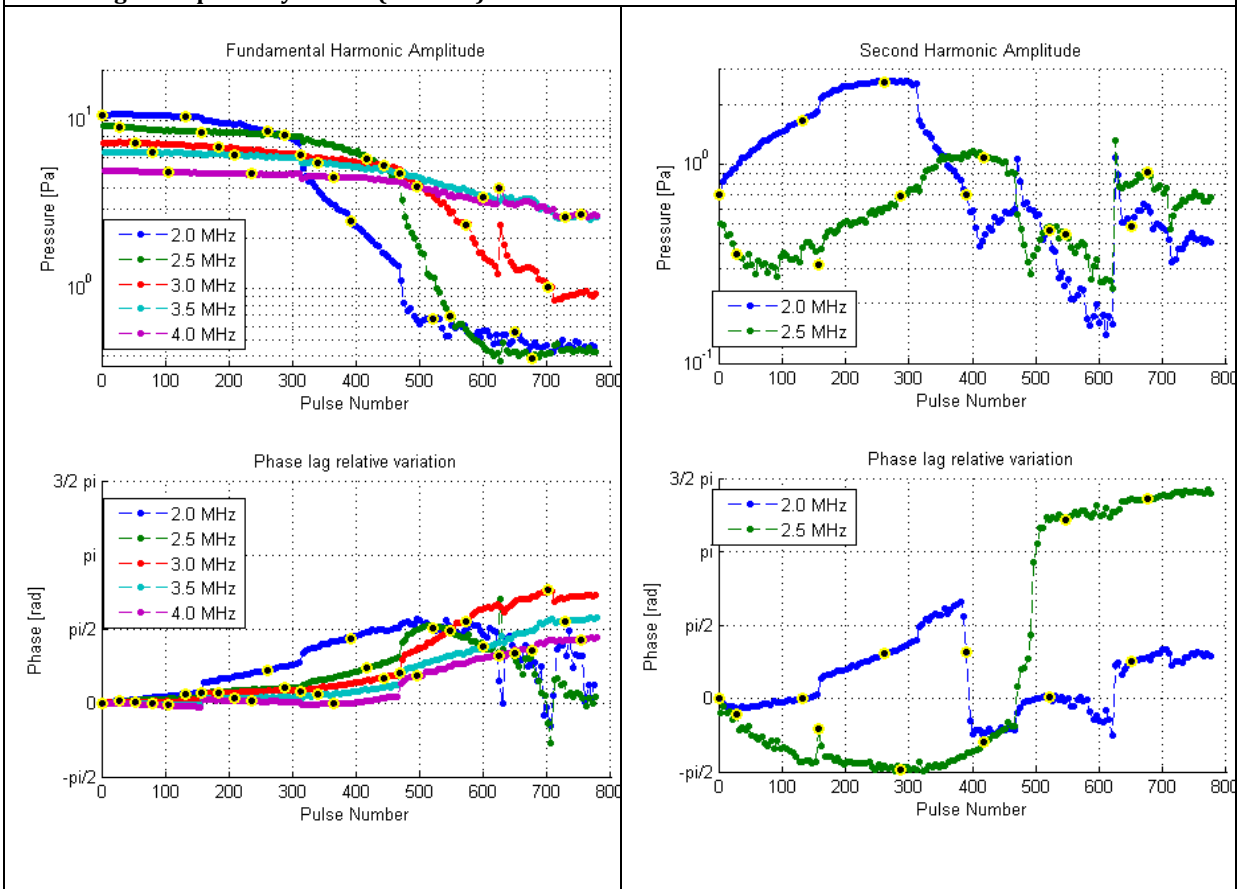


**Figure 2: Fundamental harmonic amplitude (top left) and phase lag (bottom left) of bubble echoes; 2nd harmonic echo amplitude (top right) and phase lag (bottom right) for 2.0 MHz and 2.5 MHz TX pulses. Circled stars mark acoustic echoes for which an optical recording was also performed.**

# Effect of Albumin Concentration on Ultrasound and Microbubble mediated Gene Transfection in vivo: a preliminary in vitro and in vivo investigation

***Richard J Browning[1], Helen Mulvana[1], Mengxing Tang[2], Jo V Hajnal[1], Dominic J Wells[3], Robert J Eckersley[1]***

*[1] Imaging Sciences Department, Imperial College London, UK;*
*[2] Bioengineering Department, Imperial College London, UK;*
*[3] Department of Veterinary Basic Sciences, Royal Veterinary College, London, UK.*

**Introduction**

Ultrasound and microbubble mediated gene transfection is a rapidly advancing field with great potential for the targeted treatment of many diseases. Studies have shown that the contrast agent selection influences transfection efficiency (Alter *et al.*, 2009) with albumin shelled microbubbles, such as Optison (GE Ltd.) performing better than lipid shelled agents such as SonoVue (Bracco Suisse SA). However, optimisation of the albumin shell for the purposes of gene transfection has not been undertaken.

Previously, Porter *et al.* (1995) investigated the influence of albumin concentration on the acoustic response of microbubbles for imaging, though detailed bulk and single bubble acoustics were not performed. Yong-feng *et al.* (2001) investigated the influence of the sugar shell additive on bubble stability. Shell composition strongly determines microbubble behaviour under ultrasound, however, few transfection studies include their detailed acoustic investigation making interpretation of *in vivo* results challenging.

We present detailed acoustic characterisation of microbubbles with varying albumin concentrations from 2 – 10% using high speed imaging, bulk acoustics and modelling. The results were used to plan our pre-clinical work and some preliminary results of their application *in vivo* are also discussed.

**Methods**

Filter-sterilised, recombinant human serum albumin at 2%, 5% and 10% albumin and 0.9% saline solutions were diluted four-fold with a filter-sterilised solution of 20% dextrose and 0.9% saline solution and heated to 60$^{o}$C. Octafluoropropane gas was bubbled through the solution before sonication (Sonicator 3000, Misonix) for 1 minute (20kHz, 33-42W). The resulting suspension was immediately centrifuged at 500rpm for 1 minute, and the liquid phase aspirated using a syringe. The resulting microbubble suspension was imaged using a microscope (Nikon Eclipse 50i) and the images analysed using a program developed in MATLAB (The Mathworks Inc.) specifically for this purpose (Sennoga *et al*., 2010). (All concentrations are listed as weight per volume, and all materials were purchased from Sigma-Aldrich.)

High speed imaging (Cordin 550) was used to assess the influence of albumin concentration on the dynamic behaviour of single bubbles excited at moderate (~100 kPa) acoustic pressures. A dilute microbubble suspension was injected into a 200 μm diameter cellulose capillary fibre held within a tank of filtered, de-ionised, gas-saturated, isotonic water at 37°C. Single, isolated bubbles were excited with a 12 cycle, 0.5 MHz, Gaussian windowed pulse using a 0.5 MHz single element focused transducer ($f$ = 40 mm). The high speed camera was run at 2.5 MHz and a series of 58 images obtained for each insonation. Images were post-processed in Matlab to obtain time vs. diameter plots, and diameter measurements pre- and post-excitation for each bubble.

The time vs. diameter data were used to derive shell properties for each albumin formulation. Modelling was performed using the Marmottant model (Marmottant *et al.*, 2005) in MATLAB. The derived shell parameters were used to model anticipated microbubble behaviour following excitation at 6 MHz, the frequency employed during our pre-clinical investigations (Browning *et al.*, 2010). For reference, comparison was also made against the contrast agent SonoVue employed during this work, using established shell properties (Marmottant *et al.*, 2005).

Acoustic scattering and attenuation measurements of bulk microbubble suspensions were performed using the set-up previously described in Mulvana et al. (2010) in gas saturated, body temperature water. A sufficient volume of contrast agent to generate an approximate 50% attenuation of the total transmitted signal was added to a 300 ml acoustically transparent vessel at the mutual focus of a pair of single element transducers (Videoscan V380 Panametrics-NDT). One transducer was driven with a stepped pressure ramp made up of a series of pulse-inversion (PI) pairs where the pulse was a 2 cycle Gaussian windowed sinusoid with centre frequency 3.5 MHz over a pressure range from 22 - 217 kPa in 30 kPa increments. A pulse repetition frequency (PRF) of 2 Hz was used, while the intra PRF between the incremented pressure ramp pulses was 5 kHz. The acquisition was repeated every 30 seconds for 10 minutes. Signals were generated in MATLAB and uploaded to an arbitrary signal generator before power amplification. Scattered signals were received using a second, matched transducer and amplified (PR5800, Panametrics-NDT), while attenuated signals were acquired in the far field using a 1 mm diameter needle hydrophone (Precision Acoustics Ltd.) connected to a pre-amp. All signals were acquired via a digitizer to a PC for post-processing in MATLAB to recover the attenuation, total scatter and non-linear scatter component of the receive signals in each case. Measurements were normalised against the actual volume of contrast agent added to generate each measurement and its measured gas concentration, and used to calculate a ratio of scatter to attenuation ratio (STAR) and non-linear STAR (nSTAR).

Preliminary *in vivo* transfection experiments were performed on the myocardium of 6-8 week old, female, CD1 mice (Harlan). 150 µL of 5% albumin microbubbles and 50 µL (4 µg/µL) of pGL4.13[luc2/SV40] (Promega), a plasmid encoding Firefly luciferase, were administered intravenously by a 27G needle prior to 2 minutes of ultrasound exposure (Siemens Accuson Sequoia, 15L8, 6 MHz, 1.6 MI, focal depth 0.75 mm). 72 hours post treatment, intra-peritoneal injection of luciferin and *in vivo* bioluminescence imaging (IVIS 100, Xenogen) were used to identify areas of myocardium transfection.

**Results**

Bubble manufacture produced suspensions with similar characteristics, with some variation between each albumin concentration and size distribution, as presented in Table 1.

| Albumin Concentration | Mean Diameter (µm) | Concentration (MBs/ml) | Gas Concentration (µl/ml) |
|---|---|---|---|
| 2% | 1.3 ±0.14 | 6.5e8 ±2.28e8 | 2.2 ±1.46 |
| 5% | 1.8 ±0.07 | 2.0e9 ±1.68e9 | 14.0 ±9.8 |
| 10% | 1.7 ±0.01 | 1.1e9 ±0.03e9 | 7.4 ±0.42 |

**Table 1. Microbubble suspension size and concentration analysis.**

During high speed imaging, both 5% and 10% albumin bubbles showed similar maximum bubble excursions during insonation, with a peak excursion of approximately 5.5µm for 13µm diameter bubbles (Fig. 1). Both showed an average decrease in bubble size after insonation of up to 0.6 µm at 13 µm and a mean decrease for all bubbles of 2.3%. In contrast, 2% albumin bubbles showed a far greater radial expansion under the same acoustic conditions, up to a peak of over 10 µm for a 12 µm bubble (Fig. 1) and a greater decrease in diameter following insonation of up to 2.5 µm for a 12 µm or a mean decrease for all bubbles of 5.2%.

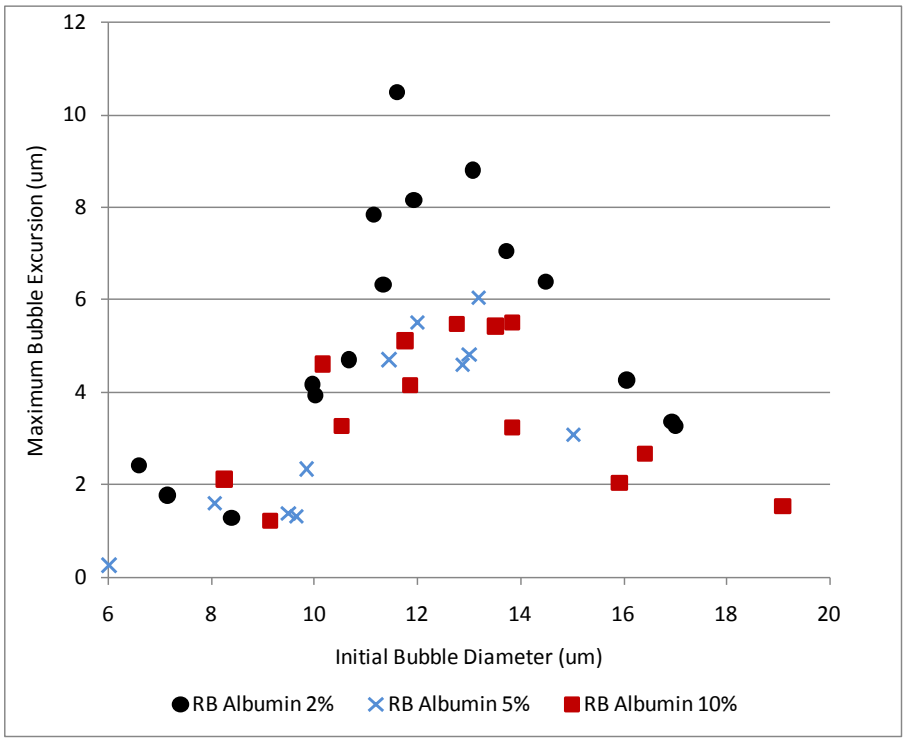


**Figure 1. Maximum bubble excursion during insonation.**

Modelling results are presented in Figure 3 as maximum radial excursion against initial microbubble diameter. The data suggest that albumin microbubbles may be capable of greater radial oscillation than SonoVue when driven at 6 MHz, leading to the expectation that in-house fabricated microbubbles may be capable of greater acoustic activity under these conditions. In contrast to our high speed imaging conducted at 0.5 MHz, modelling at 6 MHz indicates that 5% and 10% albumin preparations may be capable of greater radial excursion than 2% albumin microbubbles. We hypothesise that this apparent disparity may be a symptom of parameterising the model appropriately and further work is required to investigate the suitability of the model in this context.

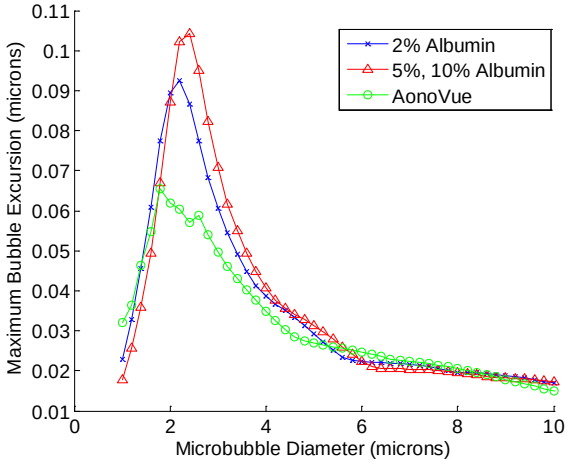


**Figure 3. Maximum microbubble excursion following excitation with a 10 cycle, gauss-windowed, 0.04 MI, 6 MHz pulse for three microbubble preparations: 2% Albumin, 5% and 10% Albumin and SonoVue.**

Bulk investigation showed that both 5 and 10% albumin preparations exhibit similar acoustic behaviour, while 2% albumin bubble suspensions were characterised by greater total and non-linear scattering (Fig. 2).

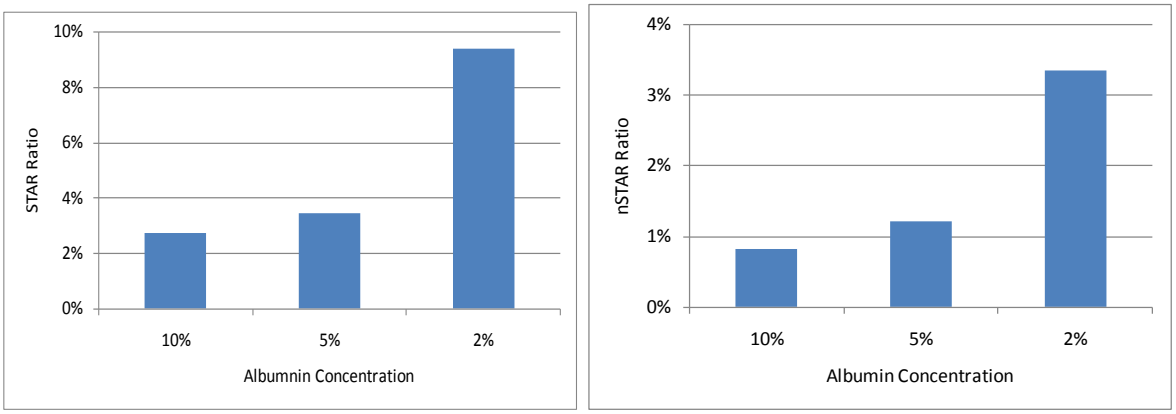


**Figure 2. Linear scattering to attenuation ratio (STAR) and non-linear scattering to attenuation ratio (nSTAR) plotted against albumin concentration.**

Preliminary *in vivo* work has demonstrated the use of our in-house fabricated 5% albumin bubbles for transfection of the mouse myocardium under the influence of 6MHz ultrasound. The level of transfection using freshly prepared microbubbles is comparable to our previous work with Sonovue (Browning *et al*., 2010), however the level of transfection was seen to decrease with time post microbubble fabrication, with a correlation between microbubble suspension gas concentration and transfection observed. Mice which were treated with microbubbles fabricated more than 4 hours prior to administration displayed negligible levels of transfection.

**Summary**

Our findings indicate that the acoustic properties of albumin microbubbles can be manipulated for the purposes of gene transfection by controlling the concentration of albumin used during fabrication, without compromising the microbubble yield or significantly influencing the mean diameter. A reduction in albumin concentration results in more flexible microbubbles which exhibit greater radial excursion during single bubble investigation at low frequency, and greater total and non-linear scattering during bulk acoustic studies at clinical imaging frequencies.

Single bubble modelling was used to anticipate the behaviour of the microbubble preparations at 6 MHz, as employed during our pre-clinical work. These results indicate that similar improvements in acoustic response may be expected for in-house prepared albumin microbubbles over SonoVue at higher acoustic frequencies, and we hypothesise that manipulation of microbubble elasticity will lead to greater acoustic activity and may be used to improve transfection *in vivo* as compared to stiffer microbubble preparations.

Our preliminary *in vivo* results indicate that in-house fabricated 5% albumin microbubbles can be used to effectively generate transfection *in vivo* with levels similar to those achieved during our previous work using SonoVue. Work is on-going to establish the relative improvement in transfection which may be achievable, but has been limited by the poor stability of our in-house albumin preparation. These preliminary results have also led to the discovery that the ability for microbubbles to be used for transfection is significantly reduced when administered more than 4 hours post fabrication.

It was observed that the reduction in albumin required to generate more flexible microbubbles (2% albumin) had a further impact on stability, as indicated by the greater size reduction observed following insonation. As discussed above, poor stability could present challenges for the application of these microbubbles *in vivo*. Our results also indicate that 5% and 10% albumin concentration microbubbles exhibit similar acoustic properties. Further work will focus on improving microbubble stability, further optimisation of microbubble parameters and more comprehensive investigation of their application and efficacy *in vivo*.

## Conclusions

Bulk acoustics, high speed optical imaging and modelling has improved our understanding of the differences in behaviour of bubbles made at different albumin concentrations. These findings will be used to inform our *in vivo* transfection work using these bubbles and demonstrates that detailed acoustic characterisation forms an important step in optimisation of microbubbles for any application.

*This work was supported by an EPSRC grant (EP/F066740/1).*

*All animal work was conducted under the authority of a UK Home office project licence as required by the Animals (Scientific Procedures) Act 1986.*

**References**

4. Browning, R.J., Mulvana, H., Wells, D.J., Eckersley, R.J., Effect of needle gauge on microbubble mediated cell transfection in vivo. British Medical Ultrasound Society Annual Scientific Meeting and Exhibition, 28-30th September, 2010.
5. Marmottant, P., van der Meer, S., Emmer, M., Versluis, M., A model for large amplitude oscillations of coated bubbles accounting for buckling and rupture. J. Acoust. Soc. Am., 118 (6), pp. 3499-3505, 2005.
6. Mulvana, H., Stride, E., Hajnal, J.V., Eckersley, R., Temperature behaviour of ultrasound contrast agents. Ultras. Med. Biol., 36 (6), pp. 925-934, 2010.
7. Porter, T.R., Xie, F., Kricsfeld, A., The mechanism and clinical implication of improved left ventricular videointensity following intravenous injection of multi-fold dilutions of albumin with dextrose. Int. J. Cardiovasc. Imaging 11 (2) pp. 117-125, 1995.
8. Sennoga, C., Mahue, V., Loughran, J., Casey, J., Tang, M., Eckersley, R.J., On sizing and counting of microbubbles using optical microscopy. Ultras. Med. Biol., 36 (12) pp. 2093-2096, 2010.
9. Yong-feng, D., Ming-xi, W., Wen-ming, Z., Study on the preparation of a new sugar albumin microbubble ultrasound contrast agent. Yaoxue Xuebao. 36 (11) pp. 859-862, 2001.

# Microbubbles as contrast agents for acousto-optic measurement of blood oxygenation: theoretical and experimental studies

***Jack Honeysett[a,b], Eleanor Stride[c], Terence Leung[a]***

*[a]Dept. of Medical Physics and Bioengineering, University College London, UK*
*[b]CoMPLEX (Centre of Mathematics and Physics in the Life Sciences and Experimental Biology), University College London, UK*
*[c]Dept. of Mechanical Engineering, University College London, UK*

Optical measurements in biological tissue are already in use for clinical monitoring, including measurement of tissue oxygen saturation[1]. This technique (commonly known as near infrared spectroscopy or NIRS) is, however, limited by strong optical scattering in tissue. The measurement accounts for a large volume of tissue, therefore NIRS provides only a bulk estimate of tissue oxygenation rather than being sensitive to more localised changes in blood oxygenation.

Combining focused ultrasound (US) with diffuse light provides a way to improve this unsatisfactory spatial resolution[2]. Hybrid acousto-optic techniques rely on US to modulate the properties of the tissue (such as the refractive index and scattering) in a highly localised region, which in turn modulates the optical field. The time-varying portion of the detected light then provides information about photons which have passed through the US focal region.

However, this US-modulated light signal is very weak compared with the un-modulated light which does not pass through the focal region. It has previously been shown by the authors using a computational model that microbubbles can enhance the US-modulated signal[3] (Figure 1), by exploiting the changes in optical scattering that occur when microbubbles oscillate under US. This technique is proposed as a method for improving the sensitivity of NIRS to large blood vessels[4]. Experimental work with tissue phantoms is used to verify the results of the model. A phantom consisting of a blood-filled tube surrounded by a scattering medium is insonified by a 1 MHz US transducer (tone burst), in the beam path of 632 nm laser light (CW). The ratio of modulated light to un-modulated signal is measured by a photodetector to demonstrate the change in US-modulation due to the presence of microbubbles in the blood.

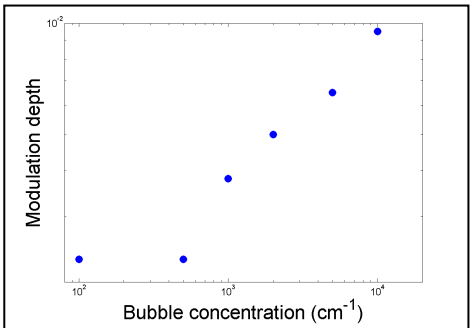


**Figure 1: Effect of bubble concentration on US-modulated optical signal strength**

The applications of this technique for non-invasive clinical monitoring will be discussed: in particular measurements of blood oxygenation from the jugular vein and pulmonary artery.

**References**


1. Gibson A. P., Hebden J. C., Arridge S. R.: “Recent advances in diffuse optical imaging” Phys. Med. Biol. 50, R1-R43 (2005)
2. Murray T. W., Roy R. A.: “Illuminating sound: Imaging tissue optical properties with ultrasound” Acoustics Today, vol. 3 (2007)
3. Honeysett J., Stride E., Leung T.: “Monte Carlo simulations of acousto-optics with microbubbles” Proc. of SPIE, vol 7564, p 75640K (2010)
4. Honeysett J. E., Stride E., Leung T. S.: “Feasibility study of non-invasive oxygenation measurement in a deep blood vessel using acousto-optics and microbubbles” Advances in Experimental Medicine and Biology (under review)

# Bubble Oscillations near an Elastic Wall

***M.Fujiwara, T.Sugiura***

*Mechanical Engineering, Faculty of Science and Technology, Keio University, Japan*

**Introduction**

Microbubbles are widely used in medical imaging with ultrasound, to enhance endocardial boundary delineation. Furthermore, its potential use for drug and gene deliveries attracts attention in recent years. Bubble dynamics have to be clarified for practical use of such systems.

Bubble-wall interactions have been investigated by many researchers. Effects of walls cannot be neglected for bubbles located in narrow capillaries and near walls. However, most studies regard a wall as rigid and thus neglect their elasticity. Microbubbles are usually confined in space through a blood vessel or an elastic capillary fiber, therefore the elasticity of the wall has to be considered. To the best of our knowledge, the effect has not been quantified clearly to this date.

**Method**

In this study, we try to clarify the dynamics of a bubble near an elastic wall. We regard the wall as a beam, so as to express the wall elasticity. For the first step of this study, we consider only the first mode of the beam vibration; therefore, the model can be more simplified as a spring-mass system.

**Results**

We compared results of an elastic wall model with those of a rigid wall model using the method of image. In both cases the bubble resonance frequency decreases with decreasing distance to the wall. On the other hand, the most noticeable difference between the interaction of the bubble with the rigid wall and that with the elastic wall appears in the maximum amplitude of oscillation at the wall, which increases in the case of a rigid wall and decreases for an elastic wall.

**Conclusion**

We proposed a simple spring-mass model for analysis of the bubble oscillations near an elastic wall. The model can approximately describe effects of the elastic wall on bubble oscillations.

# Optical Characterization of Individual Liposome Loaded Microbubbles

***Ying Luan, Telli Faez, Ilya Skachkov, Nico de Jong***

*Biomedical Engineering, Erasmus MC, the Netherlands*

**Introduction**

Accurate characterization of drug loaded contrast agent is important to support mechanism study of ultrasound triggered drug delivery. Liposome loaded microbubble is a newly developed system, and it has been proved for considerable improvement of gene transfer efficiency [1]. This study mainly focuses on characterization of liposome loaded microbubbles through ultra-high speed imaging. Physical parameters of microbubbles are derived from resonance spectroscopy for better understanding of ultrasonic behavior of liposome loaded microbubbles.

**Methods**

Liposome loaded bubbles were characterized by comparing with non liposome loaded bubbles through optical approach. Individual microbubbles with radius ranging from 0.5μm-4μm were insonified with ultrasound with frequency range of 0.5-4MHz and pressures of 50kPa & 100kPa. Ultra-high speed imaging was used to record images through the whole frequency range in a single run. Characteristic resonance curve, which varies with microbubble sizes and viscoelastic properties, can be constructed through frequency spectrum of radius time curves.

Resonance curve provide two parameters: resonance frequency and damping coefficient.
Shell elasticity can be determined by fitting the spectroscopy curve with a linear oscillator model from Marmottant *et al*. In addition, shell viscocity of microbubbles can be derived from damping coefficient of resonance curve [2].

**Results**

Resonance curve of microbubbles were compared, which gives an indication of the different characteristics between liposome loaded and non liposome loaded microbubbles. See Figure 1. In general, compared with bare bubbles, liposome loaded microbubbles have lower elasticity and higher viscosity, which is in accordance with different surface structure and rheology of the two groups of microbubbles.

## Conclusions

Resonance spectroscopy with high speed imaging was proved to be an effective method to characterize liposome loaded microbubbles. Resonance frequency, elasticity and viscosity parameters derived from this study can be applied in further modeling of liposome loaded microbubbles. This study will facilitate future ultrasound parametric study of drug delivery with drug loaded contrast agents.

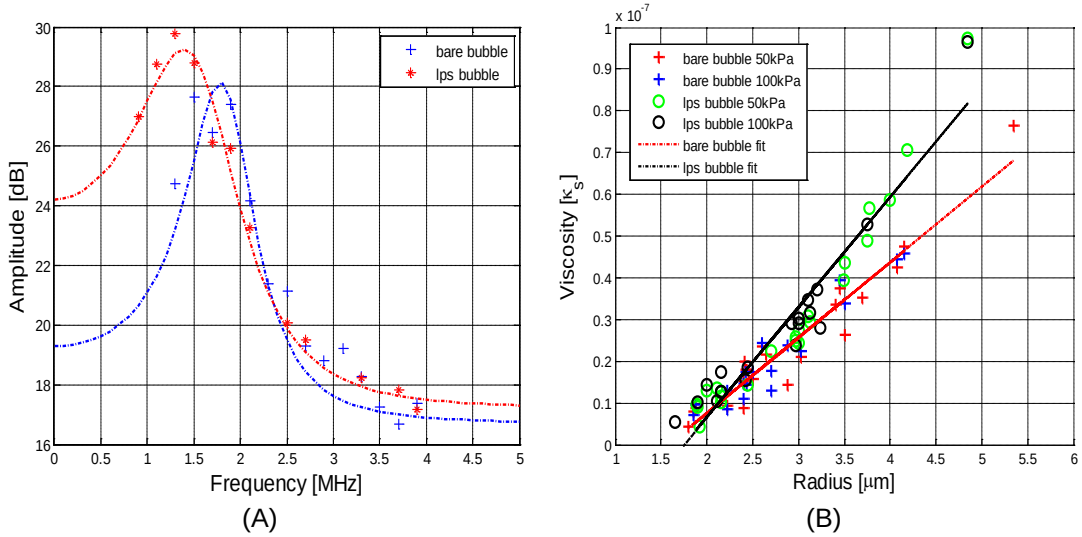


**Figure 1. Resonance curve of bare bubble and liposome loaded microbubble, both of which have radius of 4.8μm(A). For bare bubble, eigenfrequency f0= 1.9MHz, damping coefficient δ=0.49. For liposome loaded bubble, f0=1.74, δ=0.84. Viscosity values are derived from f0 and δ (B)**.


## Acknowledgements

We would like to thank Ine Lentacker and Bart Geers from Ghent Research Group on nanomedicines, Ghent University, for providing microbubble samples.This work is supported by Sonodrugs Project (NMP-4-LA-2008-213706) with financial support of the European Union.


## Reference


1. I. Lentacker, et al., "Lipoplex-loaded microbubbles for gene drug delivery: a trojan horse controlled by ultrasound," *Adv.Funct.Mater.* **17**, 1910-1916(2007)
2. S.M.van der Meer, et al., "Micorbubble spectroscopy of ultrasound contrast agents", *J. Acoust.Soc.Am.* **121**(1), 648-656(2007)

# The use of ultrasound contrast agents in cancer immunotherapy: The use of mRNA-loaded microbubbles for transfection of dendritic cells

***Dewitte H.[1], De Temmerman M-L.[1], De Smedt S.C., Rejman J., Lentacker I.***

*Ghent Research Group on Nanomedicine, Department of Pharmaceutical Sciences, Ghent University, Harelbekestraat 72, 9000 Ghent, Belgium*

**[1] Both authors contributed equally to this work**

**Introduction and aim of the study**

In cancer immunotherapy the patient's immune system is triggered to selectively recognize and eliminate tumor cells in the body. One way to achieve that is by loading dendritic cells (DCs) – the most potent antigen presenting cells – with tumor associated antigens (TAAs). In the DC's, the antigens can be processed and presented to T-cells, thus giving rise to a tumor-specific immune response.

The central effector cells in antitumor immunity are cytotoxic T-lymphocytes (CTLs). These CD8+ T-cells are formed upon recognition of antigens presented in MHC class I molecules by antigen presenting cells. To obtain MHC class I presentation, the antigens have to be loaded directly into the cytosol of the DC. This can be accomplished by transfecting the DCs with messenger RNA encoding a TAA. The advantages of mRNA over pDNA for this very purpose are numerous: (a) mRNA does not integrate in the genome of the host cell, therefore there is no risk of insertional mutation; (b) since translation of mRNA to proteins takes place in the cytosol, there is no need for mRNA to enter the nucleus; (c) mRNA – in contrast to DNA – does not require specific promoter and terminator sequences.

In this study mRNA loaded microbubbles will be evaluated for ultrasound-guided transfection of DCs**.** **Figure 1** gives an overview of the application of this technique in cancer immunotherapy.

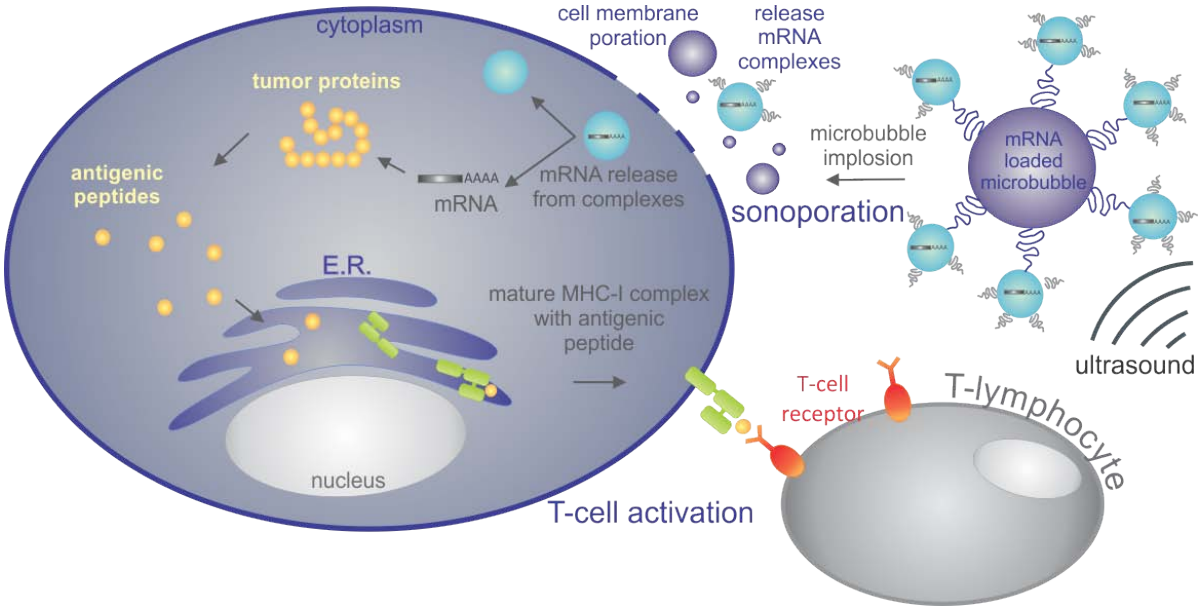


**Figure 1**

**Results**

mRNA was complexed with cationic lipids and loaded onto the microbubble surface via avidin-biotin interactions, as shown in **Figure 2**.

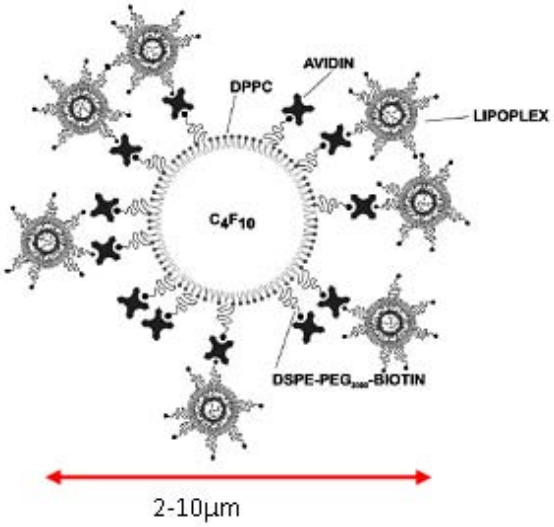


**Figure 2**

Bone marrow- derived DCs were seeded in OptiCells™. Microbubbles were loaded with mRNA complexes encoding luciferase, and after a short incubation with the cells, ultrasound was applied (1MHz, 50% duty cycle, 30s). Luciferase expression was then measured at different time points. As shown in **figure 3** ultrasound-mediated delivery of mRNA complexes led to efficient transfection of DCs. No luciferase was detected when only mRNA lipoplexes were added to the cells. Maximal levels of luciferase were detected 6 hours after ultrasound exposure.

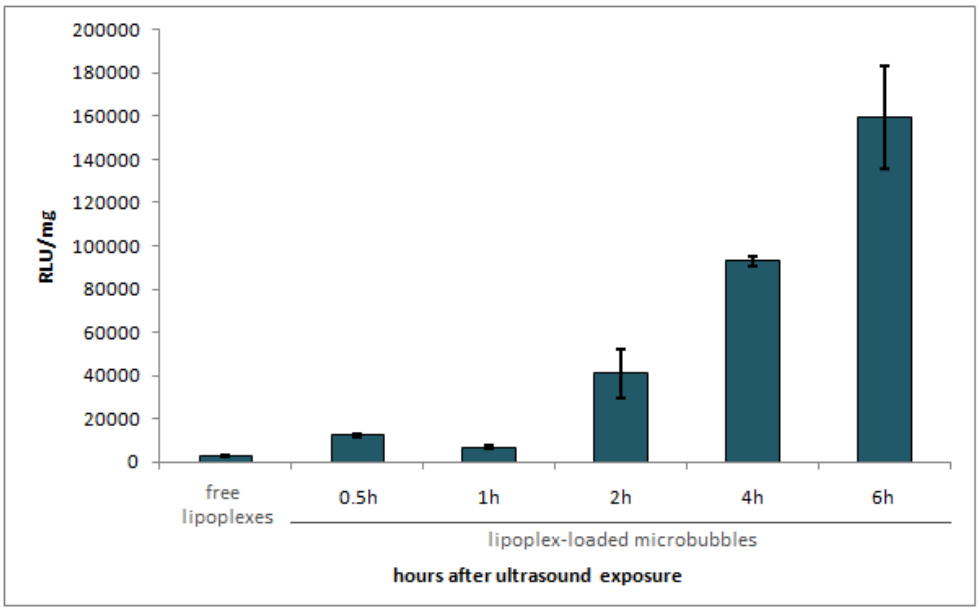


**Figure 3**

To visualize the mRNA transfection, mRNA encoding EGFP (Enhanced Green Fluorescent Protein) was loaded into the DCs. Confocal images revealed that a substantial number of DCs expressed EGFP 1 day after exposure to ultrasound and mRNA-microbubbles (**Figure 4**).

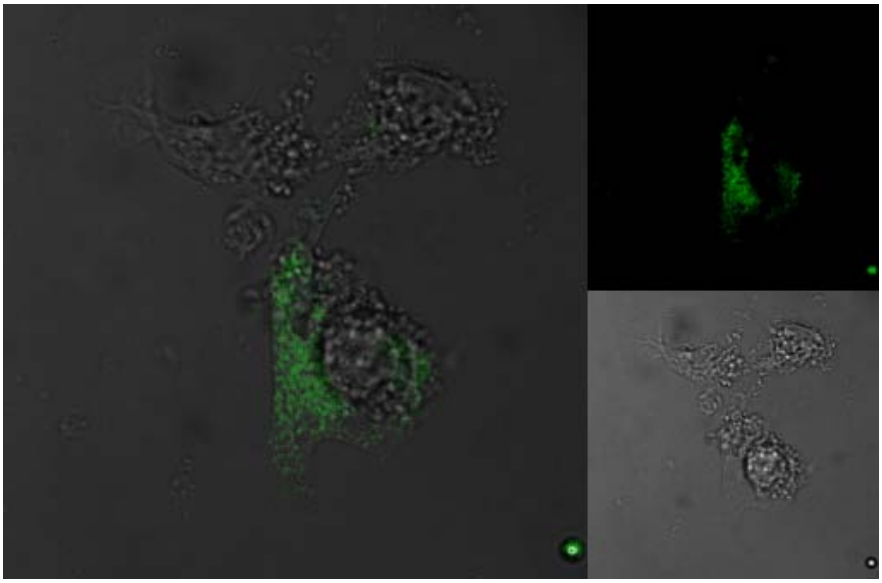

**Figure 4**

Our data demonstrate a proof-of-concept that mRNA loaded microbubbles and ultrasound can be used to transfect DCs. In contrast to current *ex vivo* transfection methods applied in the field of DC-based vaccines, this technique offers interesting perspectives towards future *in vivo* loading of DCs. First of all, ultrasound-guided delivery assures local uptake of nucleic acids, only in ultrasound exposed tissues. Secondly, microbubbles are FDA approved as contrast agents in ultrasonic imaging.

**Acknowledgements**

Heleen Dewitte is a doctoral fellow of the Institute for the Promotion of Innovation through Science and Technology in Flanders, Belgium (IWT-Vlaanderen). Ine Lentacker is a postdoctoral fellow of the Fund for Scientific Research in Flanders, Belgium (FWO-Vlaanderen).

# Myocardial Contrast Echocardiography: Barriers to Widespread Utilization

***Thomas R Porter***

Although the Food and Drug Administration has only approved ultrasound contrast agents for left ventricular opacification, a large number of clinical trials demonstrating the incremental value of myocardial perfusion imaging (MPI) with myocardial contrast echocardiography (MCE) have emerged. During dobutamine, exercise, or vasodilator stress echocardiography, the incremental data provided with MPI has improved the detection of significant coronary artery disease, and MPI was better than wall motion at predicting outcome. It has also assisted in the evaluation of chest pain in the emergency department, and provided prognostic data in the evaluation of a patient following ST segment elevation myocardial infarction. Barriers to its widespread utilization include a) lack of formal training programs which will teach both cardiologists and other health professionals how to perform these studies; b) lack of approval to utilize ultrasound contrast for perfusion imaging from regulatory agencies throughout the world; c) lack of any reimbursement for performing perfusion imaging with rest or stress echocardiography; and d) insufficient data from multi-center trials to support it as a replacement for radionuclide perfusion imaging. Nonetheless, there is consistent data from single center studies to support the concept that MPI with MCE improves the prediction of patient outcome following dobutamine, exercise, and vasodilator stress echocardiography, and that the spatial and temporal resolution of real time MCE exceeds that of radionuclide imaging. The barriers to widespread utilization can be overcome by a) developing advocacy groups who will provide evidence to regulatory agencies supporting the safety and incremental efficacy of MPI with MCE; b) developing physician-initiated multi-center trials which will test the efficacy of MPI with MCE in detecting coronary artery disease and predicting patient outcome during both rest and stress echocardiography; and c) providing training programs to assist academic centers in developing MPI with MCE as part of their educational curriculum to train physicians, cardiology fellows, and sonographers. The utilization of diagnostic ultrasound to perform bedside MPI still has the potentnial to dramatically improve the detection of coronary artery disease and improve patient risk stratification, while simultaneously reducing the need for more costly non-invasive and invasive testing that require significant amounts of ionizing radiation.

**References**


1. Tsutsui JM, Elhendy A, Anderson JR, Xie F, McGrain AC, Porter TR. Prognostic value of dobutamine stress myocardial contrast perfusion echocardiography. Circulation 2005; 112:1444-1450.
2. Porter TR, Li S, Kricsfeld D, Armbruster RW. Detection of myocardial perfusion in multiple echocardiographic windows with one intravenous injection of microbubbles using transient response second harmonic imaging. J Am Coll Cardiol 1997;29:791-799.
3. Cwajg J, Xie F, O'Leary E, Kricsfeld D, Dittrich H, Porter TR. Detection of angiographically significant coronary artery disease with accelerated intermittent imaging after intravenous administration of ultrasound contrast material. Am Heart J 2000;139:675-683.
4. Elhendy A, O'Leary EL, Xie F, McGrain AC, Anderson JR, Porter TR. Comparative Accuracy of Real-Time Myocardial Contrast Perfusion Imaging and Wall Motion Analysis During Dobutamine Stress Echocardiography for the Diagnosis of Coronary Artery Disease. J Am Coll Cardiol 2004;44:2185-2191.
5. Porter TR, Xie F, Silver M, Kricsfeld D, O'Leary E. Real-time perfusion imaging with low mechanical index pulse inversion Doppler imaging. J Am Coll Cardiol 2001;37:748-753.
6. Tsutsui JM; Elhendy A; Xie F, I'Leary EL, McGrain AC, Porter TR. Safety of dobutamine stress real-time myocardial contrast echocardiography. J Am Coll Cardiol 2005;45:1235-1242.
7. Dolan M, Gala SS, Dodla S, et.al. Safety and efficacy of commercially available ultrasound contrast agents for rest and stress echocardiography a multicenter experience. J Am Coll Cardiol 2009; 53:32
8. Xie F Dodla S, O'Leary E, Porter TR. Detection of Subendocardial Ischemia in the Left Anterior Descending Coronary Artery Territory with Real-Time Myocardial Contrast Echocardiography During Dobutamine Stress Echocardiography. J Am Coll Cardiol Img 2008;1:271-278
9. Shimoni S; Zoghbi WA; Xie F; et al. Real-time assessment of myocardial perfusion and wall motion during bicycle and treadmill exercise echocardiography: comparison with single photon emission computed tomography. J Am Coll Cardiol 2001;37:741-747.
10. Kaul S, Senior R, Dittrich H, Raval U, Khattar R, Lahiri A. Detection of coronary artery disease with myocardial contrast echocardiography: Comparison with 99mTc-sestamibi single-photon emission computed tomography. Circulation 1997;96:785-792.
11. Heinle SK, Noblin J, Goree-Best P,et al.. Assessment of myocardial perfusion by harmonic power Doppler imaging at rest and during adenosine stress: Comparison with (99m) Tc-sestamibi SPECT imaging. Circulation 2000;102:55-60.
12. Janardhanan R, Senior R. Accuracy of dipyridamole myocardial contrast echocardiography for the detection of residual stenosis of the infarct-related artery and multivessel disease early after acute myocardial infarction. J Am Coll Cardiol 2004;43:2247-2252.
13. Balcells E, Powers ER, Lepper W,et al.. Detection of Myocardial Viability by Contrast Echocardiography in Acute Infarction Predicts Recovery of Resting Function and Contractile Reserve. J Am Coll Cardiol 2003;41:827-833.
14. Main ML, Magalski A, Morris BA, Coen MM, Skolnick DG, Good TH. Combined assessment of microvascular integrity and contractile reserve improves differentiation of stunning and necrosis after acute anterior wall myocardial infarction. J Am Coll Cardiol 2002;40:1079-1084
15. Swinburn JM, Lahiri A, Senior R. Intravenous myocardial contrast echocardiography predicts recovery of dysynergic myocardium early after acute myocardial infarction. J Am Coll Cardiol 2001;38:19-25.
16. Tsutsui J, et.al. Eur Heart Journal 2008;29:377-385
17. Lepper W, Hoffmann R, Kamp O, et al: Assessment of myocardial reperfusion by intravenous myocardial contrast echocardiography and coronary flow reserve after primary percutaneous transluminal coronary angiography in patients with acute myocardial infarction. Circulation 2000;101:2368-2374.
18. Dwivedi G, Janardhanan R, Hayat SA, Swinburn JM, Senior R. Prognostic value of myocardial viability detected by myocardial contrast echocardiography early after acute myocardial infarction. J Am Coll Cardiol 2007;50:327-334.
19. Galiuto L Garramone B, Scara A, et.al. The extent of microvascular damage during myocardial contrast echocardiography is superior to other known indexes of post-infarct reperfusion in predicting left ventricular remodeling. J Am Coll Cardiol 2008;51:552-559.
20. Shimoni S, Frangogiannis NG, Aggeli CJ, et al. Microvascular structural correlates of myocardial contrast echocardiography in patients with coronary artery disease and left ventricular dysfunction: implications for the assessment of myocardial hibernation. Circulation 2002;950-956.
21. Shimoni S, Grangogiannis NG, Aggeli CJ et.al. Identification of hibernating myocardium with quantitative intravenous myocardial contrast echocardiography: comparison with dobutamine echocardiography and thallium -201 scintigraphy. Circulation 2003;107:538-544.

22. Hayat SA, Dwivedi G, Jacobsen A, Lim TK, Kinsey C, Senior R. Effects of left bundle branch block on cardiac structure, function, perfusion, and perfusion reserve: implications for myocardial contrast echocardiography versus radionuclide perfusion imaging for the detection of coronary artery disease. Circulation 2008;117:1832-1841.
23. Senior R, Monaghan M, Main ML, et al. Detection of coronary artery disease with perfusion stress echocardiography using a novel ultrasound imaging agent: two Phase 3 international trials in comparison with radionuclide perfusion imaging. Eur J Echocardiogr 2009;10:26-35.
24. Xie F, Hankins J, Mahrous HA, Porter TR.Detection of coronary artery disease with a continuous infusion of Definity ultrasound contrast during adenosine stress real time perfusion echocardiography. Echocardiography 2007;24:1044-1050.
25. Lonnebakken MT, Bleie O, Strand E, Staal EM, Nygard OK, Gerdts E. Myocardial contrast echocardiography in assessment of stable coronary artery disease at intermediate dobutamine-induced stresss level. Echocardiography 2009;26:52-60.
26. Miszalski-Jamka T, Kuntz- Hehner, S, Schmidt H, et al. Real time myocardial contrast echocardiography during supine bicycle stress and continuous infusion of contrast agent. Cutoff values for myocardial contrast replenishment discriminating abnormal myocardial perfusion. Echocardiography 2007;24:638-648.
27. Lipiec P, Wejner-Mik P, Krzemińska-Pakuła M, et al. Accelerated stress real-time myocardial contrast echocardiography for the detection of coronary artery disease: comparison with 99mTc single photon emission computed tomography. J Am Soc Echocardiogr. 2008;21:941-947
28. Mor-Avi V, Koch R, Holper EM, et al. Value of vasodilator stress myocardial contrast echocardiography and magnetic resonance imaging for the differential diagnosis of ischemic versus nonischemic cardiomyopathy. J Am Soc Echocardiogr. 2008;21:425-432.
29. Olszowska M, Kostkiewicz M, Tracz W, Przewlocki T. Assessment of myocardial perfusion in patients with coronary artery disease. Comparison of myocardial contrast echocardiography and 99mTc MiBI single photon emission computed tomography. Int J Cardiol 2003;90:49-55.
30. Elhendy A, Tsutsui JM, O'Leary EL, Xie F, Porter TR. Noninvasive diagnosis of coronary artery disease in patients with diabetes by dobutamine stress real-time myocardial contrast perfusion imaging. Diabetes Care 2005;28:1662-1667.
31. Xie F, Tsutsui JM, McGrain AC, et al. Comparison of dobutamine stress echocardiography with and without real-time perfusion imaging for detection of coronary artery disease. Am J Cardiol 2005;96:506-511.
32. Main ML, Magalski A, Chee NK , et al. Full-motion pulse inversion power doppler contrast echocardiography differentiates stunning from necrosis and predicts recovery of left ventricular function after acute myocardial infarction. J Am Coll Cardiol 2001;38:1390-1394.
33. Hillis GS, Mulvagh SL, Gunda M, et al. Contrast echocardiography using intravenous octafluoropropane and real-time perfusion imaging predicts function recovery after acute myocardial infarction. J Am. Soc Echocardiogr 2003;16:638-645.
34. Janardhana R, Swinburn JM, Greaves K, et al. Usefulness of myocardial contrast echocardiography using low-power continuous imaging early after acute myocardial infarction to predict late functional left ventricular recovery. Am J Cardiol 2003;92:493-497.
35. Tong KL, Kaul S, Wang XQ, et al. Myocardial Contrast Echocardiography Versus Thrombolysis in Myocardial Infarction Score in Patients Presenting to the Emergency Department with Chest Pain and a Nondiagnostic Electrocardiogram. J Am Coll Cardiol 2005;46:920-927.
36. Peltier M, Vancraeynest D, Pasquet A, et al. Assessment of the physiologic significance of coronary disease with dipyridamole real-time myocardial contrast echocardiography. Comparison with technetium-99m sestamibi single-photon emission computed tomography and quantitative coronary angiography. J Am Coll Cardiol 2004;43:257-264.
37. Dodla S, et.al. Heart 2010;96:220-225.
38. Korosoglou G, Labadze N, Giannitsis E, et al. Usefulness of real-time myocardial perfusion imaging to to evaluate tissue level reperfusion in patients with non ST-elevation myocardial infarction. Am J Cardiol 2005;95:1033-1038.
39. Haung WC, Chiou KR, Liu CP, et al. Comparison of real-time contrast echocardiography and low-dose dobutamine stress echocardiography in predicting the left ventricular functional recovery in patients after acute myocardial infarction under different therapeutic intervention. Int J Cardiol 2005:104:81-91.
40. Sbano JC, Tsutsui JM, Andrade JL, et al. Detection of functional recovery using low-dose dobutamine and myocardial contrast echocardiography after acute myocardial infarction treated with successful thrombolytic therapy. Echocardiography 2005;22:496-502

41. Abe Y, Muro T, Sakanoue Y, et al. Intravenous myocardial contrast echocardiography predicts regional and global left ventricular remodeling after acute myocardial infarction: comparison with low dose dobutamine stress echocardiography. Heart 2005;91:1578-583.

# Bubble detection for perfusion: Are we at the end of our technological development?

***Michalakis Averkiou***

*University of Cyprus, Nicosia, Cyprus*

Over the years we have witnessed a surge on the scientific interest for bubble imaging techniques which peaked around 2000 and has almost disappeared in the recent years. The scientific interest was well balanced between academic institutions and equipment industry during the peak years, with industry being the first to express loss of interest. There was a clear shift in the scientific community from bubble imaging to quantification and parametric imaging, therapy monitoring, molecular imaging, and drug delivery. Shift towards 3D ultrasound and matrix arrays was also observed, but for contrast has meant extending current 2D knowledge in 3D without breaking any new ground in bubble imaging. As for matrix arrays, it is quite unfortunate that such technology was utilized only for quick electronic beamforming and missed the opportunity to solve complex acoustic problems including improvements of bubble imaging.

The current state of the art for bubble imaging consists of various flavors of nonlinear pulsing schemes (pulse inversion, power modulation, and their hybrid combinations). Matched filtering, chirps, and codes have also been investigated and used by some companies and researchers but to a lesser degree. And recently radial modulation, low frequency manipulation of bubbles while imaging at a higher frequency, has also been investigated, but it has not yet found its way on clinical systems. Technology has utilized some of the important properties and physical phenomena bubbles such as destruction, nonlinearity, low MI excitation for nondestructive imaging and tissue cancellation, nonlinear pulsing schemes, and use of complimentary apertures for amplitude modulation. However there are still some other properties not fully utilized such as more complicated forms of codes and matched filtering, radial modulation, sub-harmonic response, acoustically induced deflation, self-demodulation, and bubble specific beam forming.

The apparent imaging "*technology stagnation*" is attributed to a variety of reasons. The clinical approval situation (especially for radiological applications) and more specifically in the USA/FDA is a major obstacle. In addition, most ultrasound equipment manufacturers are based in the USA, a country that is also the largest business sector for the main ultrasound companies, where contrast agents are not approved. The emergence of the Chinese/Asian markets has the potential to change this situation, but not in the near future. Early on the clinical and financial promise of bubble technology was too high but major technological advances were needed that took time and money to be achieved and thus the

interest fizzled out. Another reason for the technology stagnation is the cost of bubbles and added complexity of the contrast exam. The $20 vial would probably have gone much further... It is also possible that most efforts in larger companies were led by very few individuals ("running wild" on their own) that slowly diffused away.

**Do we need further contrast imaging? Is it adequate what we currently have? What are the problems that must be solved today?**

In answering the above questions we find that most premium/high-end systems have contrast capabilities to a certain degree but not the mid-range and low-end. Bubble sensitivity which is the most important requirement in perfusion imaging remains penetration limited for average patients, and weak in tough patients (cirrhotic livers, large individuals, difficult access). Another important clinical requirement is image resolution which is medium at best, low usually, and terrible at times. Additionally, micro/macro-vessel separation is inadequate, e.g., vessels are "lost" in liver parenchyma in portal phase. High frequency-low flow imaging (breast, vasa-vasorum) are still not fully addressed with present technology. It is hoped that newer techniques like radial modulation can better address high frequency imaging.

**Are we at the end of our technological development?**

The answer that would be given by any scientist in this field is of course, "No"!! However, some of the issues mentioned above suggest a possible slow down that may be perceived by some as the end of a technological development. The worst case scenario would be that slow progress will be observed for the foreseeable future and new technologies will also be made available for contrast as well when they become available for the rest of diagnostic ultrasound, e.g, automated procedures, spatial compounding, 3D, matrix arrays, aberration correction, speed of sound correction, motion compensation, etc. The best case scenario would be that industry and scientific community together will "rediscover" bubble imaging and continue to advance bubble imaging in order for it to reach its true potential.

# BR38, A New Ultrasound Blood Pool Tracer

***Professor Roxy Senior, Consultant Cardiologist***

*Northwick Park Hospital, Harrow, Middx, UK*

**Objectives**

To evaluate BR38, a new microbubble-based blood pool agent for contrast-enhanced ultrasound imaging.

**Materials and Methods**

The size characteristics of BR38 microbubbles were measured by Coulter counting The backscatter coefficients and attenuation were determined as a function of frequency Additional measurements included the surface charge, osmolality, viscosity and resistance to hydrostatic pressure A complete set of pharmacological and toxicological studies were conducted on the final formulation, mainly in rats and dogs The blood levels and elimination of the gaseous component $C_4F_{10}$ were determined in the rabbit Contrast-enhanced echographic examinations were performed in pigs focusing on the myocardium and the liver Finally safety testing and preliminary imaging experiments were performed in a Phase I trial on human volunteers.

**Results**

BR38 suspensions are isotonic, non -viscous and show a high resistance to hydrostatic pressure Their backscatter coefficient is high from 2 MHz and above and attenuation shows a maximum at 4MHz, slowly decreasing at higher frequencies The no effect levels (NOEL) of 1 µL/kg (rats) and 5µL/kg (dogs) observed in repeated toxicology studies correspond to 50 and 250 times the expected imaging dose, respectively No effects on cardiovascular parameters (in dogs) or respiratory parameters (in rats) were observed $C_4F_{10}$ is eliminated within minutes from blood and excreted in expired air Imaging showed strong and persistent enhancement of the myocardium and of the liver A late phase was observed in the liver No serious adverse events or no significant changes in vital signs, ECGs and laboratory tests were observed in Phase I.

**Conclusions**

BR38 shows a very good safety profile. Its long persistence, reduced shadowing and high efficacy over a wide range of frequencies will be particularly valuable for myocardial perfusion imaging and abdominal imaging BR38 may also be a promising agent for high frequency imaging during carotid ultrasound.

# Contrast-enhanced low mechanical index sonography in children

***Martin Stenzel***

*University Hospital Jena, Germany*

**Purpose/Objective**

Ultrasound is the first-line imaging method in children and adolescents.

Ultrasound contrast media (USCM) are used increasingly to assess vesicoureterorenal reflux (VUR) in children. The obvious advantage of the method is lack of ionising radiation.

On the other hand, intravenous application of USCM is being performed extremely rarely in children. There is one main reason to explain that: experience of the method for intravascular use is very limited, mainly because there is no approval by the EMEA for intravascular use in children.

To assess nature and perfusion of focal lesions and extent of inflammatory diseases, investigators cannot do without contrast media, irrespective of imaging modality.

**Material/Methods/Experience**

The author practises i.v. USCM based sonography for 6 years in adults, mainly in hepatic and renal lesions, but also for detection of organ injuries. For the last 3 years the technique was performed in children and adolescents for characterisation of focal organ lesions, detection of injury impacts and in tumour disease follow-up.

The issue regarding off-label use has to be dealt with. Careful informing patients and parents and the informed consent are mandatory.

**Results**

Over a period of 3 years i.v. USCM sonography examinations in about 40 children and adolescents were performed. Liver, spleen, kidney, thyroid and the small intestine were assessed.

All examinations were of diagnostic value. No adverse reactions in the patients occured.

**Discussion/Conclusion:**

Intravenous administration of USCM in children and adolescents is not officially approved in Europe. Consequently, there is very little expertise in paediatric sonographers.

Regarding the author's experience, USCM enhanced sonography is safe, effective and very helpful in some cases. Children should benefit from this technique the same way as adults do. Nevertheless, spread of expertise's knowledge is important and help from the manufacturers should be demanded.

# Myocardial contrast echocardiography for the study of perioperative myocardial perfusion

***Carolien S.E. Bulte [1,2], Jeroen Slikkerveer [1,3], Otto Kamp [1,3], Stephan A. Loer [1,2], Christa Boer [1,2] and R. Arthur Bouwman [1,2]***

*[1]Institute for Cardiovascular Research, VU University Medical Center, Amsterdam, The Netherlands. Departments of [2]Anesthesiology and [3]Cardiology, VU University Medical Center, Amsterdam, The Netherlands.*

**Introduction**

General anesthesia is associated with an increased activity of the sympathetic nervous system, which may lead to alterations in myocardial blood flow (MBF). Historically, the lack of a suitable, intraoperative and noninvasive imaging technique impeded investigation of the influence of general anesthesia on MBF. Myocardial contrast echocardiography (MCE) is a noninvasive, bedside method for assessment of MBF. It is unclear whether this technique is applicable in the intraoperative setting, since positioning of the anesthetized patient and mechanical ventilation may influence the quality of transthoracic images necessary for quantification of flow. Therefore, the aim of this study was to investigate the feasibility of MCE for intraoperative measurement of MBF and to study the effect of general anesthesia on myocardial perfusion.

**Methods**

Eight cardiovascular healthy patients (3 women, 5 men; age 33-68 years) scheduled for general anesthesia were included. Integrity of cardiovascular autonomic control was confirmed using autonomic function tests. MCE was performed before and during the administration of 1.0 MAC sevoflurane and included MBF measurements at rest and during adenosine-induced hyperemia. MCE provides absolute quantification of MBF in ml/min/gr tissue by analysis of replenishment curves obtained during continuous contrast infusion (Sonovue, Bracco, Switzerland). Flow reserves were calculated by $MBF_{hyperemia}/MBF_{rest}$. Data are presented as mean ± SD. Paired t-tests were used for comparison of dependent samples. A p-value $<0.05$ was considered to reflect a significant difference.

**Results**

In the preoperative setting, basal MBF was 1.13 ± 0.38 ml/min/gr and increased to 3.38 ± 0.73 ml/min/gr during adenosine-induced hyperemia ($p<0.001$). In all patients intraoperative opacification of the myocardium was feasible resulting in a basal MBF of 1.17 ± 0.30 ml/min/gr, which increased to 2.18 ± 0.41 ml/min/gr during hyperemia ($p=0.001$). Alterations in MBF in response to adenosine-

induced hyperemia were comparable for the preoperative and intraoperative measurements, indicated by flow reserves of 3.5 ± 2.1 and 2.0 ± 0.9 respectively (p=0.07).

**Conclusions**

Quantification of myocardial blood flow using myocardial contrast echocardiography is safe and feasible in the intraoperative setting. These preliminary data show no significant difference in flow reserve for the preoperative and intraoperative setting. However, more measurements should be performed to confirm this observation.

# Consensus on guidelines and protocol for tumour vascularity for phase trials

***Edward Leen***

*Imperial College London - Hammersmith Hospital Campus London*

The advent of several novel therapies targeting tumour angiogenesis and vascularity used clinically over the last decade has highlighted the need for more accurate and reproducible quantitative techniques to assess more subtle alteration in tumoral vascularity. Imaging modalities such as CT, MRI and positron emission tomography (PET) have been used to assess perfusion changes in monitoring anti-vascular therapies in cancer patients. However all these modalities have disadvantages such as invasiveness, availability and costs which may limit their application into routine clinical practice. With hundreds of oncology therapeutics in current and future development, assessment of early response has invariably proved to be disappointing to date as compared with the pre-clinical animal studies.

Traditional medical imaging techniques, such as dynamic contrast-enhanced computerized tomography (CT), magnetic resonance imaging (MRI), and ultrasound (US), have been used routinely to monitor the therapeutic effects of cancer intervention. Current assessment of response using these conventional methods is purely based on interval evaluation of the tumour sizes using the Response Evaluation Criteria In Solid Tumours (RECIST) (3). However as anti-angiogenic or anti-vascular therapies are predominantly cytostatic, current criteria for monitoring response are clearly inadequate as they reflect only late changes and are unable to identify non-responders at an early time-point (4). In addition, the development of vascular-targeted agents and their clinical usage are also costly; hence accurate, reproducible and non-invasive imaging methods of assessing their effectiveness at an earlier stage are required.

The Experimental Cancer in Medicine Center (ECMC) network in UK recently organized a meeting of experts in Ultrasound, CT, MR and PET for assessment of tumour vascular support, to establish guidelines and protocols for each modality. The outcome of the meeting will be presented.

# CEUS Imaging Needs in Drug Development

***Theresa Tuthill***

*Pfizer Inc, Groton, CT USA*

Contrast enhanced ultrasound, along with imaging in general, is gaining a larger role in the development of new therapeutic agents. The associated needs of pharmaceutical companies can be broken into three groups: today (current imaging biomarkers), tomorrow (targeted imaging), and future (site drug delivery).

Currently in oncology clinical trials, CEUS is used for quantification of tumor blood flow and associated perfusion surrogate endpoints. These imaging biomarkers can serve not only in the monitoring of treatment, but also in stratification of patients and in development of prognostic factors. Numerous institutions have developed potential methodologies, but to apply CEUS in multi-site clinical trials, standardization is needed in techniques and in analysis with implementation independent of equipment.

Healthcare is moving towards more personalized medicine, and target identification can help to understand underlying biological processes and pathways and to assist in patient selection. While genetics provide information on effectiveness of therapeutic interventions, phenotyping through targeted imaging is needed for determining disease susceptibility and/or progression. A prime example is in oncology where recent studies have been aimed at tailoring therapies based on tumor characteristics such as protein expression.

A longer term goal in the pharmaceutical industry is for site-targeted drug delivery. The conversion from standard parenteral delivery of compounds would result in asymmetric, preferential drug distribution to desired tissues and cells leading to increased drug concentration at desired sites and decreased toxicity elsewhere. Delivery platforms through microbubble encapsulated/attached drugs would improve therapeutic index for compounds both on the market currently and in development. Research areas of relevance include enabling extravasation, demonstrating efficacy, monitoring clearance, determining off-target toxicity, and establishing feasibility in the clinic.

# HIREC (High Resolution Contrast) – a novel technique for contrast imaging

***Dr HP Weskott***

*Klinikum Siloah, Hannover, KRH. Germany*

Different low MI techniques like pulse inversion, power amplitude exist for contrast imaging have been developed during the last decade.

Due to its imaging process, temporal and spatial resolution, partly being caused by blooming artifacts, are lacking behind B-mode imaging. Most contrast software solutions have a low dynamic range as well, so differences in local contrast concentration cannot be dissolved adequately. A homogeneously enhanced image over the whole depth is often missed, which is a major limitation in the sensitivity to detect small liver lesions.

Using a low MI coded harmonic imaging technique these clinical relevant disadvantages can be overcome – as long as the power of the received echoes is sufficient and the background tissue is greatly cancelled out. A frame rate like in B-mode imaging allows the visual detection of flow direction even in arteries. It ranges between 26 fps and 55 fps depending on the image size (width, line density and to some extend to its depth). Using a high dynamic range differences in bubble concentration can be imaged for example in tumor tissue and infectious disease. The different bubble concentration in hepatic arteries and veins can be clearly seen during the arterial phase. A high spatial resolution is mandatory for the detection of focal organ lesions. Pixel size in HIREC mode (no company name) is comparable to that of B-mode images and thus allows the detection of liver metastases down to 3mm.
Disadvantage of HIREC may come up when echogenic tissue is not suppressed sufficiently, so a contrast wash out cannot go below the pre-contrast level and may therefore be missed. Clinical examples of HIREC performance in liver, kidney and vessel studies will be demonstrated.

# Detection and Characterization of Liver Tumors using Sonazoid Contrast Imaging

***Fuminori Moriyasu, M.D., Ph.D.***

*Department of Gastroenterology & Hepatology, Tokyo Medical University*

Sonazoid has been launched in Japan since 2007 and used clinically for diagnosis of liver tumor lesions. Not only characterization but also detection of the liver tumor is the role of Sonazoid contrast imaging because Sonazoid has a liver specific Kupffer phase imaging.

**Detection of Liver Tumors**

We have compared conventional B-mode ultrasound (US) alone with the combination of conventional B-mode US and contrast enhanced ultrasound (CEUS) with Sonazoid in the Kupffer phase for the detection of hepatic metastases by using a jackknife free-response receiver operating characteristic (JAFROC) analysis.

Twenty-seven patients with 57 hepatic metastases and 6 patients without hepatic metastasis underwent conventional B-mode US and CEUS in the liver-specific Kupffer phases of Sonazoid. We used the diagnoses established by contrast-enhanced multi-detector row computed tomography (MDCT) as the standard of reference. All ultrasound scanning was performed by an experienced radiologist with a routine clinical procedure. All scanning data were archived with digital cine clips. A Windows-PC based review system, which can display pairs of cine clips for B-mode and contrast-enhanced US side by side, was developed for off-site observer study. Seven radiologists interpreted each case individually first conventional B-mode only, and then the combination with contrast-enhanced US by identifying locations of possible candidates for hepatic metastasis with their confidence ratings. The figure of merit (FOM) values, sensitivity, and false-positives per case were estimated for B-mode US alone, and for the combination of conventional B-mode and contrast-enhanced US. The analysis of variances for multi-reader-multi-case matrix of pseudo FOM values was used for testing a statistically significant difference between two modes of interpretations.

For all readers, the sensitivities of the combined US imaging (mean 72.2%) were clearly improved from that of conventional US alone (mean 41.6%) by reducing the average number of false positives from 1.1 to 0.5 per case. In the jackknife analysis, there was a statistically significant difference between mean FOM values for the combined imaging (0.76) and for conventional US alone (0.44, $P < .00001$).

The combination of conventional and contrast-enhanced US could improve physicians' accuracy in the detection of hepatic metastases.

**Characterization of Liver Tumors**

Computer-aided diagnosis (CAD) could be useful for characterizing focal liver lesions on Sonazoid-enhanced US; thus, it would potentially improve radiologists' accuracy for focal liver lesions.

To evaluate the clinical utility of a computer-aided diagnosis (CAD) scheme for the improvement of diagnostic performance of radiologists for differentiation of focal liver lesions on contrast enhanced ultrasound with Sonazoid.

Our data set contained 107 focal liver lesions from 106 cases, consisted of 27 metastases, 27 hemangiomas, and 53 hepatocellular carcinomas (HCCs). Histological differentiation of HCCs is as follows; 17 well-differentiated, 26 moderately differentiated, and 10 poorly differentiated hepatocellular carcinomas. Pathologies of all cases except for hemangiomas were determined based on biopsy or surgical specimens. The CEUS images were obtained with use of Aplio XG (Toshiba, Nasu, Japan), including B-mode, vascular imaging with micro-flow imaging (defined as <60 seconds after injection), and Kupffer phase (defined as 10 minutes after injection). The CAD displayed vascular imaging as movie files, B-mode and Kupffer images as static images. The observer study was conducted with seven radiologists with experience in CEUS of the liver, all of whom were first asked to give confidence ratings regarding benign or malignant; second, if malignant, whether metastasis or HCCs; finally to select one of 5 classifications matched to the unknown focal liver lesions. Each radiologist read cases first without CAD and immediately thereafter with CAD. Observers' rating data were analyzed with the multi-reader multi-case receiver operating characteristic (ROC) analysis.

The overall sensitivity of our CAD for differentiation of 5 types of focal liver lesions included in the database was 76.6% (82/107). For all seven participants, as to benign vs. malignant, the mean area under the ROC curve (AUC) values were improved significantly from 0.861±0.068 without CAD to 0.942±0.045 with CAD ($p<0.001$). In addition, as to metastasis vs. HCC, the mean AUC values were also improved significantly from 0.707±0.09 to 0.776±0.075 by use of the CAD ($p=0.035$). The overall sensitivity of all observers was also improved from 52.6% to 66.5%.

The use of the CAD can significantly improve the diagnostic performance of radiologists for differential diagnosis of the focal liver lesions on CEUS.

# Molecular Imaging in Cardiovascular Medicine: New Developments

***Jonathan R. Lindner, MD***

*Oregon Health & Science University*
*Portland, Oregon, USA*

New methods for evaluating atherosclerotic disease with ultrasound have been developed that go beyond simple anatomic characterization and instead yield information on plaque or vascular phenotype. This talk will focus on new developments in ultrasound molecular imaging techniques. For atherosclerotic disease high-risk molecular phenotype has either focused on the detection of early but aggressive disease or the development of complex end-stage plaques that are prone to atherothrombotic events. This talk will focus on how molecular imaging of endothelial cell adhesion molecules that are involved in the inflammatory component of atherosclerosis, as well as activated hemostatic pathways which produce a prothrombotic and pro-inflammatory phenotype. How these technologies can be used to evaluate risk and to assess new therapies that are targeted at high risk events will be discussed. Part of this discussion will also involve the molecular and cellular participants in the remodeling of the vasa vasorum and development of plaque neovessels which have been associated with propensity for disease progression and atherothrombotic events. Molecular imaging of angiogenesis in peripheral vascular disease will also be discussed. In this setting, molecular imaging in concert with perfusion imaging has been able to provide important insight into the regulatory process of arteriogenesis and also to evaluate the mechanism of effect of pro-angiogenic therapies such as stem cell therapy.

# Advances in Contrast Enhanced Imaging with Micro-Ultrasound

***A. Needles[1], J. Mehi[1], N.C. Chaggares[1], R. Castelino[2], N. Sacadura[1], A. Heinmiller[1], C. Bilan-Tracey[1], C. Theodoropoulos[1], D. Hirson[1], and F.S. Foster [1,2]***

*[1.] VisualSonics, Toronto, Canada*
*[2.] Sunnybrook Health Sciences Centre, Toronto, Canada*

## Introduction

Contrast Enhanced Ultrasound Imaging (CEUS) has historically been applied at conventional ultrasound frequencies (1-15 MHz) and involves the intravenous injection of gas-filled microbubble contrast agents. By increasing the center frequency of the ultrasound system and maintaining bandwidth, the resolution of the CEUS image can be greatly improved. An increase in frequency will inevitably result in a tradeoff in sensitivity to the microbubbles, as their resonant frequencies are in the low MHz range and nonlinear propagation from tissue signals becomes more problematic at higher frequencies. Micro-ultrasound systems (>15 MHz), typically used for pre-clinical imaging of small animals, require both high resolution and sensitivity. This talk will focus on the advances in the field of contrast imaging aimed at trying to solve issues related to resolution and sensitivity, and outline areas where tradeoffs exist. Recent developments in transducer and system technology will be presented, along with Photoacoustic (PA) imaging combined with micro-ultrasound. This is an exciting technique that uses laser light to create ultrasound, and can improve sensitivity to contrast agents that are undetectable with ultrasound alone, while maintaining equivalent resolution.

## Methods

### *Transducer Development*

A comparison study between two high-frequency array transducers was conducted with a commercially available micro-ultrasound system (Vevo 2100, VisualSonics). A 256 element linear array transducer (MS250, VisualSonics, $f_c$ = 21 MHz, 70% -6dB two-way bandwidth, elevation focus = 15 mm, elevation f-number = 5.3) was compared with a newly developed transducer with identical frequency characteristics (MS-250SC, VisualSonics) but elevation characteristics optimized for mouse imaging (elevation focus = 8 mm, elevation f-number = 5). The original MS250 transducer was used in previous studies for contrast imaging in mice (Needles et al. 2010) simply due to its frequency characteristics. It was originally designed for small animal imaging at depths corresponding to the penetration of 20 MHz ultrasound (15-20 mm). Its success in contrast agent detection in the 20 MHz range was owed to its frequency characteristics, but its elevation resolution, particularly in the near field (5-10 mm), was

always less then optimal. This is often apparent in the corresponding B-Mode image used to guide the placement of a nonlinear contrast imaging scan plane.

A prototype phantom (Gammex Inc., Middleton, WI, USA) was used to assess resolution of the two transducers. The phantom contained randomly distributed anechoic spheres (diameters on the order of 1 mm) for assessing resolution in the elevation dimension, and 50 µm wire targets for assessing lateral and axial resolution. The transmit focus of the ultrasound system was set to 8 mm, corresponding to the geometrically-fixed elevation focus of the new MS250SC transducer. The images of the phantom spheres and wires were then compared, qualitatively and quantitatively, between the two transducers to assess near-field elevation resolution, lateral resolution and axial resolution.

Finally, the two transducers were compared *in vivo* using MicroMarker™ (VisualSonics) contrast agent in the kidneys of healthy adult mice (n = 3). The animals were administered two 50-µl intra-venous boluses of contrast agent ($1.2 \cdot 10^7$ bubbles per bolus), one for each transducer, with 10 minutes between each injection. The image planes were aligned as closely as possible between each scan, and were chosen to encompass as much of the kidney cortex and medulla as possible for assessing the perfusion of the microcirculation, while avoiding the larger renal blood vessels. The simultaneously acquired B-Mode and Contrast images were compared qualitatively, and a contrast-to-tissue ratio (CTR) was calculated.

***Increasing the Frequency of Nonlinear Microbubble Detection***

The same micro-ultrasound system (Vevo 2100, VisualSonics) was modified to perform nonlinear contrast imaging at 30 MHz, using an amplitude modulation based approach (Needles et al. 2010).
A 256 element linear array transducer (MS-400, VisualSonics, $f_c$ = 30 MHz, 70% -6dB two-way bandwidth, elevation focus = 9 mm, lateral res. = 110 µm, axial res. = 50 µm) was used for 30 MHz imaging. The transducer was compared to the lower frequency (21 MHz) transducer described in the previous section (MS-250SC) using the 50 µm wire phantom. The effect of scaling the frequency up to 30 MHz was also assessed in the same kidney model (n = 3), as well as in a mouse tumour model on the hind limb (n = 1). In the case of the tumour model, two 50 µL bolus injections were performed; one at the typical concentration ($1.2 \cdot 10^7$ bubbles per bolus) and one at double the concentration ($2.4 \cdot 10^7$ bubbles per bolus).

***Photoacoustic Contrast Imaging***

A modified version of the same micro-ultrasound system (Vevo 2100, VisualSonics) was operated with two different 256 element linear array transducers (MS250 and MS550D, VisualSonics, $f_c$ = 21 MHz and $f_c$ = 40 MHz respectively, both with 70% -6dB two-way bandwidth) retrofitted with a housing that

held rectangular fiber optic bundles (25.4 x 1.25 mm) to either side of the transducer at an angle of 30º. The rectangular bundles were bifurcated ends of a single bundle that was coupled to a tuneable laser (Rainbow NIR, OPOTEK Inc., Carlsbad CA, 680-970 nm). The μUS system was synchronized with the laser and PA signals were acquired with a fluence < 20 mJ/cm$^2$, beamformed in software, and displayed at 5-20 Hz. Microbubbles were loaded with gold nanoparticles (GNP) using a previously described technique (Seo et al. 2010**)** and were flowed through a 1 mm diameter wall-less vessel phantom (2% agar**)** and imaged at 21 MHz with the system in both Contrast Mode and a newly implemented PA-Mode (Needles et al. 2010b) using an optical wavelength of 800 nm. Both GNP (Nanopartz Inc., Loveland CO, USA), and Methylene Blue (MB) (www.riccachemical.com) were also imaged *in vivo*. For determination of the presence of MB signal *in vivo*, PA images of the axillary lymph node were collected at 21 MHz using 680 nm and 760 nm laser light, both pre- and post-infusion of MB into the forepaw of an adult CD1 mouse and a subtracted image was generated. Axillary and brachial lymph nodes were excised and imaged to verify the source of the MB signal. In the case of GNP, *in vivo* images were assessed at 40 MHz with 800 nm light in a mouse tumour model on the hind limb, following the intravenous bolus injection of the agent (200 μL).

**Results**

***Transducer Development***

Results from the cyst phantom are shown in Fig. 1. It is clear that in the near field (< 10 mm) improving the elevation focus has a dramatic effect on the elevation resolution. Some of the anechoic spheres (1 and 2) are barely visible with the current contrast transducer (MS250) and others of smaller diameter are not visible at all due to out of plane clutter (3). Deeper spheres (4) are not well focused as the transmit focus is located at 8 mm in both images, however, they are visible in the MS250 image due the 15 mm elevation focus of this transducer. It is also apparent that the shallower elevation focus of the MS250SC leads to poorer imaging penetration depth as signal level starts to fall off below 12 mm.

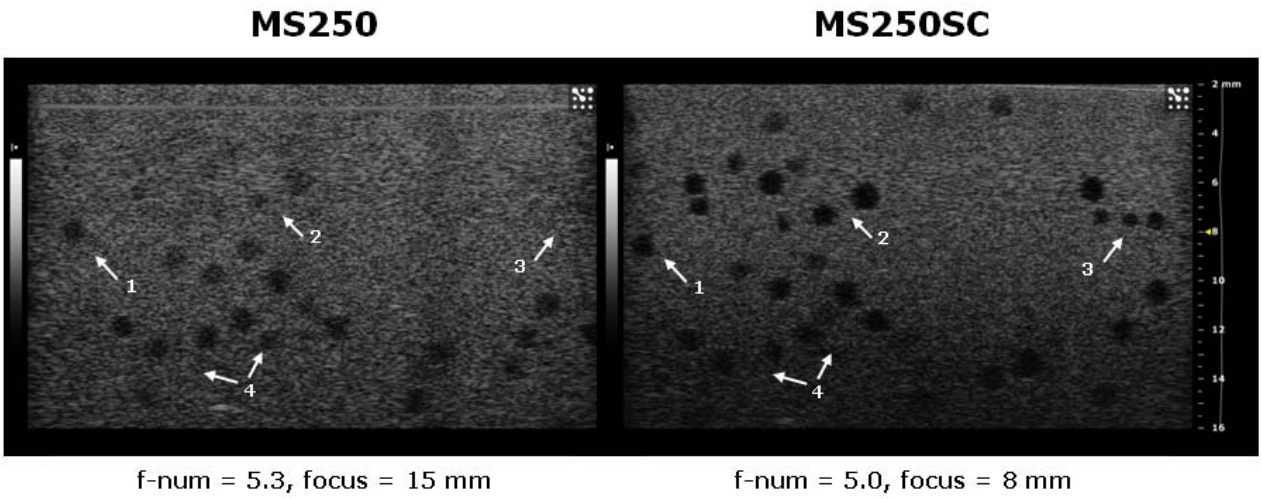


**Figure 1 – Cyst phantom comparison.**

As expected, the measured lateral and axial resolutions were identical (164 µm lateral, 75 µm axial). This can be observed in the image of the wire phantom shown in Fig. 2.

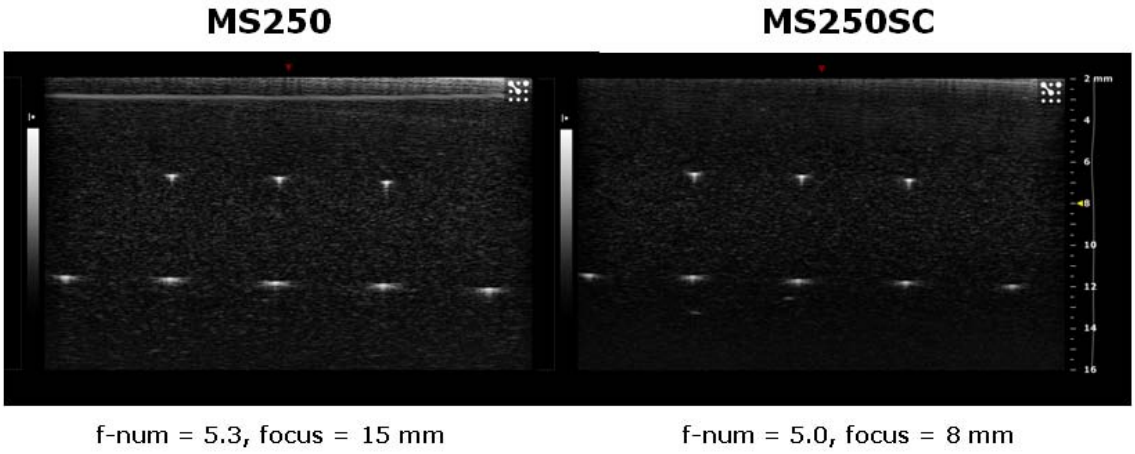


**Figure 2 – Wire phantom comparison.**

Results from the *in vivo* comparison are shown in Fig. 3. The differences between the two transducers are subtle, but nonetheless difference can be observed, particularly in the B-Mode images. The MS250SC image has better detail around the border of the kidney (1), which is likely a result of less out of plane clutter in the near field. In terms of the nonlinear contrast image, the larger slice thickness of the MS250 leads to more bubbles contributing to the contrast image and a larger signal. For example, in the tissue surrounding the kidney (2) the signal appears very bright and cannot be separated from the organ itself. Compared to the MS250SC, which has a smaller slice thickness, there is better delineation between the highly vascularized kidney and the surrounding tissue. In terms of the peak intensity of contrast detection in the kidney, both transducers had a CTR in the range of 12-13 dB.

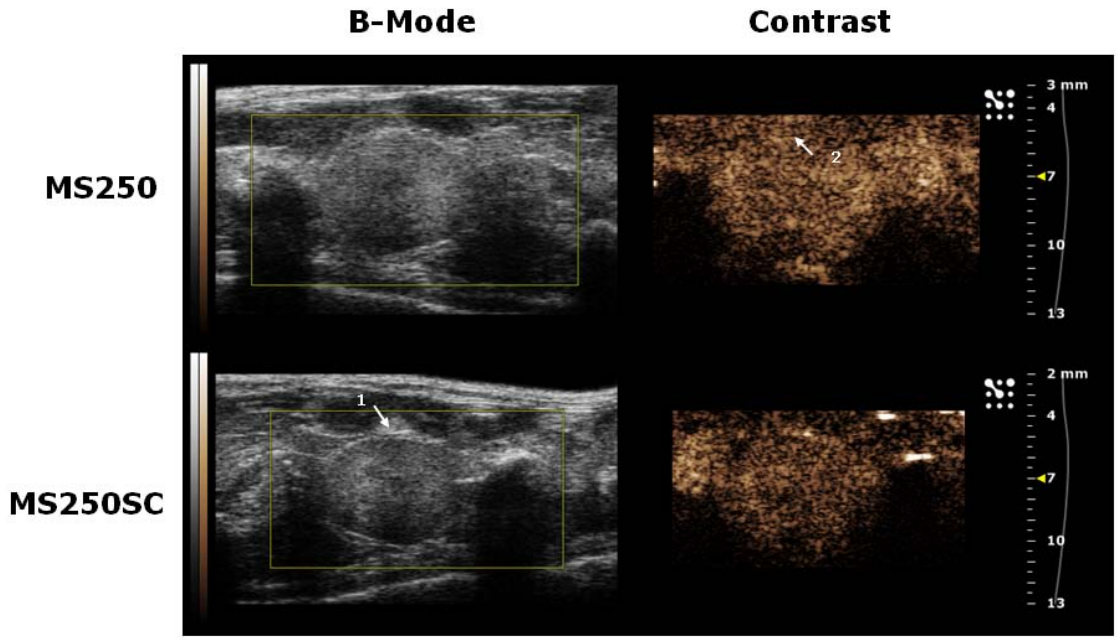


**Figure 3 – In vivo transducer comparison (kidney).**

***Increasing the Frequency of Nonlinear Microbubble Detection***

When comparing the performance of 30 MHz contrast imaging to 21 MHz in the kidney it was clear that the effects of attenuation coupled with increased tissue signal and lower sensitivity to the microbubbles, caused very little enhancement in signal (2-3 dB). However, when moving to the hind limb tumour model, the improvements in resolution in both the B-Mode and Contrast images were noticeable, as expected from wire target measurements (not shown) and observed in Fig. 4. Despite the improvements in resolution, however, the CTR was 4 dB lower in the 30 MHz image (MS400) compared to the 21 MHz image (MS250SC). It should also be noted that the 21 MHz image in Fig. 4 was generated with the lower contrast agent dose ($1.2 \cdot 10^7$ bubbles per bolus) and the image at 30 MHz was generated with the higher contrast agent dose ($2.4 \cdot 10^7$ bubbles per bolus).

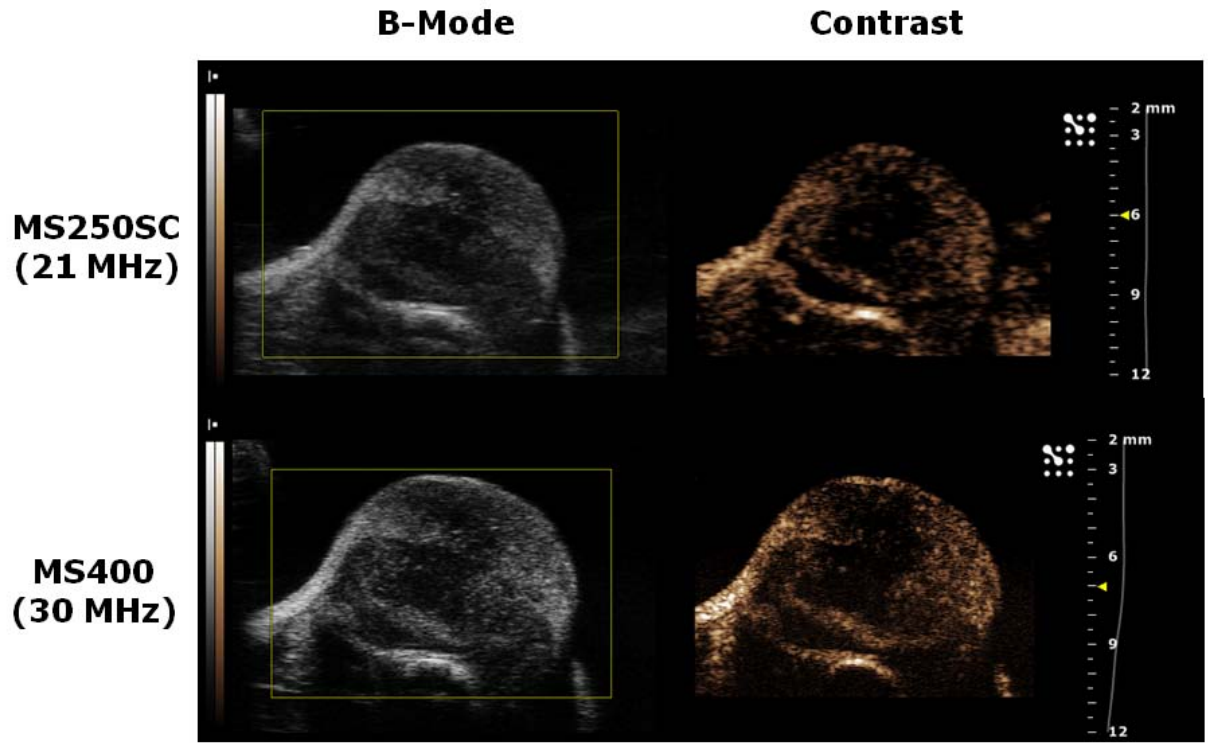


**Figure 4 - In vivo transducer comparison (tumour).**

***Photoacoustic Contrast Imaging***

Results from the microbubbles loaded with GNP in the agar flow phantom are shown in Fig. 5. This figure demonstrated the ability of the micro-ultrasound system to image a dual contrast agent. Nonlinear ultrasound detection is capable of detecting the microbubbles, while PA imaging can also detect the GNP bound to the bubble shell. The PA image of the tube shows the characteristic response of the PA signal in this frequency range for a 1 mm diameter absorber. For example, the primary frequency component, generated by the PA effect, of a 1 mm tube filled with GNP will be around 1 MHz. Since the data in Fig. 5 was collected with a 21 MHz transducer (70% BW), only the high frequency components at the edges of the channel are detected. For the *in vivo* data, excision of the lymph nodes showed that the MB had migrated to the axillary lymph node. Images of this node confirmed this and are shown in Fig. 6. Since the MB is highly absorbent to light near 680 nm, the PA signal was much stronger than at 760 nm. By subtracting the 760 nm image from the 680 nm image a contrast enhanced PA image was obtained, and yielded a contrast enhancement improvement of 8 dB.

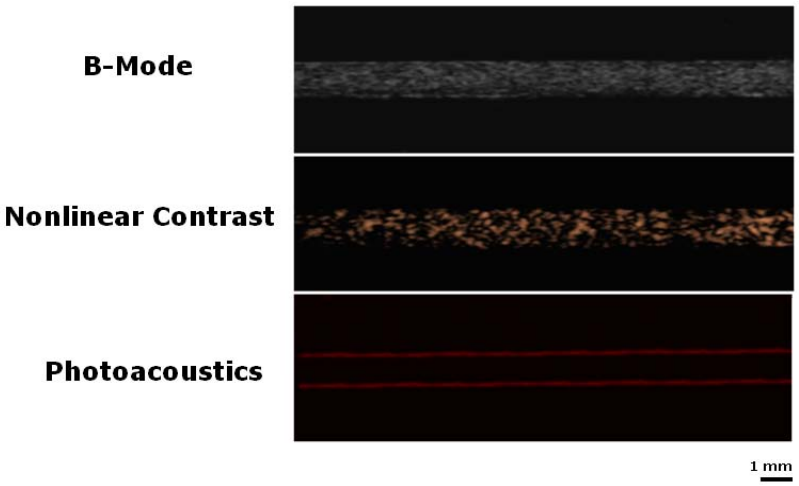


**Figure 5 – Vessel phantom containing microbubbles loaded with gold nanoparticles.**

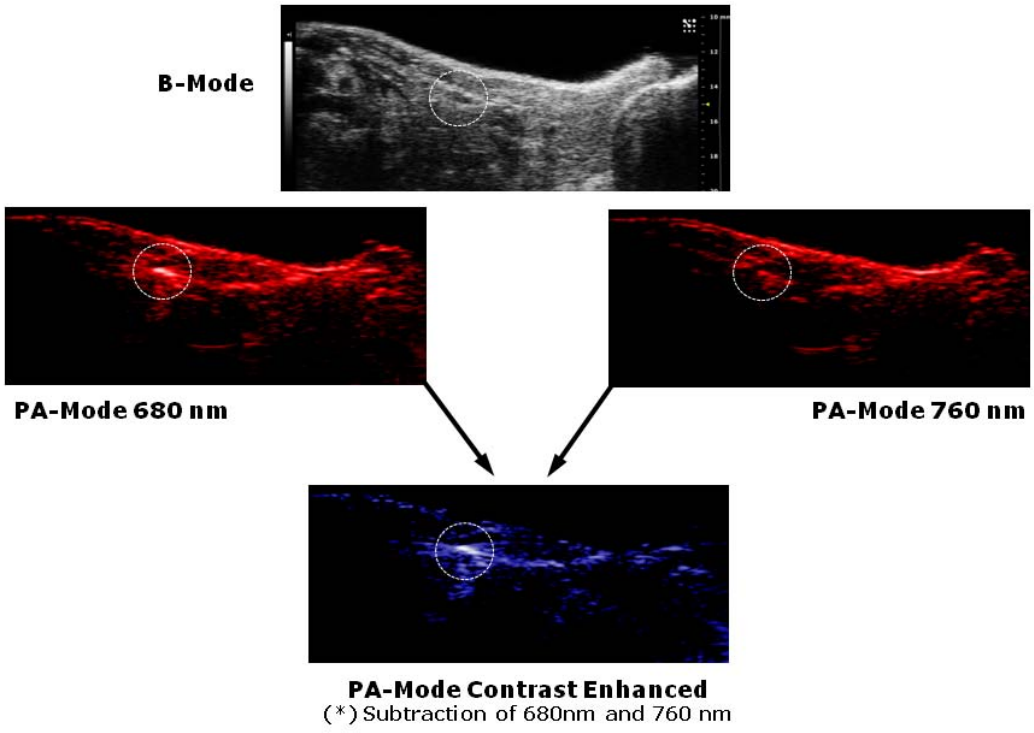


**Figure 6 – Photoacoustic Imaging of methylene blue contrast agent the axillary lymph node in a mouse. The contrast enhanced image is a subtraction of the single wavelength images at 680 nm and 760 nm.**

Images of the tumours injected with GNP are shown pre and post-inection in Fig. 7. The B-Mode images illustrates how GNP are undetectable under ultrasound alone, but are visible using PA imaging. Two things are notable about this image: that a new method of contrast detection can be utilized with a micro-ultrasound system, and the fact that this image was obtained using a 40 MHz transducer, a higher frequency than currently used for nonlinear microbubble detection. It remains to be determined if the nanoparticles in this image are confined to the vascular space, or if they have migrated into the surrounding tissue. Due to the size of the nanoparticles, it is reasonable to hypothesize that the latter is

true, thus providing the ability of micro-ultrasound systems to image beyond the vasculature with contrast agent.

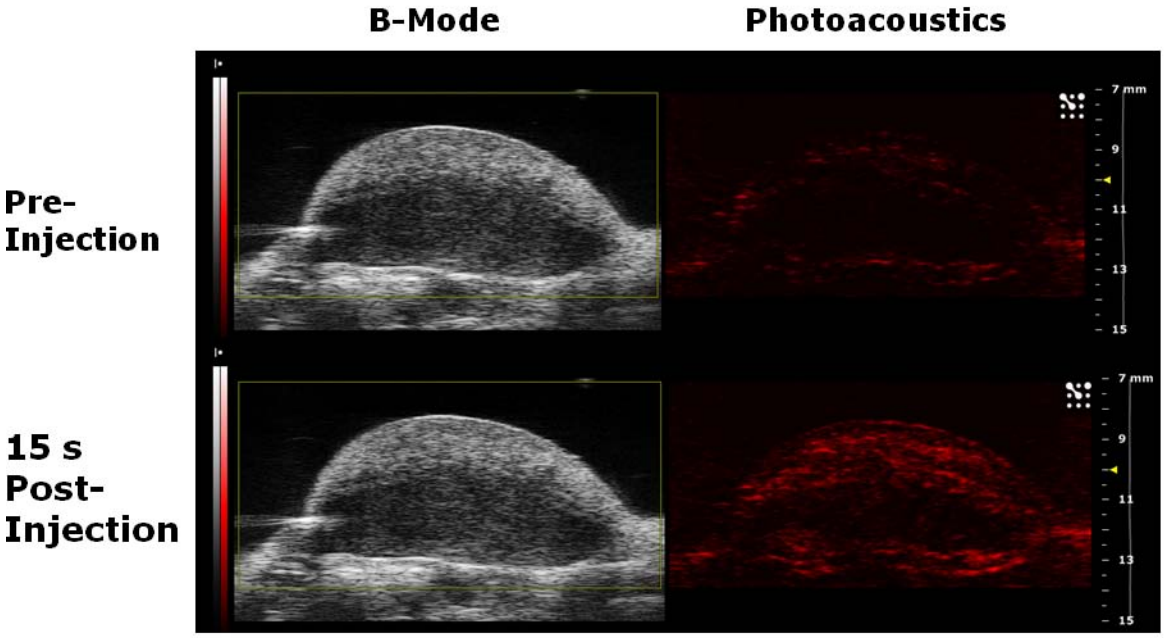


**Figure 7 - Photoacoustic Imaging of gold nanoparticles in a mouse tumour at 40 MHz with 800 nm light.**

**Discussion and Conclusions**

This study has provided an overview of new developments in contrast imaging with micro-ultrasound. Changes to an existing transducer improved the resolution and out of plane clutter rejection for mouse abdominal imaging, and were demonstrated both *in vitro* and *in vivo*. It was also demonstrated qualitatively that an increase in imaging frequency to 30 MHz helped to improve the image resolution for nonlinear microbubble imaging, but should be limited to superficial structures. The improved resolution came with a trade-off in increased tissue signal (~2-3 dB) and lower overall sensitivity to the microbubbles. In the case of the tumour images at 30 MHz, a doubled dose of microbubbles needed to be administered to see equivalent results as at 21 MHz, and even then the CTR was still 4 dB lower. Different techniques than amplitude modulation, such as radial modulation (Måsøy et al. 2008) or self-demodulation (Vos et al. 2010), will likely be required to push nonlinear microbubble imaging beyond 30 MHz. In terms of increasing frequency, however, PA imaging presents a new method of detecting contrast *in vivo* at higher imaging frequencies, as demonstrated by 40 MHz images of GNP in a mouse tumour. Binding GNP to microbubbles creates a dual contrast agent that can be imaged with nonlinear ultrasound, and PA-Mode. Finally, PA imaging can also improve sensitivity to contrast agents such as MB that are undetectable with ultrasound alone. This has the potential to open up new areas of contrast imaging previously unheard of with micro-ultrasound.

**References**


1. Måsøy SE, Standal O, Näsholm P, Johansen TF, Angelsen B, Hansen R. SURF Imaging: In vivo demonstration of an ultrasound contrast agent detection technique. IEEE Trans Ultrason Ferroelec Freq Contr 2008;55:1112-1121.
2. Needles A, Mehi J, Arditi M, et al. Nonlinear contrast imaging with an array-based micro-ultrasound system. Ultrasound Med Biol 2010a;36:2097-2106.
3. Needles A, Heinmiller A, Ephrat P et al. Development of a combined photoacoustic micro-ultrasound system for estimating blood oxygenation. Proc IEEE Ultrason. Symp, San Diego, 2010b (in press).
4. Seo M, Gorelikov I, Williams R, Matsuura N. Microfluidic assembly of monodisperse, nanoparticle-incorporated perfluorocarbon microbubbles for medical imaging and therapy. Langmuir 2010;26;13855-13860.
5. Vos HJ, Goertz DE, de Jong N. Self-demodulation of high-frequency ultrasound. J Acoust Soc Amer 2010;127:1208.

# Chirp reversal power modulation contrast imaging

***Anthony Novell and Ayache Bouakaz***

*UMR Inserm U 930, CNRS ERL 3106, Université François Rabelais de Tours, 37044 Tours, France*

**Aim**

It is known that chirp excitations increase significantly the signal to noise ratio (SNR). Besides, we have shown earlier that chirp reversal improves the contrast detection through an increased contrast to tissue ratio (CTR) [1]. Chirp reversal consists in transmitting a first excitation signal being an up-sweep chirp (UPF) of increasing frequencies with time and a second excitation signal, the down-sweep (DNF), being a replica of the first signal, but time reversed with a sweep of decreasing frequencies with time. The aim of our study is to evaluate the combination of chirp reversal with power modulation (CRPM) for contrast agent imaging. In comparison to standard pulse inversion or power modulation, CRPM turned to provide a significant increase in both CTR and SNR.

**Material and Methods**

Experiments were performed using a 128 elements PZT linear array probe centered at 4 MHz. The probe was connected to a fully programmable open scanner equipped with analog transmitters (M2M, France). Chirp reversal and other traditional contrast agent imaging schemes (pulse inversion, power modulation) and combinations of them were implemented into the open scanner. Chirps with linear frequency modulation were transmitted. The chirps were centered at 2.5 MHz with 55% bandwidth. The chirp length was set to 8 µs giving thus the same frequency bandwidth as the equivalent transmitted pulse (traditional 2 cycles Gaussian pulse (<2 µs)). A flow phantom was used in which SonoVue® microbubbles (Bracco Research, Switzerland) at a dilution of 1/2000 was introduced. RF data were recorded and then filtered using a matched filter in order to compress the scattered signals and recover the axial resolution. The compression filter was designed in order to recover both the fundamental and the harmonic components. The transmitted peak negative acoustic pressure was 350 kPa corresponding to a non derated mechanical index of 0.22. Traditional multi-excitations schemes such as pulse inversion (PI), power modulation (PM) and their combination PIPM were implemented using chirps with and without chirp reversal approach. The CTR and SNR were quantified for each transmitted sequence.

## Results

Chirp reversal (CR) provided an increase of approximately 3 dB in both SNR and CTR in comparison to PIPM. The combination of chirp reversal with PI (CRPI) did not improve the contrast detection in comparison to CR alone. However the combination of CR and PM increased significantly both the CTR and the SNR. The CTR using CRPM was 25.3 dB while PM alone and CR alone provided a CTR of 20.7 dB and 21.8 dB respectively. In table 1 are given the CTR and SNR for the different detection strategies. Figure 1 displays an example of contrast images obtained after compression for PI and CRPM approaches.

**TABLE I**
**SNR and CTR for different detection strategies**

| | PI | PM | PIPM | CR | CRPI | CRPM | CRPIPM |
|---|---|---|---|---|---|---|---|
| SNR (dB) | 38.7 | 40.8 | 40.0 | 43.0 | 43.4 | 45.8 | 43.2 |
| CTR (dB) | 17.2 | 20.7 | 19.1 | 21.8 | 20.9 | 25.3 | 21.5 |

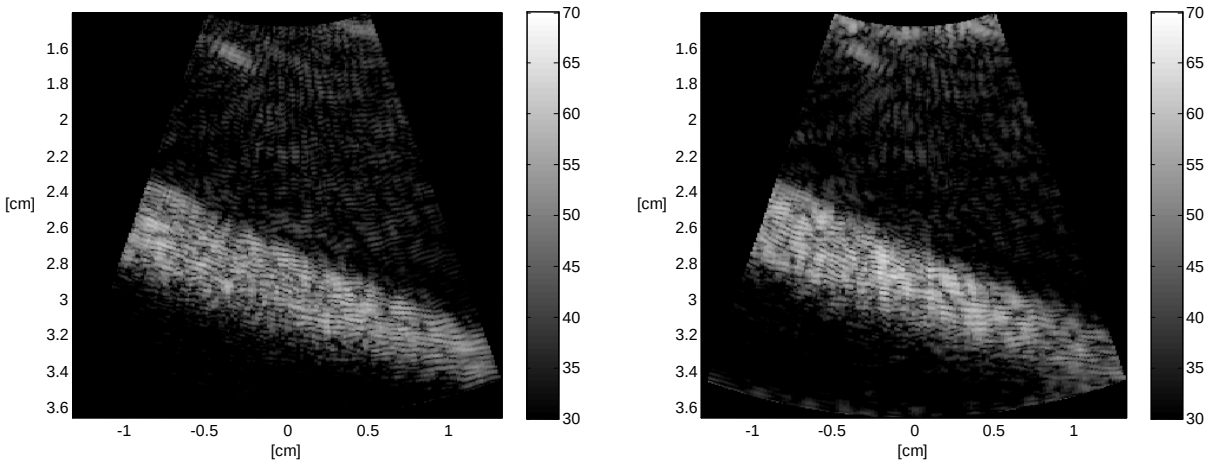


PI CRPM

**Figure 1. PI and CRPM contrast images after compression at an applied MI = 0.22**

## Conclusion

These results demonstrate the ability to increase both the CTR and the SNR when chirp reversal imaging is performed in combination with power modulation technique.

**Reference**

A. Novell, S.M. van der Meer, M. Versluis, N. de Jong and A. Bouakaz "Contrast agent response to chirp reversal: simulations, optical observations and acoustical verification," IEEE Trans Ultrason Ferroelectr Freq Control, 2009 Jun, 56(6), pp 1199-206.

# Subharmonic Imaging for *vasa vasorum*

***Telli Faez[a], Marcia Emmer[b], Michel Versluis[c], Nico de Jong [a,b,c]***

*[a] Biomedical Engineering Thoraxcenter, Erasmus Medical Center, Rotterdam, The Netherlands*
*[b] Interuniversity Cardiology Institute of The Netherlands, Utrecht, The Netherlands*
*[c] Physics of Fluids Group, Department of Science and Technology, University of Twente, The Netherlands*

Atherosclerosis, a chronic, inflammatory disease involving the development of atherosclerotic lesions in the major arteries of the vasculature, is the uppermost underlying cause of cardiovascular disease[1] and a major cause of stroke[2]. Cardiac events and stroke are often caused by atherosclerotic plaque rupture. It has been shown that *vasa vasorum* plays an important role in atherosclerotic plaque pathogenesis and stability.[3,4]

Ultrasound is an established tool to measure carotid atherosclerosis for the diagnosis and monitoring of patients at risk of stroke.[5,6] The carotid artery is a relatively superficial artery that is easily accessible for ultrasound imaging. Recent advances in contrast-enhanced ultrasound have shown that this technique can characterize the carotid *vasa vasorum* and intra-plaque angiogenesis and thus it is potentially a new diagnostic tool to detect plaque vulnerability.[7,8,9,10,11,12,13]

The contrast to tissue ratio (CTR) can be further improved by exploiting the nonlinear properties of the contrast bubbles e.g. in harmonic imaging: pulse inversion[14] and power modulation[15]. However for the transmit pressures used in these methods the CTR is lowered as a result of nonlinear propagation of the ultrasound wave through the tissue, which causes that the tissue scatter signal also contains second harmonic energy which contaminates the bubble echo signal.

Propagating ultrasound wave does not contain energy at the subharmonic frequency, which revives a strong interest in subharmonic emissions (backscattered energy at half the transmit frequency) from contrast agents.[16,17] Subharmonic imaging has potentially a larger CTR compared to other imaging methods[18]. In recent studies[19] subharmonic imaging (SHI) has been used for the diagnosis of breast cancer at the transmitting frequency of 4.4 MHz. SHI appears to improve the diagnosis of breast cancer relative to conventional ultra-sonography and mammography.

In this study, the subharmonic scattering of phospholipid-coated contrast agents (BR14, Bracco Research S.A., Geneva, Switzerland) in the frequency range preferred for carotid imaging (5-15 MHz) has been investigated optically and acoustically *in vitro*.

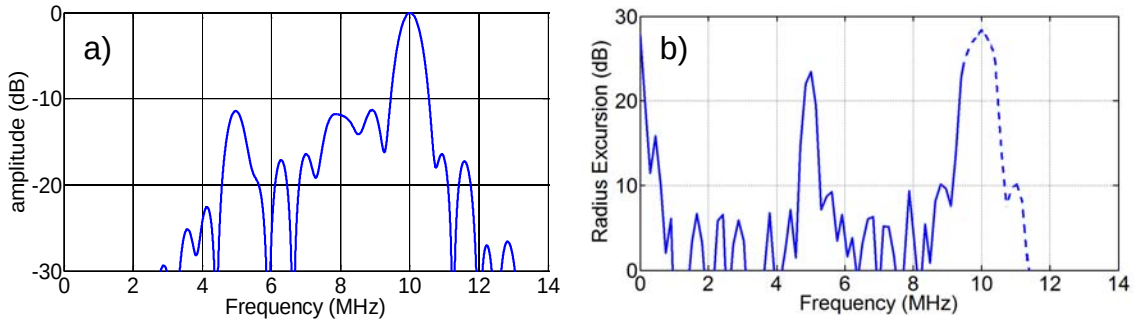


**FIG. 1- The amplitude of the subharmonic response of a BR14 contrast agent microbubble measured at driving frequency of 10 MHz a) acoustically and b) optically.**

The results of the measurements indicated that:

- The subharmonic scattering of the phospholipid-coated contrast agent microbubbles is sufficiently detectable in the frequency range around 10 MHz at low acoustic pressures.
- However, not all the microbubbles respond nonlinearly.
- The frequency in which the subharmonic response is maximum increases with increasing the amplitude of acoustic pressure; in contrary to what has been observed for the fundamental response.
- The subharmonic scattering signal can be enhanced up to 20 dB by increasing the ambient pressure in a quasi-static manner up to 30 kPa.

In conclusion, we have shown from single bubble measurements that the subharmonic imaging has a great potential to be exploited in the frequency range mostly suited for carotid imaging. However this study has to be complemented with forthcoming in vivo studies.

**References**


1. Yach D, Hawkes C, Gould CL, Hofman KJ. The global burden of chronic diseases - Overcoming impediments to prevention and control. JAMA 2004;291:2616-2622.
2. Golledge J, Greenhalgh RM, Davies AH. The Symptomatic Carotid Plaque. Stroke 2000; 31:774-781.
3. Barger AC, Beeuwkes R, Lainey LL, Silverman KJ. Hypothesis: vasa vasorum and neovascularization of human coronary arteries. N Engl J Med 1984;310:175-177.
4. Zamir M, Silver MD. Vasculature in the Walls of Human Coronary Arteries. Arch Pathol Lab Med 1985;109:659-662.
5. Eliasziw M, Rankin RN, Fox AJ, Haynes RB, Barnett HJM. Accuracy and Prognostic Consequences of Ultrasonography in Identifying Severe Carotid Artery Stenosis. Stroke 1995;26:1747-1752.
6. Baldassarre D, Amato M, Bondioli A, Sirtori CR, Tremoli E. Carotid Artery Intima-Media Thickness Measured by Ultrasonography in Normal Clinical Practice Correlates Well With Atherosclerosis Risk Factors. Stroke 2000;31:2426-2430.
7. Feinstein SB. Atherosclerotic Plaque Neovascularization Contrast Ultrasound Imaging of the Carotid Artery Vasa Vasorum and Atherosclerotic Plaque Neovascularization. J. Am. Coll. Cardiol. 2006;48:236-243.
8. Shah F, Balan P, Weinberg M, Reddy V, Neems R, Feinstein M, Dainauskas J, Meyer P, Goldin M, Feinstein SB. Contrast-enhanced ultrasound imaging of atherosclerotic carotid plaque neovascularization: a new surrogate marker of atherosclerosis? Vasc. Med. 2007;12:291-297.
9. Vicenzini E, Giannoni MF, Puccinelli F, Ricciardi MC, Altieri M, Di Piero V, Gossetti B, Benedetti Valentini F, Lenzi GL. Detection of Carotid Adventitial Vasa Vasorum and Plaque Vascularization With

Ultrasound Cadence Contrast Pulse Sequencing Technique and Echo-Contrast Agent. Stroke 2007;38:2841-2843.
10. Coli S, Magnoni M, Sangiorgi G, Marrocco-Trischitta MM, Melisurgo G, Mauriello A, Spagnoli L, Chiesa R, Cianflone D, Maseri A. Contrast-Enhanced Ultrasound Imaging of Intraplaque Neovascularization in Carotid Arteries: Correlation With Histology and Plaque Echogenicity. J Am Coll Cardiol 2008;52:223-230.
11. Staub D, Patel MB, Tibrewala A, Ludden D, Johnson M, Espinosa P, Coll B, Jaeger KA, Feinstein SB. Vasa Vasorum and Plaque Neovascularization on Contrast-Enhanced Carotid Ultrasound Imaging Correlates With Cardiovascular Disease and Past Cardiovascular Events. Stroke 2009;41:41-47.
12. Xiong L, Deng YB, Zhu Y, Liu YN. Correlation of Carotid Plaque Neovascularization Detected by Using Contrast-enhanced US with Clinical Symptoms. Radiology 2009;251:583-589.
13. Shalhoub J, Owen DRJ, Gauthier T, Monaco C, Leen ELS, Davies AH. The use of Contrast Enhanced Ultrasound in Carotid Arterial Disease. Eur J Vasc Endovasc Surg 2010;39:381-387.
14. Burns PN, Wilson SR, Simpson DH. Pulse inversion imaging of liver blood flow: improved method for characterizing focal masses with microbubble contrast. Invest Radiol 2000;35:58-71.
15. Brock-Fisher GA, Poland MD, Rafter PG. 1996. Means for increasing sensitivity in non-linear ultrasound imaging systems. US Patent No. 5577505.
16. Chomas J, Dayton P, May D, Ferrara K. Nondestructive subharmonic imaging. IEEE Trans Ultrason Ferroelectr Freq Control 2002;49:883-892.
17. Shi WT, Forsberg F, Hall AL, Chiao RY, Liu JB, Miller S, Thomenius KE, Wheatley MA, Goldberg BB. Subharmonic imaging with microbubble contrast agents: initial results. Ultrason Imaging 1999;21:79-94.
18. Shankar PM, Krishna PD, Newhouse VL. Subharmonic backscattering from ultrasound contrast agents. J. Acoust. Soc. Am. 1999;106:2104-2110.
19. Forsberg F, Piccoli CW, Merton DA, Palazzo JJ, Hall AL. Breast lesions: Imaging with contrast-enhanced subharmonic US-Initial experience. Radiology 2007;244:718-726.

# Prostate cancer localization by contrast ultrasound dispersion imaging based on spatial coherence analysis

***M. P. J. Kuenen [1,2], M. Mischi[1], H. Wijkstra [1,2]***

*[1] Eindhoven University of Technology, Department of Electrical Engineering, The Netherlands*
*[2] Academic Medical Center, Department of Urology, Amsterdam, The Netherlands*

**Introduction**

In 2010, prostate cancer accounts for 28% and 11% of all cancer diagnoses and deaths in the USA in 2010, respectively [1]. New focal therapies could significantly improve prostate cancer treatment, but they cannot be used efficiently due to a lack of imaging methods. In fact, the most reliable prostate cancer localization method is currently provided by systematic biopsies, which are invasive and can only provide a poor spatial accuracy.

The potential of contrast-enhanced ultrasound imaging for prostate cancer localization has been gaining interest in the past few years. In particular, techniques for quantitative measurement of microvascular blood perfusion have been proposed [2], based on the known correlation between cancer aggressiveness and angiogenesis [3]. However, no method has yet produced reliable results.

We recently proposed contrast-ultrasound dispersion imaging (CUDI) as a new alternative method [4]. Whereas angiogenesis-induced changes in the microvascular architecture can cause various opposing effects on perfusion [5], they have a direct influence on the intravascular dispersion of ultrasound contrast agents.

CUDI is based on contrast-specific ultrasound imaging of the passage of an intravenously injected contrast-agent bolus through the prostate circulation. Dispersion is then estimated from indicator dilution curves (IDCs) that are measured at each B-mode video pixel.

In a previous study, the contrast-agent transport was modeled by the convective dispersion equation, enabling the extraction of a local, dispersion-related parameter from each IDC. This study showed better results for CUDI than for perfusion quantification methods [4].

We now present a method for an indirect estimation of dispersion. Rather than focusing on each IDC individually, this method exploits the spatial dispersion dynamics by considering the similarity among spatially adjacent IDCs as an indirect measure for dispersion. The adopted coherence-based similarity analysis is compared with our previous method, as well as with quantitative perfusion estimation methods.

**Materials and methods**

Data acquisition was performed at the Academic Medical Center (AMC) in Amsterdam. A 2.4 mL SonoVue® (Bracco, Milan, Italy) bolus was injected intravenously. Transrectal ultrasound power modulation imaging (frequency 3.5 MHz, mechanical index 0.06) was performed using an iU22 scanner (Philips Healthcare, Bothell, USA) equipped with a C8-4v transducer. An IDC was measured at every pixel of the resulting B-mode video and linearized by compensating for the logarithmic compression.

The spatial coherence is the adopted IDC similarity measure for dispersion estimation. It is computed as the correlation coefficient between IDC magnitude spectra. IDC arrival time differences, which are rather a measure of perfusion, are incorporated in the IDC phase

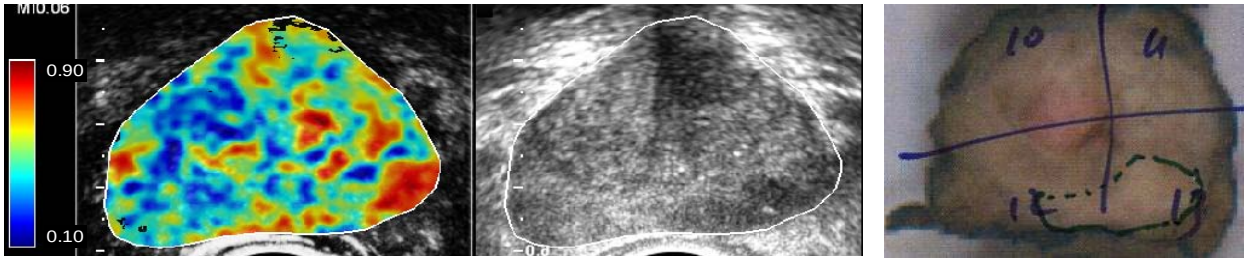


**Figure 4 CUDI coherence image (left) in which the coherence level is shown by color coding. The fundamental B-mode ultrasound image is shown in the middle, whereas the image on the right shows the correspondinghistology.**

As a result, coherence is not sensitive to IDC arrival time differences. The analysis is restricted to frequencies up to 0.5 Hz, which govern the contrast-agent transport dynamics. The DC component is also discarded, as it is determined by scanner settings.

The coherence analysis compares each pixel IDC to neighboring IDCs. A ring-shaped spatial kernel determines which pixels are used for this comparison. Because the axial scanner resolution is 0.43 mm, pixels within a distance of 0.5 mm are discarded. Pixels at distances up to 1.0 mm are included to enable detection of the smallest cancers (1.0 $mm^3$) in which angiogenesis occurs.

A preliminary validation was conducted based on four patients. Regions of interest representing cancer and normal tissue were selected based on histology data, obtained at the AMC. The sensitivity and specificity for correct pixel classification were then computed.

**Results**

On a pixel basis, there was a good agreement between the coherence images and the histology assessment. The sensitivity and specificity were 80% and 86%, respectively. The ROC curve area (0.91) was slightly higher than that of our previous CUDI method [4]. Both CUDI methods showed superior results to those obtained by testing all the other IDC parameters reported in the literature [6, 7].

## Conclusions

Coherence-based CUDI shows promising results for prostate cancer localization. Compared with other quantitative methods, this method requires no model interpolation. Alternative similarity measures, as well as a more advanced preprocessing and kernel design may provide additional improvements in the future.

**References**


1. American Cancer Society, Cancer Facts & Figures, Atlanta, 2010.
2. Pallwein, L. et al., Ultrasound of prostate cancer: recent advances, Eur. Radiol., 18, 707-715, 2008.
3. Brawer, M. K., Quantitative microvessel density. A staging and prognostic marker for human carcinoma, Cancer, 78(2), pp. 345-349, 1996.
4. Mischi, M., et al., Prostate cancer localization by contrast-ultrasound diffusion imaging, 2009 IEEE Ultrasonics Symp. Proc., pp. 283-286.
5. Delorme, S. and M. V. Knopp, Non-invasive vascular imaging: assessing tumour vascularity, Eur. Radiol., 8, 517-527, 1998.
6. Elie, N. et al., Methodology for quantifying interactions between perfusion evaluated by DCE-US and hypoxia throughout tumor growth, Ultrasound in Med. & Biol., 33(4), 549-560, 2007.
7. Strouthos, C. et al., Indicator dilution models for the quantification of microvascular blood flow with bolus administration of ultrasound contrast agents, IEEE Trans. UFFC, 57(6), pp. 1296-1310, 2010.

# Do we need new technology for Molecular Imaging?

***Alexander Klibanov [1,2], John Hossack[2], Michael Lawrence[2], Joshua Rychak[3], Klaus Ley[4]***

*[1]Cardiovascular Division, Department of Medicine, University of Virginia*
*[2]Department of Biomedical Engineering, University of Virginia*
*[3]Targeson Inc., [4]La Jolla Institute of Allergy and Immunology*

Molecular imaging is defined as visualization, characterization, and measurement of biological processes at the molecular and cellular levels in humans and other living systems. In order to perform molecular imaging with ultrasound a combination of two entities, the **CONTRAST AGENT** and the **IMAGING SYSTEM** for its detection are essential:

**Ultrasound contrast agents**, capable of selective and firm binding to the disease markers (molecules and cells), via specific molecular interactions.

**Ultrasound imaging techniques** for sensitive and quantitative detection of the ultrasound contrast in the region of interest. Detection should be achieved with a signal to noise ratio sufficient for distinguishing normal tissue from the tissue that overexpresses the target receptor, to obtain useful diagnostic information, or aid in image guided therapy or biopsy.

The inventory of technologies that are currently available includes:

1. Microbubble contrast agents, decorated with targeted ligands, are widely described in the literature and used in preclinical imaging studies (mainly in mouse models). Human application is yet to become widespread. The use of non-targeted microbubbles as blood pool markers is already common and will become generic soon.
2. Targeting ligands are now routinely attached to the microbubble shell covalently, thus avoiding the use of biotin-streptavidin linker between the ligand and the bubble, which cannot be used in humans. Bubbles can be now made quite stable on storage, and could be administered *in vivo* straight out of the vial without complicated purification steps.
3. Microbubble detection schemes (harmonic, subharmonic imaging, phase inversion, power modulation, plus combination of those methods, eg PIAM and CPS) allow suppression of tissue signal and monitoring of the behavior of individual microbubbles, with picogram mass and micrometer-scale particle size range. Manufacturing of uniform-size bubbles, now at an experimental small-scale level, may aid in bubble-specific detection imaging modalities.
4. Expanding the variety of targeting ligands beyond the use of murine monoclonal antibodies, towards the use of smaller proteins (e.g., scVEGF), peptides/peptide mimetics, and

carbohydrates improves the ease of targeted microbubble manufacturing and handling. Many of these ligands will work both in animal models and in humans.

5. Ability to improve targeting efficacy, i.e., minimize the contrast agent dose, is crucial. This can be achieved by using proper ligands and ligand combinations, understanding biomechanics of targeting events, and acoustic radiation force application as a tool to increase the probability of circulating bubbles to reach the vessel wall that carries the target.

In principle, all of these technologies are available; many of them are not exactly novel. In reality, pockets of individual technologies exist in some settings, with some equipment and imaging probes, but not all and not always.

Overall, microbubble contrast technology seems to move from discovery research to product development stage; patent expiration may be an important tool to accelerate the progress of the field.

Further progress will be achieved with other, truly novel types of agents and imaging techniques: phase-shift or liquid fluorocarbon nanoparticles, or even smaller solid nanoparticles that could easily extravasate to the interstitial space. Photoacoustic imaging, where laser light absorption by contrast nanoparticles is used to excite the acoustic response, will provide an additional boost of detection sensitivity for molecular and cellular imaging of the extravascular targets; imaging of single target cells is expected.

# A functionalized ultrasound contrast agent against the GPIIb/IIIa receptor detects activated platelets

***F. Guenther[1], A. L. Klibanov[2], M. Kramer[1], M. Schwarz[1], E. Ferrante[2], K. Peter[3], C. Bode[1], C. von zur Muhlen[1]***

*[1]University Hospital of Freiburg, Department of Cardiology*
*[2]University of Virginia, Charlottesville, Virginia, USA*
*[3]Baker Heart Research Institute, Melbourne, Australia*

**Introduction**

Membrane proteins of activated platelets are of special interest regarding molecular imaging of atherosclerosis, since platelets are not only involved in final events leading to thrombotic vessel occlusion, but also in earlier stages of atherosclerosis. The aim of our study was ultrasound molecular imaging of the activated platelet GP IIb/IIIa receptor. For this purpose, ultrasound microbubbles (MB) were linked to an antibody that binds specifically to ligand-induced binding sites (LIBS) of activated platelets.

**Methods**

The monoclonal antibody anti-LIBS was coupled to biotinylated microbubbles (lipid shell, gaseous decafluorbutane core, diameter 2-3 µm) using a biotin-streptavidin system (LIBS-MB). As negative control, a non-specific, biotinylated control antibody was attached to the MB (= control-MB). Platelets were isolated from citrate blood of healthy volunteers, activated by ADP and incubated on fibrinogen-coated culture dishes. Microbubble adhesion was assessed by using an inverted parallel plate flow chamber. A withdrawal syringe pump created a shear flow of 5, 3 and 1 dyne/cm², respectively. Adherent and passing microbubbles were counted at each shear flow calculate capture efficiency (1 minute, field of view 400 x 300 µm). As negative control substrate, fibrinogen-coated dishes without platetes were used.

**Results**

The capture efficiency of LIBS-MB (n=14) was 9.1% at a shear rate of 1 dyne/ cm² (SEM±1.59), 0.9% at 3 dyne/ cm² (SEM±0.15) and 0.5% at 5 dyne/ cm² (SEM±0.09). When using control microbubbles (n=9), capture efficiency was significantly lower ($p<0.05$): 1.3% at 1 dyne/ cm² (SEM±0.34), 0.07% at 3 dyne /cm² (SEM±0.07) and 0.04% ± at 5 dyne /cm² (SEM±0.03). The adhesion of targeted MB on fibrinogen-coated dishes without platelets was significantly lower than on platelets ($p<0.05$).

**Summary**

Molecular ultrasound imaging using LIBS-MB seems to be a promising and efficient strategy for detection of activated platelets, which play a pivotal role in endothelial inflammation and plaque rupture. Thus, non-invasive imaging of activated platelets on the surface of ruptured or inflamed atherosclerotic plaques can be feasible, which is of great clinical interest regarding non-invasive evaluation of arteriosclerosis.

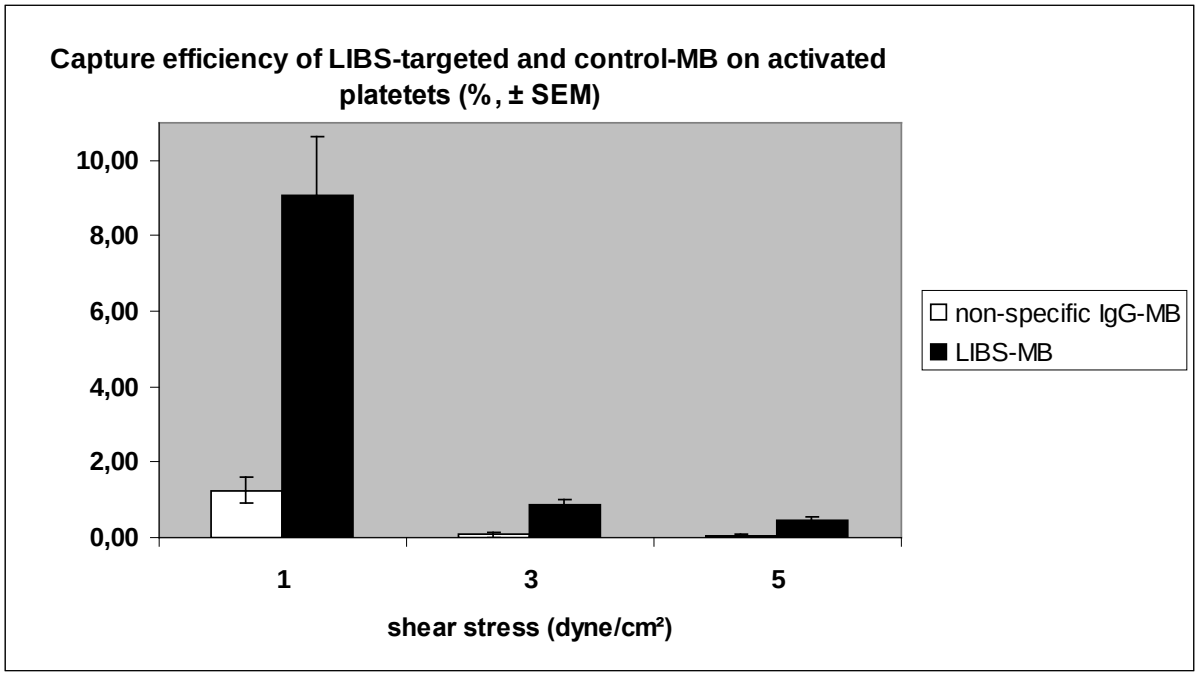

# Molecular ultrasound imaging of P-Selectin for monitoring the effects of anti inflammatory therapy.

***Bettinger T., Tardy I., Bussat P., Emmel P., Pagnod-Rossiaux S., Schneider M., Tranquart F.***

*Bracco Suisse SA, Geneva, Switzerland*

**Introduction**

New strategies have recently emerged for the treatment of inflammatory diseases, such as rheumatoid arthritis. They rely on the use of TNFα antagonists, and despite accepted effectiveness, up to 40% of the patients fail to respond to the treatment. Thus, diagnostic tools are needed to predict responsiveness and to improve patient care. Molecular ultrasound imaging using targeted microbubbles allows to monitor non-invasively the expression of vascular biomarkers in real time. Pre-treatment with TNFα antagonists has been shown to reduce the expression of various vascular markers in mice, such as P-selectin, ICAM-1 and VCAM-1 (Esposito et al., 2007). The objective of the present study was to assess the potential of targeted ultrasound contrast agents (TUCA) to monitor the expression of P-selectin (CD62P) following injection of the TNFα antagonist etanercept.

**Materials and Methods**

P-selectin specific microbubbles (P-MB) were prepared with streptavidin-bearing microbubbles (Target-Ready Contrast Agent, Visualsonics, Toronto, Canada) functionalized with a biotinylated P-selectin antibody (LYP20 clone, Biocytex). Control bubbles (C-MB) were prepared with a biotinylated isotype control antibody.

In vivo binding was measured in a rat hind limb inflammation model induced by i.m. injection of lipopolysaccharide (LPS, 1.1 mg/kg, Sigma). Twenty four hours after the onset of inflammation, randomized boluses of targeted or control bubbles were administered in the jugular vein. Bubble accumulation was assessed 10 min after the iv injection in the inflamed and in the contralateral muscle using a Siemens Sequoia ultrasound scanner (CPS mode, 15L8 probe, 7 MHz, MI of 0.25). The echo signals were expressed as linearized echo power values ($rms^2$). The expression of inflammatory markers in inflamed muscles was further evaluated by immunohistochemistry using the same P-selectin specific antibody. Monitoring of anti-inflammatory treatment efficacy was performed by pre-treating animals twenty four hours before LPS administration, with a s.c. injection of etanercept (0.45 mg/kg, Wyeth) or of saline. Blood concentration of TNFα was monitored by ELISA during the course of the experiment.

**Results**

Immunohistochemistry showed P-Selectin expression in microvessels in LPS-treated muscles (*Figure* 1). No staining was observed in the contralateral muscle.

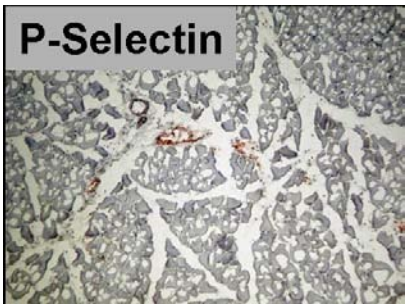


**Figure 1: Immunohistochemistry staining in inflamed rat hind limb 24 h after LPS injection showing P-selectin expression in microvessels.**

P-selectin-binding bubbles had increased signal in the LPS-inflamed hind limb vs control bubbles (echo signal: 20 ± 12 $rms^2$ vs 3.6 ± 0.8 $rms^2$, respectively).

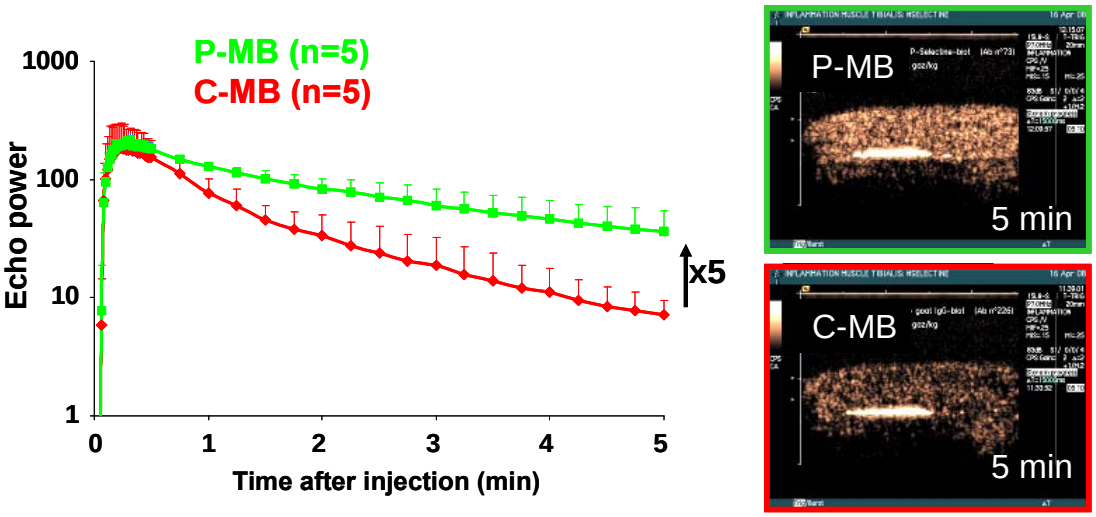


**Figure 2: Signal enhancement in the LPS-induced inflamed hind limb of rats after administration of microbubble preparations containing either anti P-selectin antibody (P-MB) or an isotype control antibody (C-MB) (±SD).**

Intramuscular injection of LPS triggered a rapid release of TNFα in blood as measured by ELISA (*Figure* 3). The concentration reached a maximum approx. 90 min after LPS injection.

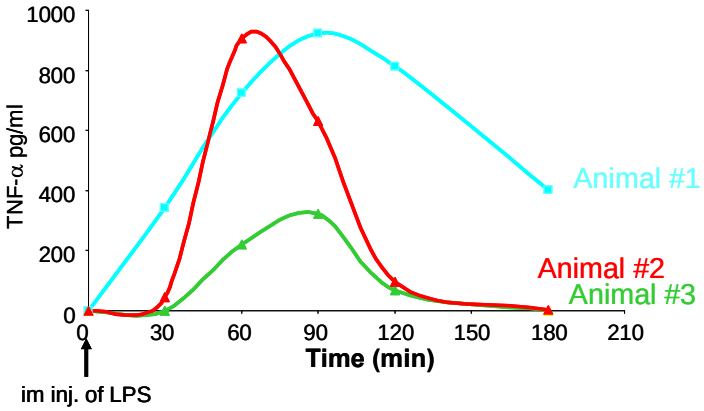


**Figure 3: ELISA titration of TNFα in the blood circulation following i.m. injection of LPS in the hind limb of rats.**

The known inhibition of inflammation achieved by administration of etanercept to prevent TNFα activity (Campbell et al., 2007), was visualized using P-MB. Animals pre-treated with etanercept, showed an almost 2-fold decrease in P-MB accumulation (13.7 ± 7.8 rms$^2$), in comparison to control animals receiving saline (24.2 ± 5.9rms$^2$) *(Figure ).*

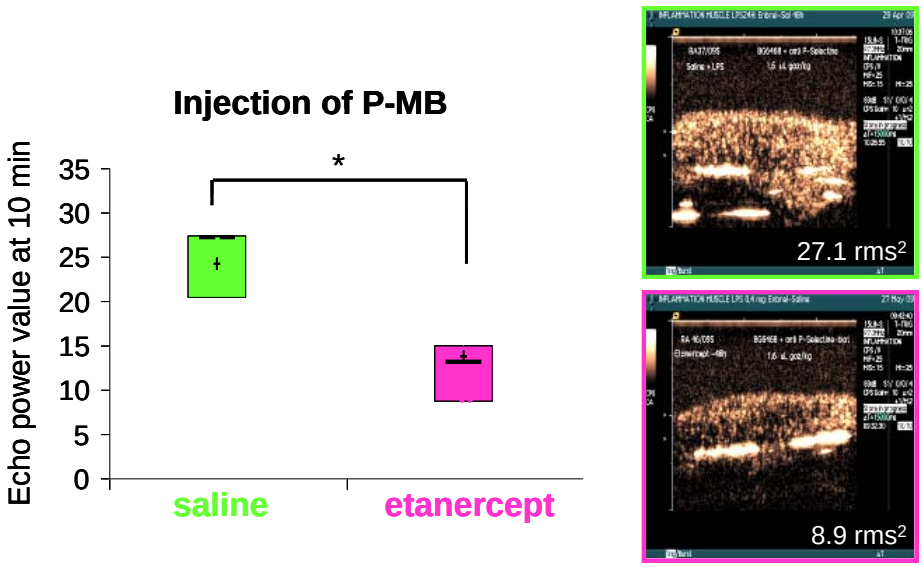


**Figure 4: Monitoring of anti-inflammatory treatment efficacy in LPS-treated animals, with microbubble containing anti P-selectin antibody (P-MB) following saline injection (n=7) or etanercept administration (n=8). *t-test unpaired p<0.05 (±SD).**

## Conclusion

This study shows the ability of TUCA to monitor P-selectin expression in the course of an anti inflammatory treatment with etanercept in the rats. Therefore, molecular ultrasound imaging has the potential to become a powerful diagnostic tool to monitor anti inflammatory treatment in man.

**References**


1. Campbell,S.J., Jiang,Y., Davis,A.E., Farrands,R., Holbrook,J., Leppert,D., and Anthony,D.C. (2007). Immunomodulatory effects of etanercept in a model of brain injury act through attenuation of the acute-phase response. J. Neurochem. 103, 2245-2255.
2. Esposito,E., Mazzon,E., Muia,C., Meli,R., Sessa,E., and Cuzzocrea,S. (2007). Splanchnic ischemia and reperfusion injury is reduced by genetic or pharmacological inhibition of TNF-alpha. J. Leukoc. Biol. 81, 1032-1043.

# Detachment of targeted microbubbles under influence of secondary acoustic radiation force

***T.J.A. Kokhuis [1,6]*, M. Overvelde[2], V. Garbin[3], K. Kooiman[1], B.A. Naaijkens [4,6], L.J.M. Juffermans [5,6], M. Versluis[2] and N. de Jong [1,2,6]***

*[1] Biomedical Engineering, Thorax Center, Erasmus MC, Rotterdam, the Netherlands*
*[2] Physics of Fluids, University of Twente, Enschede, the Netherlands*
*[3] Department of Chemical and Biomolecular Engineering, University of Pennsylvania, Philadelphia, USA*
*[4]Department of Pathology, VU Medical Center, Amsterdam, the Netherlands*
*[5]Department of Physiology, VU Medical Center, Amsterdam, the Netherlands*
*[6]Interuniversity Cardiology Institute of the Netherlands, Utrecht, the Netherlands*

**Introduction**

Targeted ultrasound contrast agents (UCA) are a promising tool within the field of molecular imaging. Compared to their non-targeted counterparts, ligands to specific targets have been added to the shell which typically encapsulates a heavy gas. Because of the presence of these ligands, targeted contrast agents will only adhere to regions of the vascular endothelium expressing specific proteins (e.g. inflammatory markers), facilitating disease-specific contrast enhancement. To be able to bind to their target, the targeted contrast agent should be in close proximity to the vessel wall. However, because of the characteristics of the blood flow profile inside the vessels, most contrast agents will be present around the center line[1], making binding to their target impossible. Acoustic radiation force has been used successfully to move circulating UCA towards the target endothelium[2]. However, it was also shown that ultrasound insonification can cause clustering of targeted microbubbles due to a mutual interaction known as secondary acoustic radiation force[3]. Secondary acoustic radiation force is the force exerted on a microbubble that arises due to the sound emitted by a neighbouring microbubble when both are pulsating in an incident ultrasound field. The instantaneous secondary acoustic radiation force over a microbubble is given by $F=-V\nabla p$ with $V$ the volume and $\nabla p$ the pressure gradient in the fluid due to the pulsating neighbouring microbubble. Because the pressure gradient over the microbubble oscillates in time, the force exerted on this bubble is alternating between attractive and repulsive. However, because the volume of this bubble also oscillates in time, there is a resulting net force exerted on this microbubble when averaged over one period. When two bubbles oscillate in phase (i.e. both have a resonance frequency above or below the insonifying frequency) the net force is attractive. The objective of this study was to investigate the behaviour of targeted microbubbles under influence of secondary acoustic radiation force using ultra high speed optical imaging with the Brandaris128 camera[4].

## Materials and methods

### *Preparation of microbubbles*

Biotinylated microbubbles with a perfluorobutane ($C_4F_{10}$) gas core were made by sonication as described by Klibanov et al.[5]. The mean diameter of the microbubble distribution was 4 μm. The coating was composed of DSPC (59.4 mol %; P 6517; Sigma-Aldrich, Zwijndrecht, the Netherlands), PEG-40 stearate (35.7 mol %; P 3440; Sigma-Aldrich), DSPE-PEG(2000) (4.1 mol %; 880125 P; Avanti Polar Lipids, Alabaster, AL, USA) and DSPE-PEG(2000)-biotin (0.8 mol %; 880129 C; Avanti Polar Lipids).

### *Preparation of target surface and sample*

The topside of an OptiCell, which consists of two polystyrene membranes, served as target surface and was coated with NeutrAvidin™ (Molecular Probes), a deglycosylated form of avidin. A 100 μl droplet of 5 μg/ml solution of NeutrAvidin™ in PBS (Molecular Probes) was put on top of an OptiCell membrane and left for incubation overnight at room temperature. As a negative control a 100 μl droplet of PBS was used. The next day, the surface was rinsed with PBS to remove all the unbound protein and incubated with for 1h with 1% Bovine Serum Albumin (BSA) to block unspecific binding. Afterwards, the surface was rinsed again with PBS and mounted in a special tank (coated side down) which was filled with PBS. Biotinylated microbubbles were injected in the tank and allowed to interact with the coated surface for 10 minutes. After that, the surface was again rinsed with PBS and the bottom (not coated) membrane was cut from the OptiCell.

### *High speed optical imaging of targeted microbubbles*

After the preparation steps, the sample was mounted in a water tank with the targeted microbubbles on top. In this way, unbound microbubbles would float out of optical focus, which confirmed once again the microbubbles were targeted to the coated surface. The water tank also held both an illumination fiber and a 2.25 MHz single element transducer (Panametrics Inc., Waltham, MA, USA). The dynamics of the microbubbles were imaged with a customized BXFM microscope (Olympus Nederland B.V., Zoeterwoude, The Netherlands) with 2× U-CA magnification and a LUMPLFL 60x water immersion objective lens (Olympus). The images were relayed to the ultrafast-framing Brandaris128 camera.

## Results and discussion

Figure 1 (left panel) shows the effect of ultrasound insonification (20 cycles, 2.25 MHz) on the distance between two targeted microbubbles ($R_0 = 2.0$ μm), initially 7.1 μm apart, imaged with a framerate of 10 MHz. The pressure was gradually increased in subsequent movies (6 in total, indicated by the green lines). The time in between subsequent movies was 80 ms. From the decrease in distance between the two microbubbles during ultrasound insonification it is clear that there is a net attraction between the

two bubbles. The right panel shows a detailed plot of distance between the two bubbles during insonification with 180 kPa (fifth movie). The distance-time curve is oscillating with a frequency equal to that of the applied ultrasound because of the alternating attractive and repulsive character of the secondary acoustic radiation force. Figure 1 shows that the microbubbles move towards each other during insonification, but by the start of the next movie, the distance between the bubbles is again 7.1 µm. Moreover, from figure 1 it can be concluded that the distance in between the microbubbles can decrease by several hundreds of nm (up to 600 nm) after which the bubbles are still able to move back to their equilibrium position. This implies that the bubbles should still be attached to the coated surface. Experiments with biotinylated microbubbles in contact with a non-coated surface did not show this behaviour (results not shown here). Because stretching of molecular bonds can not be responsible for this phenomenon, some bubble deformation is plausible, although no such deformations were observed (top view) during the experiments

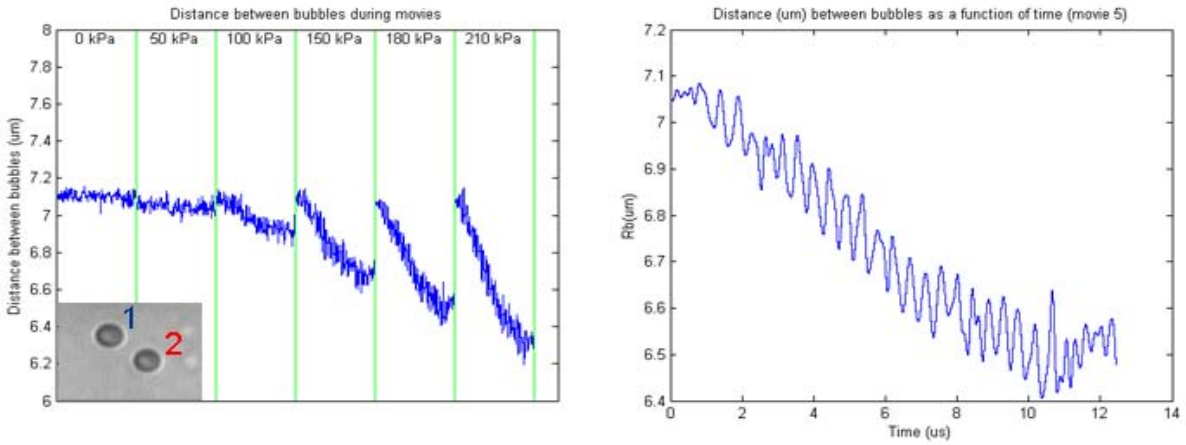


**Figure 1 Left panel** Distance in between two biotinylated microbubbles targeted to a NeutrAvidin surface during insonification with ultrasound (20 cycles, 2.25 MHz). The pressure was increased in subsequent movies (indicated by the green lines). The inset shows the two microbubbles. **Right panel** Detailed plot of the distance (µm) between the two bubbles as a function of time (µs) during insonification with 180 kPa.

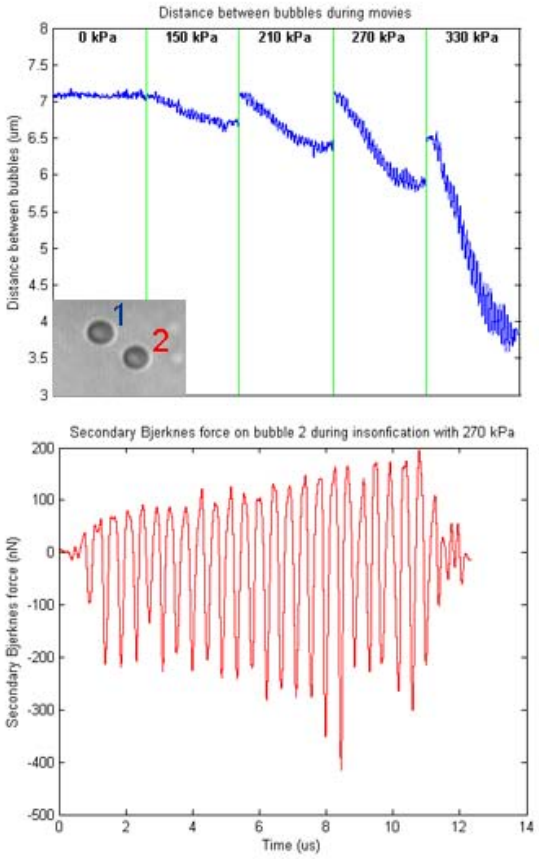


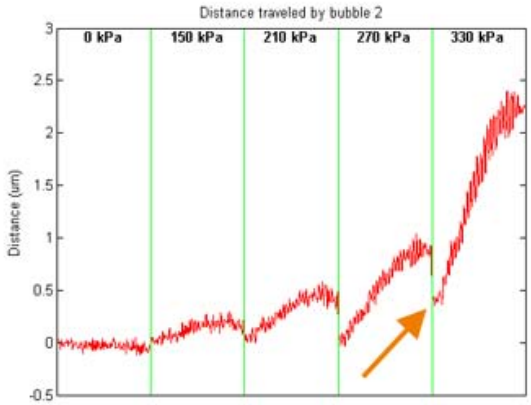


**Figure 2 Upper left panel** Distance between the two microbubbles during ultrasound insonification with (20 cycles, 2.25 MHz). The pressure was increased in subsequent movies (indicated by the green lines) up to 330 kPa. After insonification with ultrasound cycles of 270 kPa the distance between the two microbubbles had decreased by the start of the next movie. The inset shows the two microbubbles. **Upper right panel** Relative displacement of bubble 2 to its position at the start of the experiment. After insonification with 270 kPa the bubble did not get back to its original position (indicated by the orange arrow) by the start of the next movie **Bottom left panel** Corresponding secondary acoustic radiation force experienced by bubble 2 during insonification with 270 kPa. The peak value is around 400 nN.

The upper left panel of figure 2 shows that after exceeding a certain threshold in pressure (in this case 270 kPa), the distance between the bubbles was decreased by around 600 nm by the start of the next movie (which starts after 80 ms). This suggests that at least one of the bubbles detached from its adhesion point and the force exerted on this bubble was larger than its binding force. At the end of the fifth movie (insonification with 330 kPa) the microbubbles were touching. The upper right panel of figure 2 shows the displacement of bubble 2 relative to its position at the start of the experiment (which corresponds to 0 µm). After insonification with 150 kPa and 210 kPa, the bubble was again at its original starting position when the next movie started. However, at the start of the 5$^{th}$ movie (after insonification with 270 kPa during movie 4) the bubble had not moved back to its equilibrium position (indicated by the orange arrow), which suggests that the attachment to its original adhesion point was broken. The bottom left panel of figure 2 shows the corresponding secondary acoustic radiation force experienced by the same bubble (bubble 2) due to the presence of bubble 1 during insonification with 270 kPa. The maximum secondary acoustic radiation force experienced by bubble 2 during the 20 cycles is around 400 nN.

To estimate the relaxation time of the system (i.e. the time needed for a microbubble to move back to its equilibrium position after insonification), two targeted microbubbles were insonified with 20 cycles of 2.25 MHz and imaged at low frame rates to cover a larger time window (in the figure below, imaging at 1.15 MHz yielded a time window of 110 µs for each movie). The results are shown in figure 3. During insonification (in the beginning of each movie) the distance between the two microbubbles decreased. From the moment the sound is turned off (corresponding to the minimum of each curve) the distance in between the two bubbles again restored to the initial value (=10.8 µm) within less than 80 µs. However, after insonification with 300 kPa (last movie) the system did not restore to the initial value and the interbubble distance equilibrates around 10.2 µm.

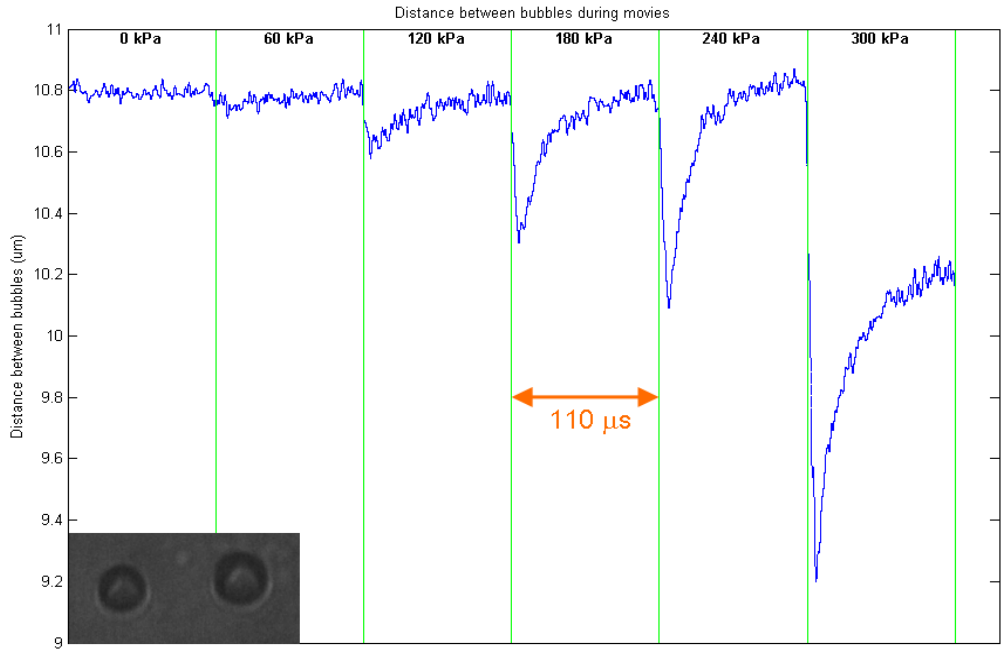


**Figure 3** Distance (µm) in between two targeted microbubbles (see inset) versus time (µs) during and after insonification with 20 cycles of 2.25 MHz. The pressure was increased in subsequent movies (indicated by the green lines). During insonification (in the beginning of each movie) the distance in between the two microbubbles decreased. After insonification the distance in between the two microbubbles restored to the initial value within less than 80 µs. However, after insonification with 300 kPa (last movie) the system did not restore to the initial value and the interbubble distance equilibrates around 10.2 µm (i.e. 600 nm decrease). The imaging frame rate was 1.15 MHz.

## Conclusion and outlook

These results show that secondary acoustic radiation force can detach a targeted microbubble from its target surface upon ultrasound insonification. We showed that the distance in between two targeted microbubbles can decrease up to several hundreds of nm during ultrasound insonification after which the bubbles still move back to their equilibrium position. This implies that the microbubbles should still be attached to their adhesion point and a restoring force should be present to account for this behaviour. We showed that above a certain threshold of the secondary acoustic radiation force (~ 400 nN in this

study and for these bubbles), the distance between the microbubbles did not restore to the initial value before ultrasound insonification. The relaxation time for microbubbles after ultrasound insonification turned out to be in the order of 80 μs (i.e. << time in between subsequent movies (80 ms)), so it is unlikely we were interfering with this time constant during our experiments. A model including the other hydrodynamic forces present will be used to distill the microbubble binding force from these data[6]. Future work will include experiments with different concentrations of surface protein (e.g. NeutrAvidin™) and ligands incorporated in the microbubble coating (e.g. biotin). Moreover, experiments will be performed using a setup allowing simultaneously viewing top and side view[7]. This might give us an indication if microbubble deformations are involved.

**Acknowledgments**

This project was funded by Stichting Technologie en Wetenschap (STW). The authors would like to thank A.L. Klibanov from the University of Virginia, Cardiovascular Division, Charlottesville, Virginia, USA for discussions about microbubble preparation.

**References**

1. Keller, M. W., Segal, S. S., Kaul, S. & Duling, B. The behavior of sonicated albumin microbubbles within the microcirculation: a basis for their use during myocardial contrast echocardiography. Circ Res 65, 458-467 (1989).
2. Rychak, J. J., Klibanov, A. L., Ley, K. F. & Hossack, J. A. Enhanced targeting of ultrasound contrast agents using acoustic radiation force. Ultrasound Med Biol 33, 1132-1139, (2007).
3. 3Schmidt, B. J., Sousa, I., van Beek, A. A. & Bohmer, M. R. Adhesion and ultrasound-induced delivery from monodisperse microbubbles in a parallel plate flow cell. Journal of Controlled Release 131, 19-26, (2008).
4. Chin, C. T. et al. Brandaris 128: A digital 25 million frames per second camera with 128 highly sensitive frames. Rev Sci Instrum 74, 5026-5034, (2003).
5. Klibanov, A. L. et al. Detection of individual microbubbles of ultrasound contrast agents: imaging of free-floating and targeted bubbles. Invest Radiol 39, 187-195, (2004).
6. Garbin, V., Overvelde, M., Dollet, B., de Jong, N., Lohse, D., & Versluis, M. (in preparation)
7. Vos, H. J., Dollet, B., Bosch, J. G., Versluis, M. & de Jong, N. Nonspherical vibrations of microbubbles in contact with a wall: a pilot study at low mechanical index. Ultrasound Med Biol 34, 685-688, (2008).

# Prostate Biopsy Guidance with VEGFR2-Targeted Microbubbles: Update from an Ongoing Study

***S. Wallack[1], D. Smith[2], Z. Du[3], AL Klibanov[3], J. Backer[4], MV Backer[4], J. Rychak[2]***

*[1.] Veterinary Imaging Center San Diego*
*[2.] Targeson, Inc*
*[3.] University of Virginia, Cardiovascular Division*
*[4.] Sibtech, Inc.*

Ultrasound molecular imaging is a developing technique with applications both in clinical practice and experimental research. Recently, we have developed a microbubble targeted to VEGFR-2, a receptor for vascular endothelial growth factor (VEGF), which is overexpressed on endothelial cells in angiogenic vasculature. This agent is a lipid-encapsulated perfluorocarbon microbubble that utilizes a unique VEGFR-2-binding ligand modeled on human VEGF, and is commercially available for use as a research reagent in preclinical applications. We now seek to investigate the utility of this agent in applications with clinical translation. In the current study, we aim to determine whether the angiogenesis-targeting microbubble can enhance the sensitivity of prostate cancer detection by targeting biopsy sampling. Current technique relies upon acquiring multiple samples under ultrasound guidance; although this technique can increase the likelihood of detection, increasing the number of samples poses additional morbidity risks. Targeted biopsy using perfusion agents has demonstrated some increase in cancer detection, although it remains to be determined whether blood flow is a truly specific indicator of malignancy. We hypothesize that molecular imaging of VEGFR2 may yield greater specificity, as it indicates the molecular components of new vessel growth, which may be detectible well in advance of perfused blood vessels.

In the current phase of this project we seek to determine whether VEGFR-2-targeting agents are retained at locations of malignancy in canines with spontaneous prostatic disease. Informed consent was acquired from all owners, and care was paid for by the study. Companion animals were referred to the study by their primary veterinarian based on suspected prostate disease. A full blood panel, chest X-ray, and abdominal ultrasound exam was performed on each animal prior to the study. Prostate biopsy was performed under general anesthesia. Microbubbles were administered IV (0.03 mL per kg), and biopsy samples were acquired 8 minutes post-contrast under transabdominal ultrasound guidance (Toshiba Aplio, harmonic mode). In animals in which contrast enhancement was evident, two samples were taken: one from the enhanced region, and one from a distant non-enhancing region. In animals in which no enhancement was observed, one sample each from the left and right the peripheral zones were acquired. Biopsy samples were read by a veterinary pathologist.

We have completed a total of nine dogs in this study. Eight were administered the VEGFR-2-targeting agent, and one was administered a non-targeted agent. Prostatic adenocarcinoma was observed in three dogs. Two of these dogs were administered targeted agents, and biopsy taken from the enhanced region(s) was determined to be carcinoma; biopsy taken from non-enhancing region did not contain cancer cells in one animal. Non-targeted agents administered to a third dog with confirmed prostatic adenocarcinoma did not demonstrate enhancement.

Inflammatory disease, with varying levels of benign hyperplasia, was observed by pathology in four dogs. Variable contrast enhancement was observed in these animals. Benign hyperplasia absent fibro-inflammatory disease was observed by pathology in two animals. No contrast enhancement was observed in either animal. No complications related to the study were observed in any animals.

Although this study remains ongoing, the data to date suggest that VEGFR2-targeting ultrasound contrast agents are retained at regions of malignant neoplasm in prostate. We have observed what appears to be non-specific contrast agent retention in cases of severe inflammatory disease, which is not unexpected as microbubble retention to activated leukocytes is a well-documented phenomenon. We did not observe microbubble retention to regions of benign hyperplasia. This data suggests that these agents may have a role in distinguishing neoplasm from benign hyperplastic disease, although further studies are required to determine whether targeted biopsy can yield increased detection efficacy.

Thursday, January 20, 2011

# Social Event

## Brewery "DE PELGRIM"
## Aelbrechtskolk 12 Rotterdam

**Tours: between 7.15 and 8.15 pm**
**Buffet: around 8.00 pm**

**Coaches will be leaving from the Hilton at 18:30 and will be back there around 23:00**

# Halting Tumor Growth Using Drug Loaded Polymeric Contrast Agent

***Michael Cochran[1], John Eisenbrey[1], Michael Soulen[2] and Margaret Wheatley[1]***

*[1]School of Biomedical Engineering, Science and Health Systems, Drexel University, Philadelphia, PA*
*[2]Division of Interventional Radiology, University of Pennsylvania, Philadelphia PA*

A polymer ultrasound contrast agent loaded with doxorubicin has been developed within our laboratory. When triggered by ultrasound, this agent has been shown to fragment resulting in drug loaded polymer shards less than 400 nm in diameter, small enough to extravasate through the leaky vasculature of a tumor and accumulate within the interstitium where they can slowly degrade and provide a sustained localized release of doxorubicin. This study investigates the use of this agent in a rat liver cancer model. Results are compared with drug loaded nanoparticles and free doxorubicin. Drug loaded ultrasound contrast agents, and 200 nm nanoparticles were prepared with 14C labeled doxorubicin. Ultrasound contrast agents, nanoparticles, free doxorubicin and a combination of ultrasound contrast agents and nanoparticles were administered intravenously into ACI rats bearing Morris 3924a hepatomas and insonated. Doxorubicin concentrations in blood plasma were measured over 30 minutes. Drug concentrations in tumors and organs were measured after 4 hours, 7 days and 14 days. Tumors were measured upon sacrifice and evaluated with autoradiography and histology. Animals treated with microbubbles had significantly lower peak plasma concentrations (0.4661 ± 0.0684%/ml) compared to and free doxorubicin (3.0328 ± 0.6120%/ml, p=0.0019). After 14 days, levels in the heart were significantly lower in animals treated with microbubbles compared to free doxorubicin (0.1676%/g tissue vs. 0.3198%/g, p=0.0088). Tumors treated with microbubbles showed significantly higher drug levels than tumors treated with free doxorubicin after 4 hours (4.1739± 0.8397 ng/mg tissue vs. 0.4162± 0.0969 ng/mg tissue, p=0.0472). These tumors showed no significant increase in size over 14 days and significantly less growth than tumors treated with free doxorubicin (p=0.0390). Doxorubicin loaded ultrasound contrast agents provided enhanced, sustained drug delivery to tumors while reducing peak plasma drug concentrations, lowering doxorubicin concentrations to the heart and arresting tumor growth.

# Risk stratification of carotid atherosclerotic lesions by standard and contrast-enhanced ultrasound: Correlation of lesion echogenicity and severity with intraplaque neovascularization

***Daniel Staub, MD [1,2], Sasan Partovi, BS[3], Arend F.L. Schinkel, MD, PhD[4], Blai Coll, MD, PhD[5], Heiko Uthoff, MD[2], Markus Aschwanden,MD[2], Kurt A. Jaeger, MD[2], Steven B. Feinstein, MD, FACC[1]***

*[1]Rush University, Medical Center, Section of Cardiology, Department of Internal Medicine, 1653 West Congress Parkway, Suite 1015 Jelke, Chicago, IL 60612, USA*
*[2]Department of Internal Medicine, Section of Angiology, University Hospital, Basel, Switzerland*
*[3]Department of Neuroradiology, University Hospital, Basel, Switzerland*
*[4]Department of Cardiology, Thoraxcenter, Erasmus Medical Center, Rotterdam, The Netherlands*
*[5]Unitat de Diagnòstic i Tractament de Malalties Aterotrombòtiques (UDETMA), Hospital Arnau de Vilanova, Institut de Recerca Biomèdica, Lleida, Spain*

**Introduction**

Current risk stratification of carotid atherosclerotic lesions is based on the evaluation of degree of stenosis and plaque morphology using standard Duplex ultrasound imaging.[1,2] High degree stenosis and echolucent plaques corresponding to histological features of plaque instability are at high risk for cerebrovascular events. Vasa vasorum derived neovascularization is also known to be an important feature in plaque development and vulnerability triggered by inflammation and hemorrhage.[3] The progression of plaques is associated with angiogenesis (microvessel formation) within the plaque, and eventually, these microvessels contribute to the instability of the plaque.[4] As recently shown, contrast-enhanced ultrasound (CEUS) provides direct visualization of the carotid plaque neovascularization.[5,6] The degree of neovascularization in atherosclerotic carotid lesions detected by CEUS is well correlated with the histological density of neovessels,[7,8] and with symptomatic patients with a history of cerebrovascular or cardiac events.[9,10]The purpose of this study was to correlate echogenicity and severity of atherosclerotic carotid lesions on standard ultrasound with the degree of intraplaque neovascularization on CEUS imaging.

**Methods**

A total of 175 patients (mean age 67±10 years, 65% male) with at least one carotid atherosclerotic lesion underwent standard and contrast-enhanced carotid ultrasound. Lesion echogenicity on B-mode ultrasound classified as uniformly echolucent (Class I), predominantly echolucent (Class II), predominantly echogenic (Class III), uniformly echogenic or extensively calcified (Class IV), degree of stenosis graded as < 50%, 50-69%, or≥ 70% stenosis based on spectral Doppler velocities, and maximal lesion thickness measured from the media-adventitia to the intima-lumen boundaries were

evaluated for each documented atherosclerotic lesion. The degree of intraplaque neovascularization on CEUS was categorized as absent (Grade 1 = no appearance of moving bubbles within the plaque or microspheres only confined to the adjacent adventitial layer), moderate (Grade 2 = moderate visible appearance of moving bubbles within the plaque at the adventitial side or plaque shoulder), or extensive (Grade 3 = extensive intraplaque neovascularization with clear visible appearance of bubbles moving to the plaque core). Correlation of neovascularization with echogenicity, degree of stenosis, and maximal lesion thickness was made using Spearman's rho and chi-square test for trend.

**Results**

The lesions's characteristics of total 293 atherosclerotic lesions are listed in Table 1. Echogenicity was inversely correlated with grade of intraplaque neovascularization (rho -0.199, p=0.001). More echolucent lesions had higher degree of neovascularization compared with more echogenic ones (p<0.001) [Figure 1A]. The degree of stenosis was significantly correlated with grade of intraplaque neovascularization (rho 0.157, p=0.003). Lesions with higher degree of stenosis had higher grade of neovascularization (p=0.008) [Figure 1B]. Maximal lesion thickness increased with the grade of neovascularization (p<0.001), and higher quartiles of maximal lesion thickness had significantly higher grade of neovascularization (p<0.001) [Figure 1C]. Maximal lesion thickness and quartiles of maximal thickness were significantly correlated with grade of neovascularization (rho 0.233, p<0.001, and 0.248, p<0.001, respectively).

**Conclusion**

These results support the hypothesis that neovascularization visualized by CEUS is correlated with morphological features of plaque instability and with lesion severity. The positive relationship between lesion echolucency, degree of stenosis, maximal lesion thickness, and contrast-agent enhancement is in agreement with the concept that more advanced atherosclerotic plaques prone for rupture, are more likely to have a greater degree of neovascularization. Therefore, CEUS may be a valuable tool for further risk stratification of echolucent atherosclerotic lesions and carotid stenosis of different degrees.

**References**


1. Hobson RW, Mackey WC, Ascher E, et al. Management of atherosclerotic carotid artery disease: clinical practice guidelines of the Society for Vascular Surgery. J Vasc Surg. 2008;48:480-6.
2. Eyding J, Geier B, Staub D. Current strategies and possible perspecitves of ultrasonic risk stratification of ischemic stroke in internal carotid artery disease. Ultraschall Med 2010;in press
3. Moreno PR, Purushothaman KR, Sirol M, Levy AP, Fuster V. Neovascularization in human atherosclerosis. Circulation. 2006;113:2245-52.
4. Sluimer JC, Daemen MJ. Novel concepts in atherogenesis: angiogenesis and hypoxia in atherosclerosis. J Pathol. 2009;218:7-29.
5. Feinstein SB. Contrast ultrasound imaging of the carotid artery vasa vasorum and atherosclerotic plaque neovascularization. J Am Coll Cardiol. 2006;48:236-43.

6. Staub D, Schinkel AFL, Coll B, et al. Contrast-enhanced ultrasound imaging of the vasa vasorum: from early atherosclerosis to the identification of unstable plaques. JACC Cardiovasc Imaging. 2010;3:761-71.

7. Shah F, Balan P, Weinberg M, et al. Contrast-enhanced ultrasound imaging of atherosclerotic carotid plaque neovascularization: a new surrogate marker of atherosclerosis? Vasc Med. 2007;12:291-97.
8. Coli S, Magnoni M, Sangiorgi G, et al. Contrast-enhanced ultrasound imaging of intraplaque neovascularization in carotid arteries: correlation with histology and plaque echogenicity. J Am Coll Cardiol. 2008;52:223-30.
9. Xiong L, Deng YB, Zhu Y, Liu YN, Bi XJ. Correlation of carotid plaque neovascularization detected by using contrast-enhanced US with clinical symptoms. Radiology. 2009;251:583-9.
10. Staub D, Patel MB, Tibrewala A, et al. Vasa vasorum and plaque neovascularization on contrast-enhanced carotid ultrasound imaging correlates with cardiovascular disease and past cardiovascular events. Stroke. 2010;41:41-7.

**Table 1. Sonographic characteristics of the atherosclerotic carotid lesions**

| Characteristics | Atherosclerotic carotid lesions (n=293) |
|---|---|
| **Severity** | |
| Stenosis < 50% | 226 (77) |
| PSV (cm/s)* | 90±22 (32 – 161) |
| Stenosis 50-69% | 49 (17) |
| PSV (cm/s)* | 166±35 (125 – 245) |
| Stenosis ≥ 70% | 18 (6) |
| PSV (cm/s)* | 315±70 (233 – 464) |
| Maximal lesion thickness (mm)* | 2.7±0.9 (1.3 to 7.9) |
| **Echogenicity** | |
| Class I | 30 (10) |
| Class II | 99 (34) |
| Class III | 111 (38) |
| Class IV | 53 (18) |
| **Neovascularization** | |
| Grade 1 | 178 (61) |
| Grade 2 | 96 (33) |
| Grade 3 | 19 (6) |

Unless otherwise indicated, data are numbers of patients and data in parentheses are percentages. *Data are means ± standard deviations and data in parentheses indicate the range. PSV = peak systolic velocity on Doppler ultrasound

**Figure 1. Grade of intraplaque neovascularization on contrast-enhanced ultrasound according to lesion echogenicity, degree of stenosis, and quartiles of maximal lesion thickness on standard ultrasound imaging.**

A: The proportion of carotid lesions with higher grade of intraplaque neovascularization is greater in more echolucent lesions ($p<0.001$ by chi-square analysis for trend). B: The proportion of carotid lesions with higher grade of intraplaque neovascularization is greater in lesions with higher degree of stenosis ($p=0.008$ by chi-square analysis for trend). C: The proportion of carotid lesions with higher grade of intraplaque neovascularization is greater in lesions of higher quartile of maximal lesion thickness ($p<0.001$ by chi-square analysis for trend).

**Figure 1**

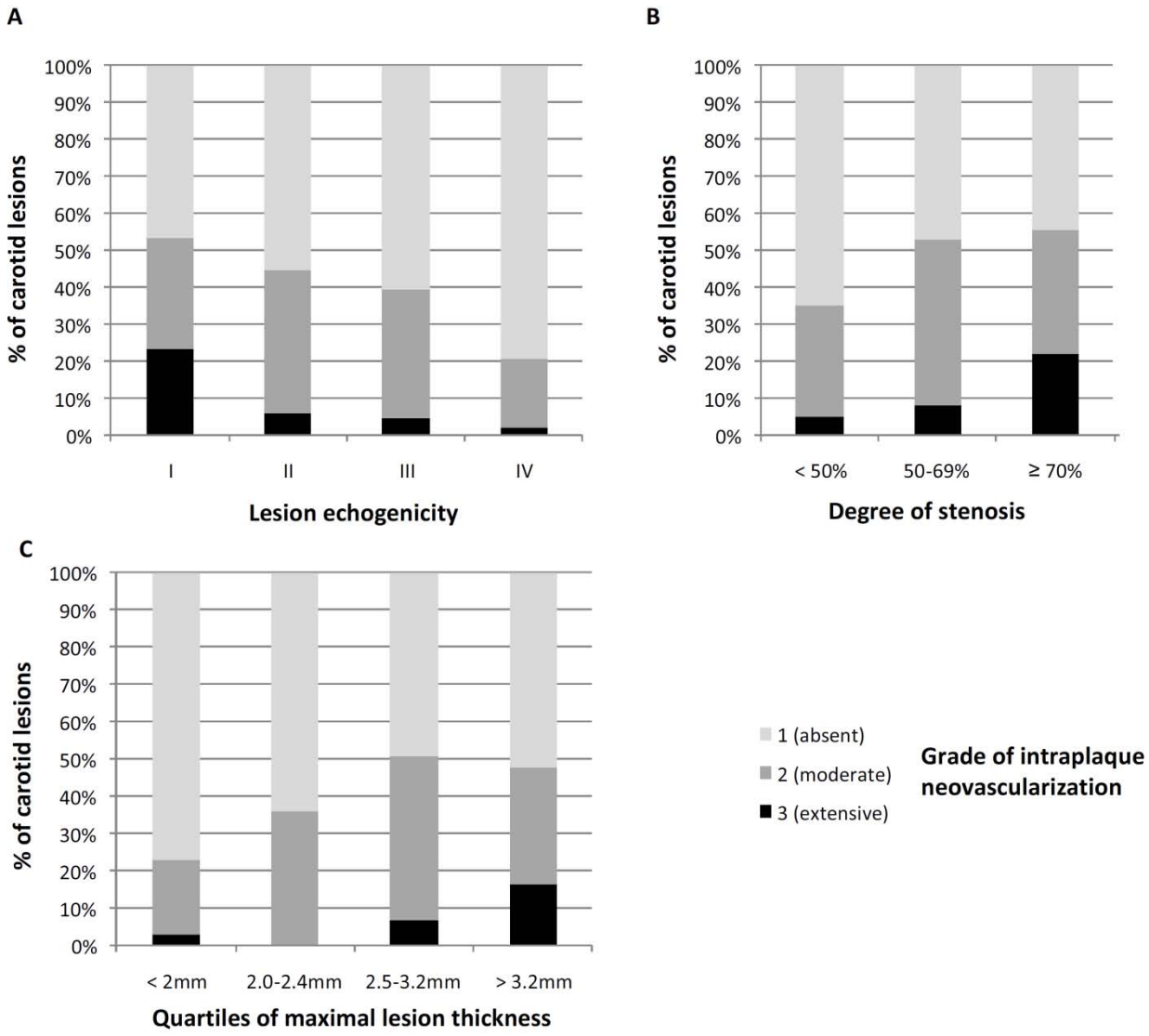

# Microbubble delivery of ApoA1 for the therapeutic elevation of HDL.

***Jason Castle***

*GE Global Research*

Apolipoprotein A1 is the predominant protein component of High-density Lipoprotein in plasma. In animal models, increasing ApoA transgenically or infusing recombinant HDL (RHDL) promotes prominent regression of atherosclerosis and enhanced macrophage-specific reverse cholesterol transport. Based on these animal models, this approach appears to offer the greatest clinical potential for HDL based therapies. There are also three intriguing small human trials demonstrating that different approaches to increasing lipid-poor ApoAI acceptors induce regression of atherosclerosis in only 6 weeks in humans.

We report on the first animal study, to consistently enhance ApoA1 transduction in the liver utilizing ultrasound and microbubbles, resulting in increased secretion of HDL into plasma. Using GE Healthcare's ultrasound contrast agent Optison, a microbubble historically used for left ventricular opacification, we demonstrate the therapeutic value of Optison used as a delivery vehicle of pharmaceutical drugs or DNA.

Targeting the liver of Sprague-Dawley rats, functional human ApoA1 DNA was intravenously injected in solution with a mixture of Optison. Upon microbubble profusion of liver as imaged by ultrasound, the appropriate amount of ultrasound energy was delivered, causing an oscillation and then disruption of microbubbles and a deposition of DNA gene payload. Once incorporated into the nucleus, the ApoA1 DNA is transformed by the rat's cellular machinery into fully functional Apo A1 protein, which consequently increases the HDL serum level.

To date we have seen up to a 34% increase in HDL level within 24 hours post procedure. Through the manipulation of all potential variables, we have determined the optimal dose energy and sequence, achieving DNA delivery efficacy rates nears 75%.

*In collaboration with SonoGene, LLC*
*NIH SBIR R44 HL095238-01*

# Successful Microbubble Stroke Sonothrombolysis without tPA in Rabbits

***William C. Culp; Aliza T. Brown; John D. Lowery; Paula K. Roberson***

*University of Arkansas for Medical Sciences, Little Rock, AR*

**Introduction**

Microbubbles (MB) combined with ultrasound (US) have been shown to produce effective clot lysis without exogenous tissue plasminogen activator (tPA) in vitro and in dog and pig models. Using an angiographic rabbit model of acute ischemic stroke we evaluate sonothrombloysis with 3 types of MB and compare it with standard tissue plasminogen activator therapy.

**Methods**

New Zealand White rabbits (n = 74; 5.2 ± 0.07 kg) received angiography, and a single 0.6 x 4.0 mm clot was injected into the internal carotid artery, occluding its branches. Emboli were prepared by placing rabbit blood into 1.5 mm glass tubes. Clotting proceeded for 6 hours at 37ºC, then at 4ºC for 72 hours. Then the clots were cut to precise length. Rabbits were randomly assigned to one of six groups. Group 1) control (n = 11) rabbits embolized without therapy; group 2) tPA without US (n = 20);
3) tPA+US (n = 10); 4) lipid MB+US (n = 16); 5) custom 3µm MB+US (n = 8); and 6) platelet-fibrin-targeted 3µm MB+US (n = 9). Treatment began one hour following angiographic verification of occlusion. Rabbits with US received pulsed wave US (1 MHz; 0.8 W/cm$^2$) for 1 hour and rabbits with tPA received intravenous tPA (0.9 mg/kg) over 1 hour. Rabbits receiving lipid MB (Definity; Lantheus Medical Imaging; North Billerica, MA) received intravenous MB (0.16 mg/kg) over 30 minutes. Rabbits administered custom 3µm MB received 5 x $10^9$ MB intravenously alone or tagged with eptifibatide and fibrin antibody over 30 minutes. Rabbits were sacrificed at 24 hours and infarct volume was determined using vital stains on brain sections.

**Results**

Infarct volume was lower for rabbits treated with lipid MB+US (1.0 ± 0.6% vs control p=0.013), custom 3µm MB+US (0.6 ± 0.9% vs control p=0.018), and targeted 3µm MB+US (0.8 ± 0.8% vs control p=0.019) compared with control rabbits (3.5 ± 0.8%). The 3 MB types collectively differed from control, p=0.004. Infarct volume averaged 2.2 ± 0.6% and 1.7 ± 0.8% for rabbits treated with tPA alone and tPA+US, respectively, and did not differ significantly from control and MB treated rabbits.

**Conclusions**

Sonothrombolysis without tPA using either untagged or platelet- and fibrin-targeted MB is effective at decreasing infarct volumes. This absence of exogenous tPA may lead to reduced hemorrhagic complications of thrombolysis. Human trials are now justified and urgently needed.

A. All microbubbles as a group are very effective at decreasing infarct volumes from control levels, P=0.004.

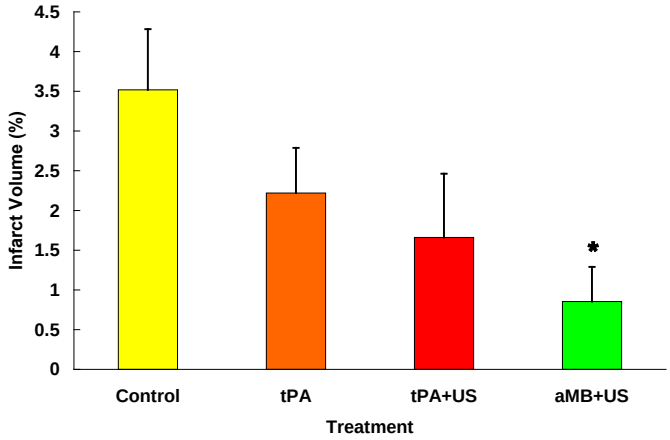


B. Individual microbubble groups are all significantly improved compared with controls but not different one from another in this animal model.

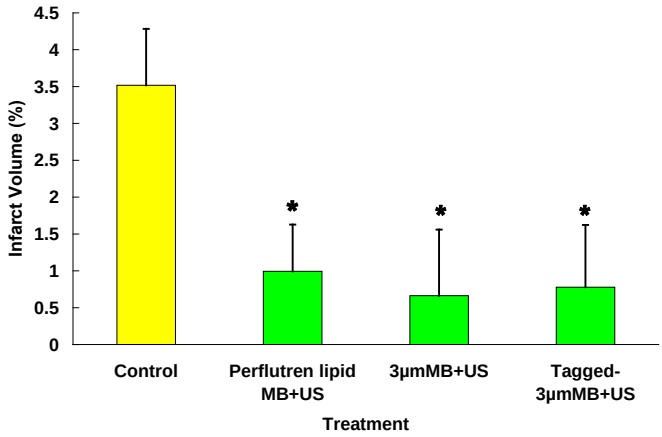


Supported in part by NIH funding, R01 HL028481

# Augmentation of Microbubble Targeting Efficacy by Red Blood Cells under Fast Flow Conditions

***Sunil Unnikrishnan[1], Michael B. Lawrence[1], Klaus F. Ley [3], Alexander L. Klibanov [1,2]***

*[1]Department of Biomedical Engineering, University of Virginia, Charlottesville, USA*
*[2]Department of Cardiovascular Medicine, University of Virginia, Charlottesville, USA*
*[3]La Jolla Institute of Immunology and Allergy, La Jolla, USA*

Microbubble ultrasound contrast agents are coming into use in clinical applications for targeted molecular imaging and intravascular drug delivery.The local hydrodynamic environment heavily influences the ability of the targeting agent to attach and firmly bind to the vascular endothelium.Microbubble targeting *in vivo* is efficient in fast flow conditions, with antibody-conjugated bubbles binding at wall shear stresses (WSS)upto 15 dyne/cm$^2$. However, microbubble adhesion is quite inefficient in flow chambersettings *in vitro* with binding occurring only at low wall shear stresses (WSS < 1.5 dyne/cm$^2$). This discrepancy points to a gap in our understanding of the targeting mechanism under physiological flow. At the same time, the presence of red blood cells (RBCs) has been shown to enhance leukocyte adhesionto the vessel wall and could be one of the factors responsible for this discrepancy. Hence, clarifying the role of RBCs in microbubble interactions with the vessel wall is required to understand and optimize the targeting process.

The effect of RBCs on the adhesion dynamics of lipid-shelled microbubbles was assessed in a parallel-plate flow chamber model. Biotinylated bubbles targeted to a streptavidin-coated surface were used for the study. Microbubble targeting was evaluated by fluorescent video microscopy both in an upright configuration, where the microbubble binding to the reactive surface is aided by buoyancy, and an inverted configuration, where buoyancy works against the binding. Adhesion efficiency was calculated as the adherent fraction of the near-wall microbubble flux.In the upright configuration, at low shear stresses RBCs did not affect the binding efficiency, but at high WSS (> 1.5 dyne/cm$^2$) presence of RBCs at physiological hematocrit enhanced binding significantly. At a WSS of 4.5 dyne/cm$^2$, the binding efficiency increased from < 0.2% in the absence of RBCs to about 12% with 40% hematocrit. This effect persisted at 20% hematocrit and when RBC deformability was modified using glutaraldehyde. The results for adhesion efficiency under the different experimental conditions are shown in fig. 1. In the inverted configuration, binding was virtually nonexistentat high WSS without RBCs, but was as much as two orders of magnitudehigher when RBCs were present, effectively nullifying gravity effects.

A reduction in the near-wall microbubble flux was also observed in the presence of RBCs at high WSS, suggesting that this augmented adhesion does not require increased margination of microbubbles. An increase in the collision frequency of the flowing microbubbles with the vessel wall due to near-wall hydrodynamic interactions with RBCs may be responsible for this behavior.

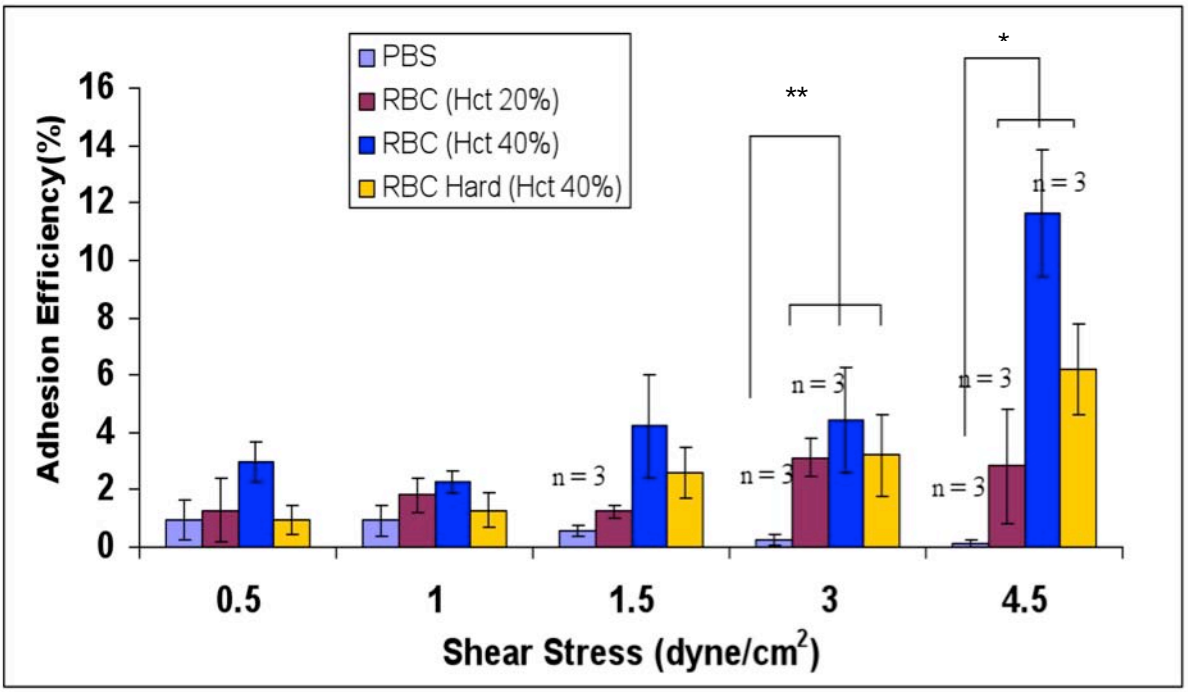


**Figure 1: Microbubble adhesion efficiency for PBS, RBC suspensions at 20% and 40% hematocrit, and hardened RBC suspension at 40% hematocrit for upright configuration (** p < 0.02, * p < 0.05)**

To examine the above-described phenomenon for a physiologic receptor, murineP-selectinwas adsorbed on to the flow chamber surface. P-selectin antibody, RB40.34, was conjugated to the biotinylatedbubbles with a streptavidin linker. The flow chamber was supported vertically to eliminateRBC sedimentation towards the surface and the accumulation of microbubbles on the surface was monitoredby ultrasound imaging. At aWSS of 4 dyne/cm$^2$, more than a two-fold increase in the mean echo intensityfrom bound microbubbles was detected in the presence of RBCs. Representative images are shown in fig. 2(a) and (b).

**Fig. 2(a): Microbubble accumulation on P-selectin without RBCs at 4 dyne/cm2**

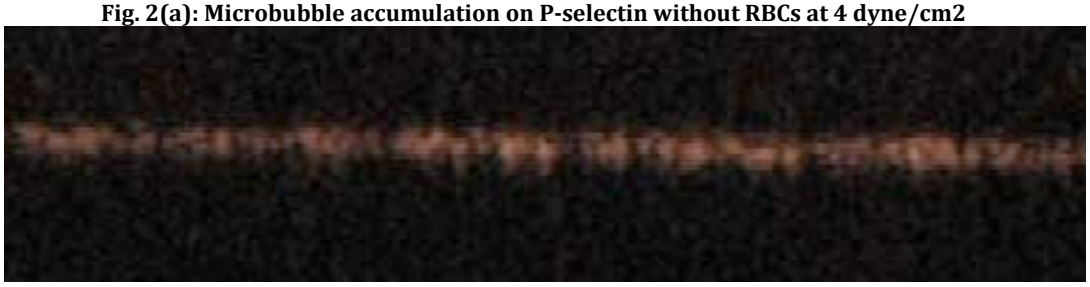

**Fig. 2(b): Microbubble accumulation on P-selectin with RBCs (40%hematocrit) at 4 dyne/cm2**

## Conclusion

Red blood cells enhance microbubble targeting under high shear stress conditions at physiologic hematocrit. Their presence in an inverted configuration effectively negates gravity effects and increases binding by nearly two orders of magnitude. The near-wall microbubble flux is significantly reduced at high shear stresses in the presence of red blood cells. This rules out increased marginationas the probable mechanism behind the enhanced adhesion.We hypothesize that this augmented binding is the result of near-wall hydrodynamic interactions between RBCs and microbubbles that lead to higher wall collision frequency and greater binding probability.In vitro flow chamber assays performed withoutRBCs may underestimate the targeting efficacy of microbubble agents. Using RBCs in the flow chamber model would improve our understanding of the targeting process andwould aid in the development of microbubbles that are optimized for targeting under physiological conditions.

# High Frequency Ultrasound Contrast Imaging of the Mouse Embryo

***J. Denbeigh, M. Puri, F. S. Foster***

The developing mouse embryo represents a dynamic model for active angiogenesis and organ development. The hemodynamics and molecular expression profiles that arise as part of this process are of great interest to the fields of developmental, cancer, and cardiovascular biology. The strategy of performing functional and molecular imaging of biological pathways using targeted microbubbles has already been employed by a number of groups to demonstrate the ability of targeted ultrasound contrast imaging to monitor molecular expression in a variety of tumour models.[1-3] Contrast imaging in the embryo, however, presents special opportunities and challenges. One the one hand we have the ability to image vascular development in many tissues (e.g. brain, heart and liver) simultaneously - a difficult feat in adult mice. Conversely, optimal infusion rates, injection volumes and uptake kinetics for microbubbles may be different in embryos than in the adult mouse and must therefore be identified. We report here on the development of techniques to infuse targeted microbubble contrast agents into whole living embryos and subsequent analysis of wash-out kinetics and molecular targets such as VEGFR-2.

Preliminary experiments were performed on litters of E15.5, E16.5, E17.5 and E18.5 mice. Mouse embryos were removed from the mother, dissected out of the uterus, and placed in chilled DMEM media fortified with Hepes, FBS and Penicillin Streptomycin. Prior to injection, each embryo was transferred to a dissecting base, the yolk sac was cut while avoiding large vessels, and the yolk sac and placenta were pinned. Pre-warmed PBS (~57C) was used to revive and warm the embryo. Once a heartbeat was visible, the embryo was covered with pre-warmed ultrasound gel and the dish was topped up with warmed PBS. 350uL of microbubble solution was drawn into a 1 mL syringe, attached to tubing and a glass cannula, and mounted on a perfusion pump. The glass needle was then trimmed to size and cleared of air, was inserted into an arterial blood vessel in the placenta, and 20 uL of microbubble solution was infused at a rate of 0.02 mL/min. A 21 MHz linear array transducer (VisualSonics) was then positioned over the embryo. See Figure 1 for a depiction of the technical set-up.

**Figure 1.** Experimental Set-up.

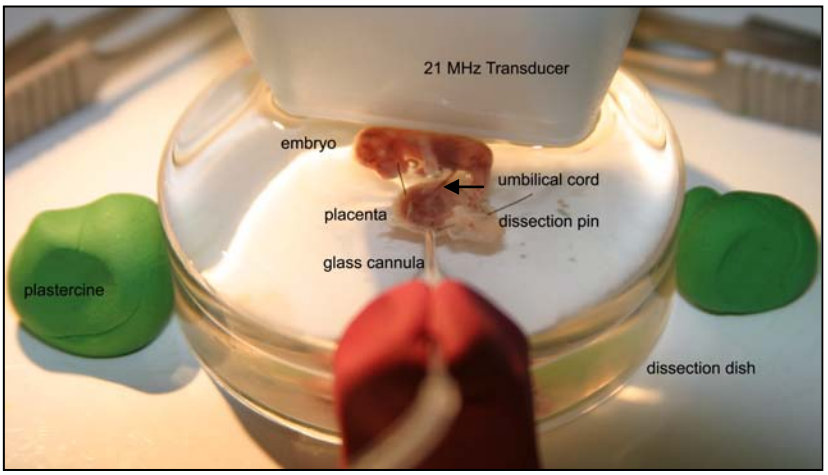


Arrangement of cannula, embryo and transducer positioned in ultrasound gel for microbubble injections.

In a pilot group of E15.5 embryos (n=3), wash-out kinetics of microbubbles in the brain, heart, and liver were studied to assess the behaviour and circulation time of the bubbles in the embryos. In our molecular imaging studies, a burst pulse was used to disrupt all bubbles in the plane of view and a sequence of nonlinear contrast image frames including both pre and post bubble disruption were obtained after permitting the microbubbles to circulate for 6 minutes at 18 MHz, using 4% power, at a frame rate of 11 $s^{-1}$, and with a contrast gain of 25dB (see Figure 2). Three populations of microbubbles (Vascular Endothelial Growth Factor Receptor -2 targeted, rat isotype $IgG_2$ control, and untargeted) were assessed at each developmental stage, with approximately 9 embryos in each group. Statistically significant increases in binding of approximately twofold ($p<0.05$) of the VEGFR2 targeted bubbles was observed at all time points, as shown in Figure 3. Immunohistochemical staining of preserved embryo sections is currently underway in an attempt to quantify the fluorescence signal for comparison with the targeted bubble binding ultrasound signal.

**Figure 2.** Molecular imaging of VEGFR-2 targeted microbubbles in a day 15.5 mouse embryo.

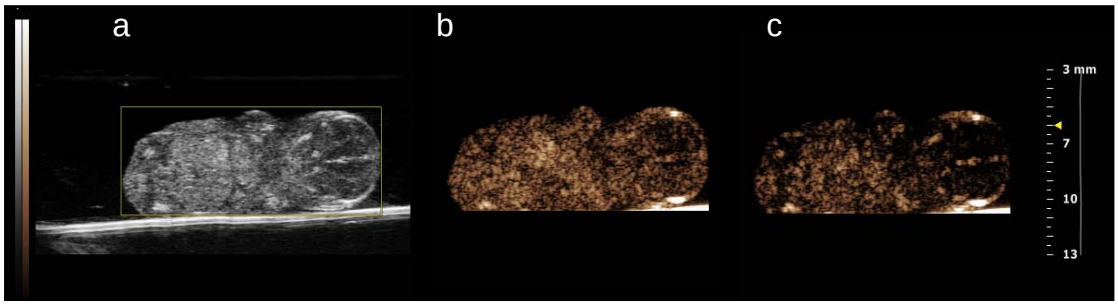


(a) B-mode image of E15.5 embryo with bubbles; (b) Nonlinear contrast mode image of bubbles circulating in E15.5 embryo after 6 minutes; (c) Non-linear contrast mode image of same embryo shortly after a burst pulse. Mean signal intensity from the bubbles decreases by a factor of approximately 2.

**Figure 3.** Microbubble binding across embryo stages.

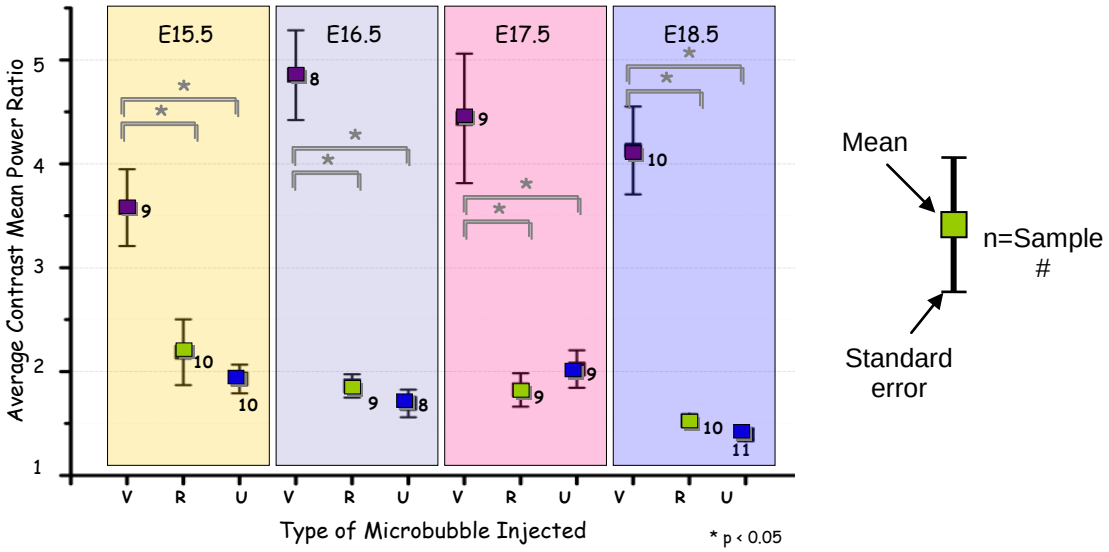


Embryos of various developmental stage (E15.5-E18.5) were injected with either VEGFR-2 targeted (V), Rat Isotype control IgG2 (R), or Untargeted (U) microbubbles. A significant difference ($p<0.05$) in the Average Contrast Mean Power Ratios was found between the binding of VEGFR-2 targeted and control bubbles ('R','U'). No significant difference in bubble binding was observed across embryo stages.

Initial results show that the technical aspect of introducing microbubbles into the living embryo vasculature is achievable and reproducible. Best results were obtained with slow infusions (0.02mL/min) of 20 uL of concentrated untargeted, rat isotype targeted, or VEGFR-2 targeted microbubble contrast agent. Careful monitoring of embryo temperature resulted in survival times of up to 4 hours while contained within the yolk sac, and approximately 30 minutes once warmed and injected. For molecular imaging, optimal destruction reperfusion experiments were carried out after a delay of 6 minutes (compared to the traditional 4 minutes in the adult mouse). This time requirement may reflect alternative mechanisms for agent clearance in the mouse embryo. Finally, Figure 3 demonstrates the feasibility of performing molecular imaging in embryos, an advantage from both a developmental biology and angiogenic perspective.

In summary, the development of useful contrast imaging methods for mouse embryos may provide a useful model for quantitative studies of angiogenic and developmental markers at high ultrasound frequencies.

**References**


1. Rychack et al., Molecular Imaging, 2007
2. Lyshchik, A., et al., J Ultrasound Med, 2007
3. Willmann, JK., et al., Radiology, 2008

# Echo Particle Image Velocimetry (Echo PIV): A novel contrast ultrasound-based method for the *in vivo* measurement of wall shear stress in human carotid arteries

***Gates PE*[1], *Zhang F*[2], *Strain WD*[1], *Gosling OE*[1], *Mazzaro L*[1], *Barker AJ*[2], *Fulford J*[1], *Shore AC*[1], *Bellenger NG*[1], *Lanning C*[3], *Aizawa, K*[1], *D'Abate, F*[1], *Shandas R*[4]**

[1]*Diabetes and Vascular Medicine, Peninsula Medical School, Exeter, Devon, United Kingdom,*
[2]*Dept of Mechanical Engineering, University of Colorado, Boulder, Colorado, USA,*
[3]*Center for Bioengineering, University of Colorado, Denver, Colorado, USA,*
[4]*Dept of Pediatric Cardiology, The Children's Hospital, Aurora, Colorado, USA*

**Introduction**

Wall shear stress (WSS) is an important factor in vascular health, vascular remodelling and plaque vulnerability. The carotid artery is at increased risk of atherosclerotic disease in areas of low or high shear stress like the bifurcation and downstream of an atheromatous plaque. At present wall shear stress is difficult to assess routinely. We have developed a novel ultrasound-based technique called Echo PIV to measure detailed blood flow and WSS. This method combines conventional B-mode ultrasound and contrast agent to generate 2-D velocity vector maps with high temporal resolution (up to 0.7 ms) and excellent spatial resolution (up to 0.4 mm) from which WSS can be calculated.

**Purpose and Methods**

In this study we compared WSS using Echo PIV to that obtained using phase-contrast MRI in the right common carotid artery in 10 healthy volunteers. Data obtained from 7-10 cardiac cycles were ensemble averaged using concurrent ECG and a blood viscosity of 3.2 centipoise was assumed.

**Results**

Wall shear stress (dyne/cm$^2$, mean±SD) for Echo PIV *versus* MRI were 21.1±6.5 *versus* 17.0±3.4 (peak systole), 4.0±1.7, *versus* 4.3±1.1 (end-diastole) and 8.7±2.5 *versus* 7.7±1.5 (mean). The overall error of Echo PIV against MRI was calculated as 10%±28%.

**Conclusions**

Reasonable agreement was found for WSS between Echo PIV and MRI. Discrepancies between the two techniques may arise from different artery slice orientations and localization between scans, inherent variability occurring at different testing times and environments. Echo PIV has is promising as a simple to use, less-costly bedside technique in the assessment of arterial haemodynamics.

# Distal arterial wall pseudoenhancement in ultrasound contrast imaging of carotids

***G. Renaud [1], G.L. ten Kate [4,3], Z. Akkus [1], S.C.H. van der Oord [1,3], A.F.L. Schinkel [4,3], J.G. Bosch [1], A.F.W. van der Steen [1,2] and N. de Jong [1,2]***

*[1] Biomedical Engineering, Thorax Center, Erasmus MC, Rotterdam, The Netherlands*
*[2] Interuniversity Cardiology Institute of the Netherlands, Utrecht, The Netherlands*
*[3] Dept. of Cardiology, Thoraxcenter, Erasmus Medical Center, Rotterdam, The Netherlands*
*[4] Division of Pharmacology, Vascular and Metabolic Diseases, Dept. of Internal Medicine, Erasmus MC, Rotterdam, The Netherlands*

Ultrasound contrast imaging of carotid intraplaque vasa vasorum was investigated in 80 patients performed with a Philips iU22 equipped with a L9-3 probe and SonoVue (Bracco S.p.a., Milan, Italy). For all patients an enhancement appears right after the distal wall of the carotid in the contrast image while the location of this enhancement is not associated with the anatomical location of a parallel vessel. Moreover after applying a flash to destroy microbubbles flowing in the field of view or observing the first arrival of contrast agent in the lumen after a new injection, the far wall enhancement turns out to be synchronized with the appearance of contrast agent in the lumen. Furthermore this enhancement describes patterns very similar to the ones observed at the same location on the B-mode image. Therefore this was suspected as being an artifact and studied in vitro using a tissue mimicking phantom.

A cylindrical vessel in the phantom is filled with SonoVue prepared with different dilutions and for native suspensions and mechanically filtered suspensions containing only small bubbles (diameter $< 3\mu m$). The phantom was then imaged with the same ultrasound system at the same low mechanical index (0.06). Whereas the artifact is barely observed with native suspensions of SonoVue, the filtered suspensions generate an enhancement right after the far wall of the vessel similar to in vivo images while no microbubbles are flowing at this location, hence this is an artifact. The artifact is thought to arise from the backscattering of the nonlinearity accumulated all along propagation from the probe to the far wall by echogenic soft tissue located right after the arterial far wall. However the artifact appears significantly if the attenuation experienced through the lumen during backpropagation is low enough.

The importance of the artifact created in vivo suggests that the attenuation induced by contrast agent in the lumen is relatively low. The flow of microbubble contrast agents through the lung capillaries and/or environmental chemical and physical conditions in blood may suppress large bubbles observed in vitro within a native suspension of SonoVue and consequently reduce the attenuation exhibited by a native size distribution of microbubbles.

The development of new imaging strategies for contrast detection or specific image post-processing is required to reduce the artifact and allow a reliable detection of intraplaque vasa vasorum at the far arterial wall.

*This research was supported by the Center for Translational Molecular Medicine and the Netherlands Heart Foundation (PARISk).*

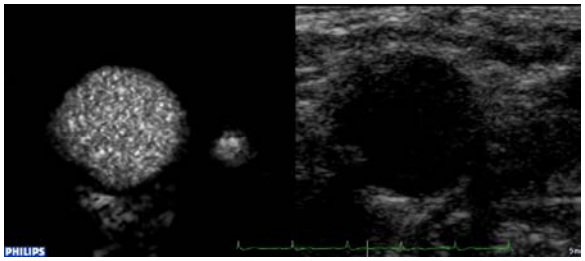


**Transversal contrast-enhanced ultrasound images of a carotid. Left: contrast mode. Right: B-mode.**

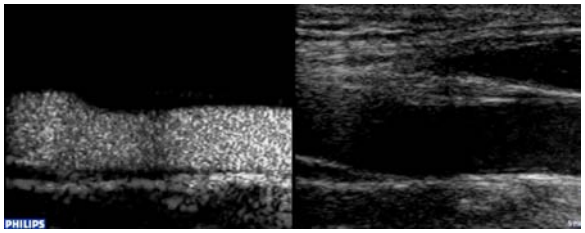


**Longitudinal contrast-enhanced ultrasound images of a carotid. Left: contrast mode. Right: B-mode.**

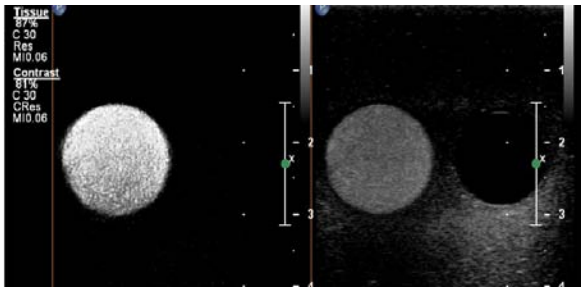


**Transversal images of the tissue mimicking phantom when the left vessel is filled with a native suspension of contrast agent. The right vessel is filled with degassed water. Left: contrast mode. Right: B-mode.**

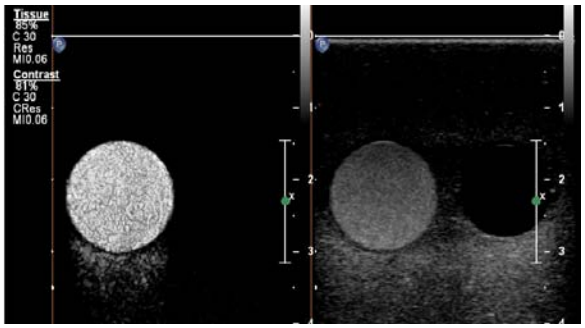


**Transversal images of the tissue mimicking phantom when the left vessel is filled with a filtered suspension of contrast agent. The right vessel is filled with degassed water. Left: contrast mode. Right: B-mode.**

# A method to create complex microvessel flow phantoms for high resolution ultrasound studies

***Ryan C. Gessner[1], Roshni Kothadia[1], Steven Feingold[1], Paul A. Dayton[1]***

*[1] - Joint Department of Biomedical Engineering - UNC and NCSU*
*Chapel Hill, North Carolina, USA*

**Introduction**

When assessing disease response to therapy, the relationship between vascularization and disease state is an important one. Indeed, many new imaging strategies are being developed to detect subtle changes in vascularization as a metric for quantifying the effects of administered therapies. The development and implementation of these imaging techniques, along with their corresponding image analysis strategies, requires an understanding of their resolution and detection sensitivity as well as their sensitivity to corruption by the realities of in-vivo imaging studies (i.e. respiratory motion, signal attenuation, etc.). In-vitro phantoms are implemented as a means to simulate anatomically relevant structures in a controlled environment to test sensitivity as well as the effects of these variables.

Blood vessel mimicking phantoms are often constructed of either acoustically transparent cellulose tubes set in gelatin for support, or wall-less gelatin bores through which contrast can be flowed and imaged. While these techniques are sufficient to test an imaging strategy's sensitivity or signal to noise ratio, they are suboptimal in creating environments for simulating blood flow which have non-trivial structures. Because the resolutions of the high-frequency ultrasound techniques are all below 1 mm, simulating vessels with structural features at or below these scales can be prohibitively difficult using wall-less bores or cellulose tubes in gelatin. This is a problem which most affects those attempting to characterize the structural morphologies of individual vessels or vessel networks as markers for disease.

We present a novel method of generating individual 3D vessel phantoms with predefined coordinates of nearly any shape. Our vessel phantoms can be constructed with < 10 μm precision. The technique is extended to the generation of entire vasculature networks with basic image addition of the independently constructed vessels. The principle behind our strategy is that an object is imaged while also being translated by a computer-controlled motion stage. If this motion occurs between imaging frames, the vessel's path will appear continuous in the final 3D image. The strategy could be beneficial for determining the accuracy and sensitivity of imaging and image-analysis techniques attempting to quantify the structural morphology of vessels or vessel networks, as well techniques quantifying blood flow speed. It can also aid in determining imaging resolution, sensitivity to artifacts, and detection

sensitivity for any of the ultrasound imaging strategies commonly implemented for vascularity assessment.

**Methods**

The complex microvessel flow phantoms generated in this manuscript were created by spatially manipulating an object being imaged between individual image captures. The physical target which we imaged was constructed from a single 200 μm cellulose tube. A polydisperse distribution of microbubble contrast agents pumped through the tube. The tube was suspended in a water bath from the arm of a precise three-axis Newport motion stage. A contrast-specific high resolution imaging method was implemented as previously described (Gessner - 2010). 3D images were acquired via the ultrasound system's translational motor stage, with an inter-frame step size of 0.05 mm.

Prior to phantom imaging, X-Y-Z coordinates of the desired vessel's centerline were created in Matlab and exported as tab-delimited text files. Nearly any arbitrarily-shaped vessel curve could be generated, provided the resulting centerline did not fail the"vertical line test". A custom LabView program was written on a PC to control the motion stage. The transducer was positioned over the tube, with the tube's axis oriented normal to the imaging plane, and parallel to the direction of the transducer's translational motor stage. The frame trigger from the ultrasound system was used to trigger the PC, which then moved the tube to the next X-Y coordinate in its centerline.

**Results**

Microvessel phantoms were generated with different morphologies, including a simple linear trajectory to measure imaging depth of field at different acoustic pulsing pressures, a single vessel with increasing tortuosity, and a four vessel network with 3 independent bifurcations. The four vessel network was generated twice, with the angles at which the vessels bifurcate modulated to simulate the onset of disease.

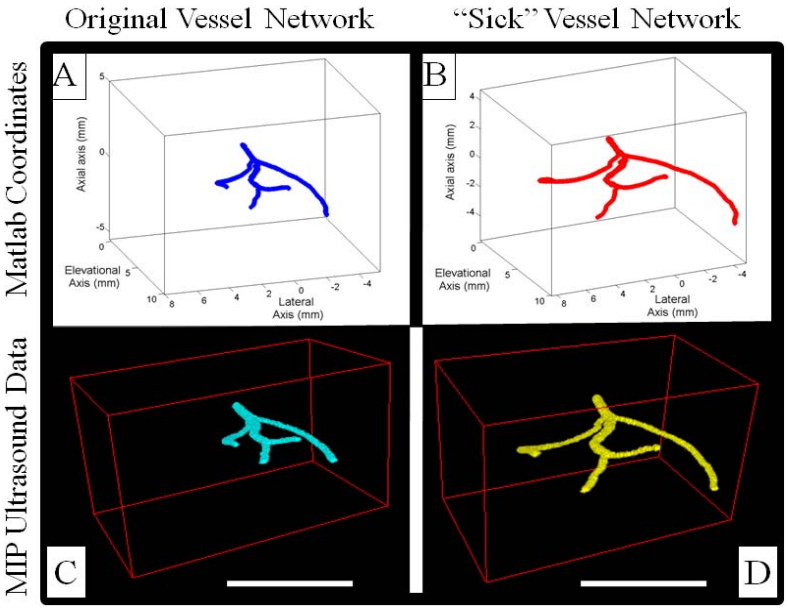


**Figure 1: A and B - 3D plots of the predefined X-Y-Z coordinates of the 4 vessel network. C and D - The corresponding ultrasound data. These ultrasound maximum intensity projections (MIPs) were created in ImageJ and have been thresholded to remove background noise. The vessel network was altered to simulate the onset of disease (Sugimoto - 2010) Scale bars in C and D represent 1 cm.**

**References**


1. Gessner R, Lukacs M, Lee M, Cherin E, Foster FS, Dayton PA. High-resolution, high-contrast ultrasound imaging using a prototype dual-frequency transducer: in vitro and in vivo studies. IEEE Trans Ultrason Ferroelectr Freq Control. 2010 Aug;57(8):1772-81.
2. Sugimoto K, Shiraishi J, Moriyasu F, Ichimura S, Metoki R, Doi K. Analysis of intrahepatic vascular morphological changes of chronic liver disease for assessment of liver fibrosis stages by micro-flow imaging with contrast-enhanced ultrasound: preliminary experience. Eur Radiol. 2010 Nov;20(11):2749-57.

# Tuning ultrasound exposure duration to microbubble sonodestruction process for bleomycin sonotransfer in vitro

***M. Tamošiūnas[1], R. Jurkonis[2], L.M. Mir[3], A. Lukoševičius[2], M.S.Venslauskas[1], S. Šatkauskas[1]****

*[1]Department of Biology, Faculty of Natural Sciences, Vytautas Magnus University, Lithuania*
*[2]Institute of Biomedical Engineering, Kaunas University of Technology, Lithuania*
*[3]UMR 8121 CNRS, Institute Gustave-Roussy, Villejuif Cedex, France;*

**Introduction**

Sonoporation is being developed as a new cancer treatment modality based on intracellular delivery of various exogenous molecules: transfer of plasmids for inactivation of oncogenes, replacement of defective tumour suppressor genes, production of proteins inducing antitumour effects, or the delivery of antiangiogenic factors, cytokines, cytotoxic proteins and therapeutic drugs. Recently, sonoporation (using the contrast agents Sonovue and Optison) in combination with administration of bleomycin (BLM) successfully reduced the volume of transplanted tumours. However, the application of ultrasound at the intensities needed for cell sonoporation often results in cell death and healthy tissue damage. Because of safety reasons these hazardous bioeffects has to be resolved before sonoporation is applied in clinical trials.

One of the reasons of uncontrolled cell damage is the lack of ultrasound exposure duration dosimetry. We tested the hypothesis that US exposure duration could be derived from the kinetics of MB disappearance after undergoing cavitation in US field (MB sonodestruction). To this end we used diagnostic ultrasound for the visualization of MB sonodestruction to find out optimal US exposure duration resulting in the highest level of BLM sonotransfer and control cell viability.

**Methods**

***Ultrasound exposure***

A 34 mm diameter ultrasound transducer (Ультразвук Т-5, ЭМА, Moscow) operating at 880 kHz was placed below the exposure well (made of plastic, the diameter of the well wall was 70 μm). The acoustic gel was used for the contact between the transducer and the well. Cell were exposed to ultrasound (100% DC) at at peak negative pressure $p_{pn}$=500 kPa for various times ranging from 0.5 to 30 s. The accuracy of the US exposure duration was assured by incorporating a high precision time relay (H5CX, Omron) with a minimal programmable time step of 0.01 s.

***Microbubble preparation***

The microbubbles were prepared after dissolving 1 mg of lyophilized powder (containing macrogol 4000, distearoylphosphatidylcholine, dipalmitoylphosphatidylglycerol, and palmitic acid) in 200 µl of the exposure medium (EM) followed by vigour pipetting. Under the preparation conditions the gas filling of the microbubbles was air. The average concentration of the microbubbles (estimated up to 2 min post microbubble preparation) was $6x10^7$ MB/ml.

***Experimental setup***

Chinese hamster ovary cells were used in experiments. The cell suspension at a final concentration of $1x10^6$cells/ml was prepared in the EM (containing 0,25M sucrose, 1 mM magnesium chloride (hexahydrate) buffered with 10 mM of disodium hydrogen phosphate, pH=7,2). To evaluate number of reversibly sonoporated cells 5 µl of BLM was administrated at the final concentration of 20 nM. 5 µl of EM was delivered for the control groups as the substitution for either MB or bleomycin BLM:

$$40\mu l(cells)+5\mu l\begin{pmatrix}BLM\\EM\end{pmatrix}+5\mu l\begin{pmatrix}MB\\EM\end{pmatrix}+US(0s;0.5s;2s;5s;15s;30s)$$

The viability of the cells in the control and US treated groups was assessed using the cell colony formation test.

***Diagnostic ultrasound imaging***

The chamber cross-section was scanned with an A/B echoscope MentorTM (Advent, Norwell, MA) with ultrasound centre frequency of 12 MHz, (pulsed wave, spatial peak pulse average intensity, $I_{SPTA3}$ = 0.3 mW/cm$^2$; MI=0.22). Period of repetition of B-scan frames was 117ms. Echoscope output video signal from SVideo terminal was connected to external USB TV tuner, which recorded video sequences of B-Scan images into computer hard-disc for data analysis. The B-scan image intensity dynamics was estimated as a function of the time in the selected regions of interest. The period of intensity estimation was assumed constant, equal to the mean inter-frame period in NTSC video record, which was estimated to be 33 ms.

**Results**

The B-Scan images of freshly prepared microbubbles (upper image) and those that were affected with therapeutic ultrasound (lower image) are shown in Fig. 1, right panel. Following the reconstitution of MB, the white pattern of the treatment chamber in the B-scan image appeared because of high sample echogenicity. The decrease of the white intensity in the B-Scan images during US exposure corresponded to the decrease of microbubble concentration. The diagrams in Fig. 1 left panel show the therapeutic ultrasound induced MB sonodestruction kinetics following a monoexponential decay with a time constant ($\tau$) of 122±10 ms. The complete MB sonodestruction by US at $p_{pn}$=500 kPa was achieved within fractions of second. The influence of diagnostic ultrasound on MB concentration decay was very weak, affecting 1.5% of MB during the first second of US exposure.

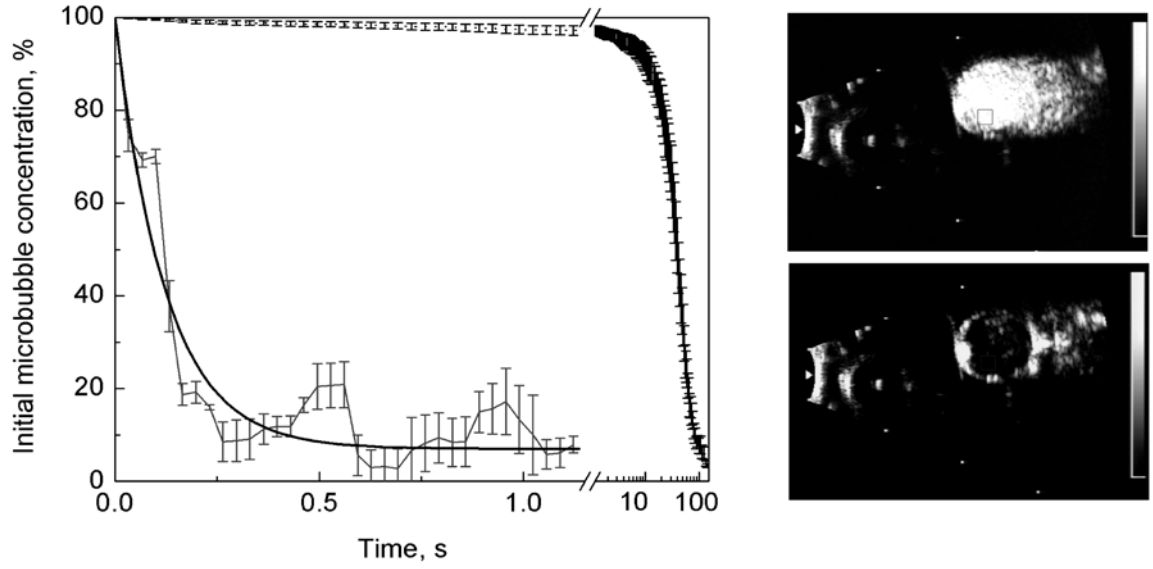


**Fig. 1. The kinetics of microbubble sonodestruction during exposure of US at acoustic pressure Ppn=500 kPa (solid line) and during exposure to diagnostic ultrasound alone (dotted line). Right panel: B-scan images of the first and the last frames in video sequence, showing high density (106 units in 200 µl) of microbubbles before (top image) and after (bottom image) exposure of US at Ppn=500 kPa for 0.5 s.**

In subsequent experiments we evaluated the number of reversibly sonoporated cells to BLM after cell exposure to US in dependence of US exposure duration (0.5, 2, 5, 15 and 30 s). Intracellular BLM entry was facilitated by US alone (in the absence of MB). At low 5-20 nM concentrations BLM has low cytotoxicity, however once inside the cell, its toxicity drastically increases. The number of bleomycin killed cells was about 8% for US exposure duration of 0.5 s (Fig. 2 open symbols). Slight but significant ($p<0.05$) increase in BLM induced cell death levelling at 16% was obtained at US exposure durations ranging between 2 and 30 s. Cell exposure to US in the presence of MB resulted in significantly larger number of reversibly sonoporated cells. Indeed, the number of reversibly sonoporated cells increased from 8 to 25% after US exposure duration of 0.5 s (Fig. 2B, filled symbols). The maximum level of

sonoporated cells was already achieved 0.5 s after the onset of the US exposure, implying that cell sonoporation to BLM was mainly the consequence of US induced microbubble cavitation. The efficiency of sonoporation was further independent on the applied US exposure duration. However the increase in US exposure duration resulted in significant decrease of cell viability (Fig. 2A). The number of cells killed both in the presence or absence of MB increased with gradual increase of US exposure duration. At the highest US-alone exposure duration tested, cell viability decreased for 25 % with no contribution to additional percentage of cell sonoporation. However, when US was applied for 0.5 and 2 s, cell viability did not decrease. Therefore, in the presence of MB, the highest level of sonoporated cells together with the lowest level of US induced cell death was achieved at 0.5 s, which corresponds to the time required for complete sonodestruction of initially prepared MB.

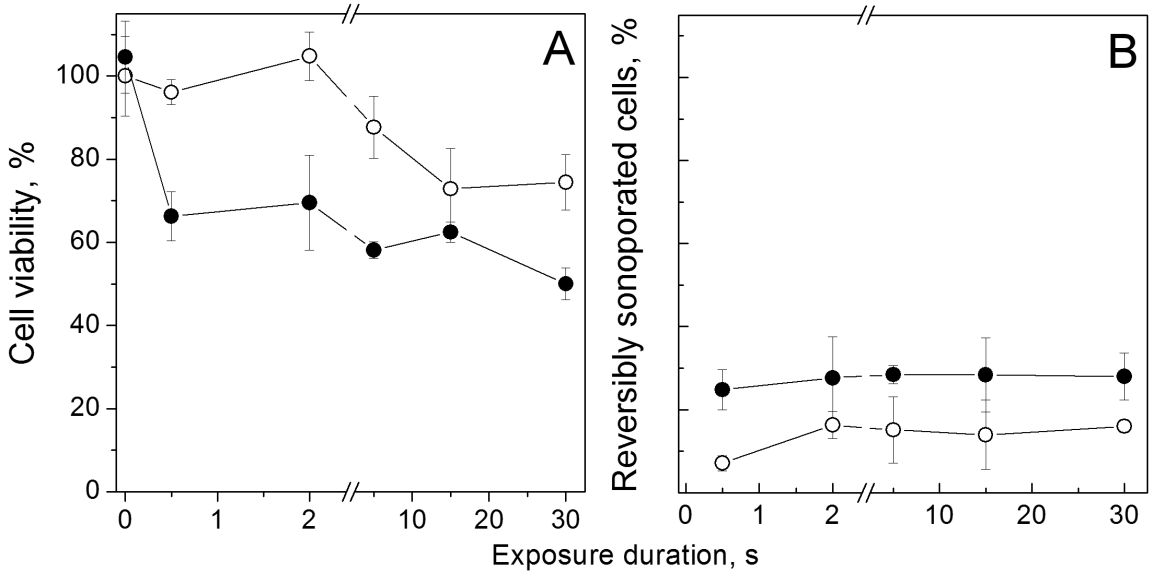


**Fig. 2. Cell viability (panel A) and number of reversibly sonoporated cells (panel B) after cell exposure to US in dependence of US exposure duration. Cells were exposed to US in the absence (panel A) and in the presence (panel B) of cytotoxic drug bleomycin (20 nM) at acoustic pressure of Ppn = 500 kPa in the absence (open symbols) and in the presence (filled symbols) of microbubbles.**

In conclusion, we propose a model for the implicit dosimetry of the US exposure duration for BLM sonotransfer. The microbubble cavitation dependent time interval was proved to be responsible for most efficient cell sonoporation to BLM. Aiming to achieve the highest level of sonoporated cells, preserving the highest level of cell viability, the duration of US exposure should not exceed the duration needed for MB sonodestruction.

# Nonlinear Propagation Models for ultrasound pulse propagation through a polydisperse bubble population

***Jean-Pierre O'Brien[1], Eleanor Stride[1], Nick Ovenden[1], Meng-Xing Tang[2], Robert J. Eckersley[2]***

*[1]University College London, United Kingdom*
*[2]Imperial College London, United Kingdom*

The presence of microbubble contrast agents in a liquid can dramatically affect the propagation characteristics of ultrasound. A number of models have been proposed to describe the effects of a bubbly medium on a travelling wave using an inhomogeneous wave equation coupled to an equation governing the bubble dynamics[1,2,3] as follows:

$$\frac{1}{c^2}\frac{\partial^2 p_l}{\partial t^2} - \nabla^2 p_l = 4\pi\rho\int\left[R^2\frac{d^2R}{dt^2} + 2R\left(\frac{dR}{dt}\right)^2\right]nda$$

$$p_{g0}\left(\frac{R_0}{R}\right)^{3\kappa} - p_l(t) = \rho\left(R\frac{d^2R}{dt^2} + \frac{3}{2}\frac{dR}{dt}^2\right) + \frac{4\mu}{R}\frac{dR}{dt} + \frac{2\sigma}{R}$$

where $p_l$ is the pressure in the liquid, $c$ and $\rho$ are the wavespeed and density of the liquid respectively, $n$ is the bubble population distribution, $R$ is the radius of the bubble, $p_{g0}$ is the initial pressure inside the bubble, $R_0$ is the initial bubble radius, $\kappa$ is the polytropic index, and $\sigma$ and $\mu$ are the surface tension and viscosity respectively. However, for polydisperse bubble populations, these models are computationally expensive and show limited accuracy when results are compared to those from experiments, particularly for concentrated suspensions of resonant bubbles.

A number of reasons have been proposed to explain these discrepancies including: (i) the nature of the shell model used; (ii) the neglect of changes in the bubble population over time due to gas diffusion and/or changes in the shell properties; (iii) the failure to account for the spatial distribution of the microbubbles and hence incorrect treatment of the effects of phase cancellation particularly between differently sized bubbles. In this study, the influence of these factors on the propagated wave was investigated through a combination of numerical simulations and analytical approximations. Strategies for reducing the computational complexity of the problem and their validity were also investigated, in particular modelling the medium as a series of homogeneous bubble "sheets"[4].

It was found that the sheet approximation accurately reproduced the results obtained from the full model with substantial improvements in computational efficiency. The reduction in computation time

was proportional to the fineness of the discretisation scheme used to model the bubble size distribution. The parameter regime within which good agreement is obtained and the underlying reasons are subject to ongoing analysis.

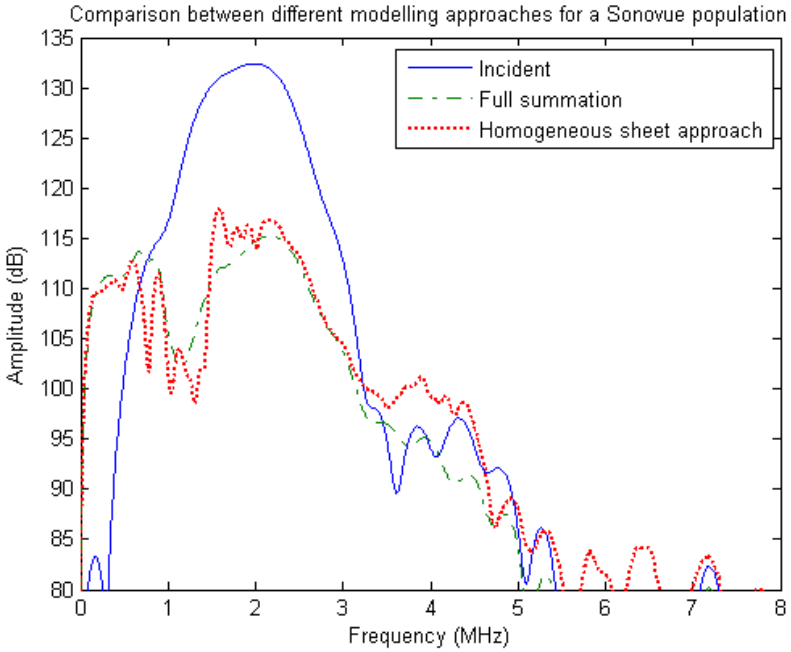


**Figure 1: Comparison of frequency spectra of pulses propagated 6cm through a Sonovue® population of concentration 4 x $10^{10}$ bubbles/m3 modelled using the old model and the homogeneous sheet approach. The blue line represents the spectrum of the incident pulse, the green line is the full model and the red line is the sheet approach. One can notice their relative similarity in sub-harmonic, fundamental and harmonic frequencies.**

Using a microbubble shell model which includes nonlinear characteristics[5] and also deterioration was found to greatly improve agreement with experimental results in terms of the predicted harmonic content.

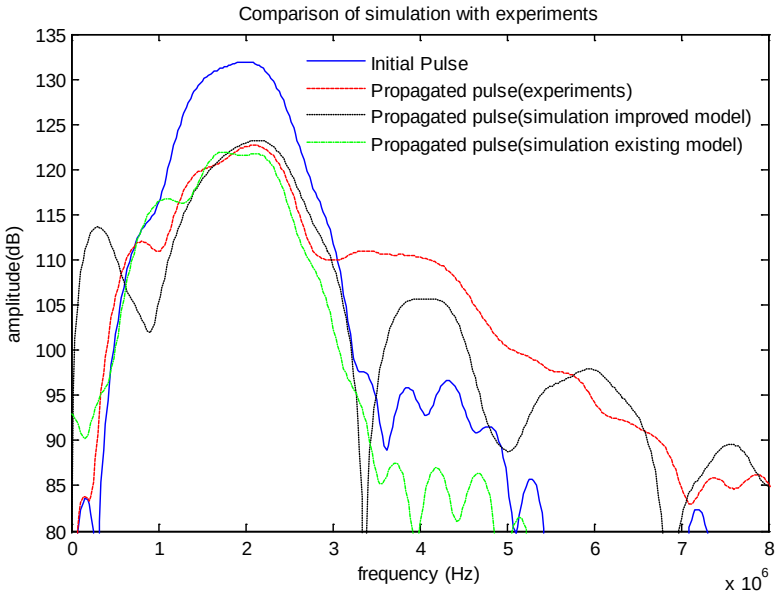


**Figure 2: Frequency spectra of propagated pulses using a nonlinear shell model: experiment vs. 2 microbubble models (shows control, existing and improved)[6]**

Results from incorporating spatial information in the form of phase differences between the responses from different bubbles also indicated that this is significant factor. It was determined however that, although the predicted rate of bubble dissolution can increase when bubbles are insonified compared to the static situation, this does not appear to have a significant effect upon the propagated wave since a dissolution time of around 0.02s remains considerably longer than that of the pulse propagation length.

Improving the predictive capability of propagation models in this way will facilitate the development of more accurate software for quantitative imaging and monitoring in therapeutic applications.

**References**


1. Commander, K and Prosperetti, A. [1989] Linear pressure waves in bubbly liquids: Comparison between theory and experiments J. Acoust. Soc. Am. 85(2), pp. 732-746
2. Stride, E. and Saffari, N. [2005], Investigating the Significance of Multiple Scattering in Ultrasound Contrast Agent Particle Populations, IEEE Transactions on Ultrasonics, Ferroelectrics and Frequency Control 52(12), 2332-2345.
3. Tang, M. and Eckersley, R. [2006], Nonlinear Propagation of Ultrasound Through Microbubble Contrast Agents and Implications for Imaging, IEEE Transactions on Ultrasonics, Ferroelectrics and Frequency Control 53(12), 2406-2415.
4. Hibbs, K., Mari, J., Stride, E., Eckersley, R., Noble, A. and Tang, M. [2007], Nonlinear Propagation of Ultrasound through Microbubble Clouds: A Novel Numerical Implementation, in IEEE Ultrasonics Symposium, pp. 1997-2000.
5. Marmottant, P., van der Meer, S., Emmer, M., Versluis, M., de Jong, N., Hilgenfeldt, S., Lohse, D. [2005], A Model for Large Amplitude Oscillations of Coated Bubbles Accounting for Buckling and Rupture, J. Acoust. Soc. Am. 118(6), pp. 3499-3505.
6. Tang M-X., Loughran J., Stride E., Zhang D. and Eckersley R.J., Effect of bubble shell nonlinearity on ultrasound nonlinear propagation through microbubble populations at low acoustic pressure, submitted to J. Acoust. Soc. Am. Express Letters.

# In-vitro measurement of flow rate with bolus injection of contrast agent and DCE-US based on indicator dilution method

***Marios Lampaskis and Michalakis Averkiou***

*University of Cyprus, Nicosia, Cyprus*

## Introduction

Dynamic contrast enhanced ultrasound imaging (DCE-US) has been used successfully to detect and characterize tumors. This technique has provided new opportunities in oncology therapy monitoring [1]. All therapy regimes need feedback so as to optimize their effectiveness, adjust doses or change to a different therapy if deemed necessary. To evaluate the effectiveness of antiangiogenic therapies, an assessment of perfusion through measurements of hemodynamic parameters related to blood volume and blood flow is needed. DCE-US coupled to indicator dilution techniques can lead us to perfusion flow measurements.

The aim of this work is to combine indicator dilution theory [2] with DCE-US to measure relative blood flow rate. Detailed in-vitro flow measurements demonstrate the range of validity of indicator dilution theory for DCE-US while at the same time the reproducibility of the method is evaluated. The relationship of indicator dilution parameters such as the mean transit time, time to peak, and the area under the curve [3, 4, 5], is correlated with relative flow rate and volume.

## Materials and method

To evaluate the relationship between flow rate and quantifiable parameters form time-intensity curves an in-vitro experiment was designed. De-ionized water was pumped with a digital peristaltic pump (Masterflex®, Cole-Palmer, Vernon Hills, IL, USA) (a pulse dampener was employed to reduce the pulsatility) into a tissue mimicking flow phantom via flow meter to confirm set flow rate, and a mixing chamber (approx. 20 ml) to ensure the homogeneity of the imaged solution. The contrast agent was injected just before the mixing chamber. A schematic representation of the flow setup is shown on figure 1 below.

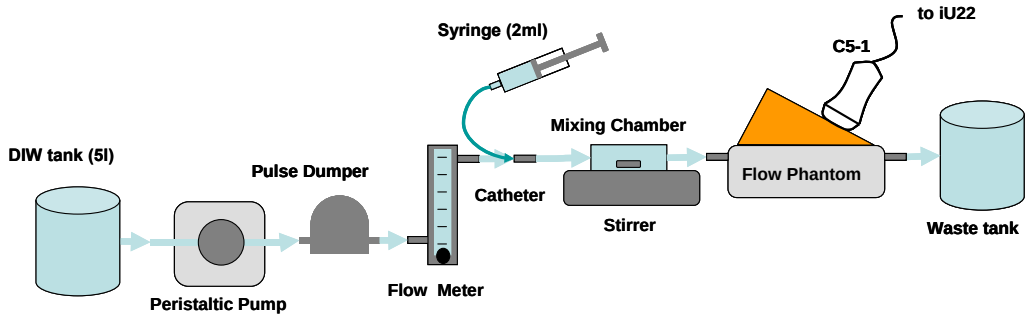


**Fig. 1 Schematic of the in-vitro flow setup**

The bolus consisted of a 0.5 ml solution of contrast agent (BR14, Bracco S.P.A., Milan, Italy) and de-ionized water (1.67%). It was administered with a 2 ml syringe as fast as possible so as to mimic an impulse input. The contrast agent concentration was scaled to mimic those expected in-vivo. A curve-linear array C5-1(iU22, Philips Medical Systems, Bothell, WA, USA) transducer was placed in line able to image an 8 mm flow channel to a depth of approximately 12 cm. Seven flow rate settings were used from 25 ml/min up to 175 ml/min at a 25ml/min interval. Five bolus injections were performed for each flow rate setting. To minimize variation in the contrast agent solutions we performed all measurements from the same vial of agent and conducted the experiment as fast as possible. The duration of the measurements was approximately one hour.

Contrast Side/Side imaging with power modulation was used. The transmit center frequency was 1.5 MHz. Image loops of 15 s to 60 s (depending on flow rate) were acquired. Image compression was set at the maximum available on the iU22 (50 dB) to best accommodate a large range of signals and avoid saturation. The 2D gain was noted and kept constant though out the experiments. The MI used was 0.05 for the contrast side (power modulation) and 0.04 for the tissue side; with a focus at 12 cm. Time-intensity curves were formed from acquired image loops using QLAB (Philips Healthcare, Andover, MA, USA). QLAB removes the logarithmic compression of the images before any further processing. The ROIs were placed exactly in the same area of the flow vessel in every loop. An example of ROI selection is shown in figure 2.

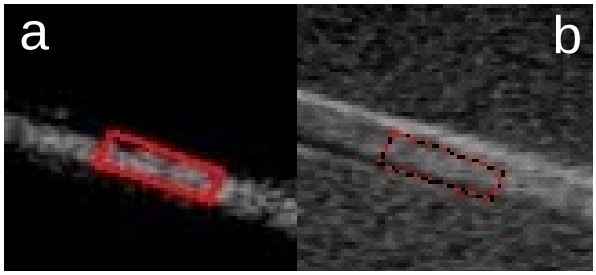


**Fig. 2 Example of ROI selection on a CEUS image of the flow phantom obtained after a bolus injection. (a) Contrast side image and (b) tissue side image.**

A lognormal model [5] was applied to each time intensity curve using purpose created MATLAB code (MathWorks, Inc., Natick, MA, USA). The MATLAB code performs an iterative non-linear regression curve fit based on the minimization of least square errors using the built-in MATLAB Trust Region algorithm. The lognormal model with a delay $t_0$ is given by:

$$I(t) = \frac{AUC}{\sqrt{2\pi}\sigma(t-t_0)} e^{\frac{[\ln(t-t_0)-\mu]^2}{2\sigma^2}} + I_0, \quad (1)$$

where *I(t)* is the backscattered signal intensity (which is proportional to indicator concentration [6] as a function of time. The variables $\mu$ and $\sigma$ are the mean and standard deviation of the normal distribution of the logarithm of the independent variable *t*. $I_0$ is the baseline intensity offset due to the noise level

present in the image and the background backscatter from the ROI (without bubbles). The inclusion of $I_0$ in (1) applies specifically to ultrasound time-intensity and is not part of the original statistical model. The *MTT is* defined as the first moment of the probability density function ($I(t)$- $I_0$) minus the bolus arrival time $t_0$, and $t_P$ are given by:

$$MTT = e^{\mu+\sigma^2/2}, \; t_P = e^{\mu-\sigma^2}. \qquad (2)$$

**Results**

According to indicator dilution theory, the shape of the time-intensity curves changes when the flow rate is changed. An example of this can be seen on figure 3 where time-intensity curves with flow rates of 25, 50, and 100ml/min, respectively, are shown.

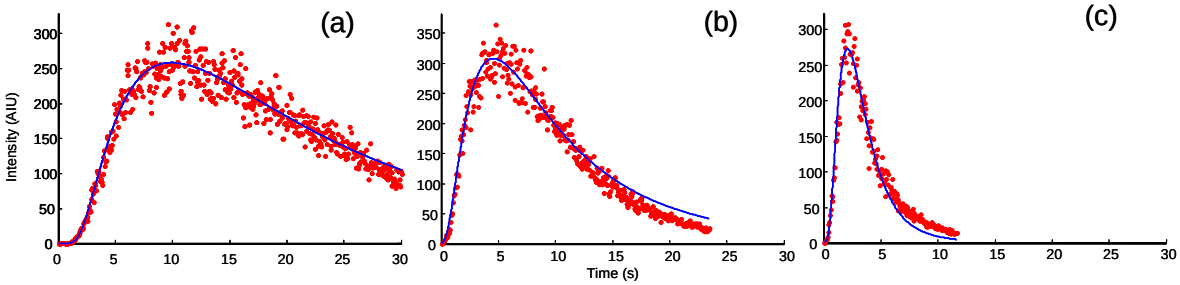


**Fig. 3 Examples of time-intensity curves obtained after a bolus injections. The flow rate is (a) 25 ml/min, (b) 50 ml/min, and (c) 100 ml/min.**

For each flow rate setting five injections were performed in order to facilitate a reproducibility study. The results obtained for each parameter are presented as a box plot to show the spread of the measurements. A box plot shows the sample maximum and minimum, the lower and upper quartile and the sample median. The results obtained for the MTT, $t_P$, AUC, and $I_P$ using lognormal model are shown in figure 4.

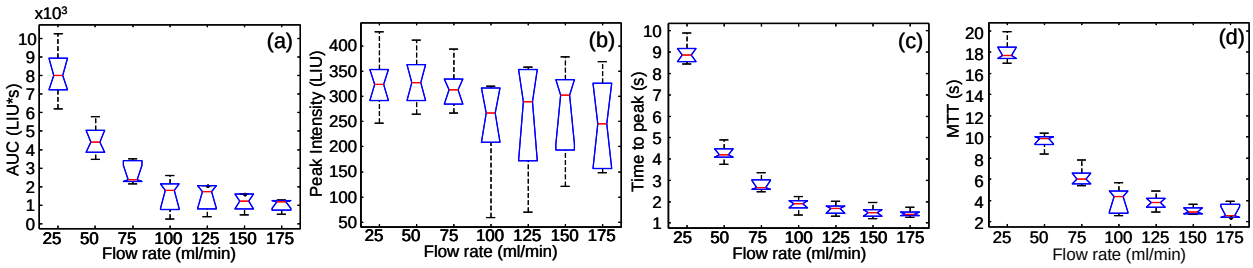


**Fig. 4 Box plots of the parameters extracted from the lognormal model and time intensity curves obtained following bolus injections for varying flow rates. (a) Area under curve, (b) peak intensity, (c) time to peak intensity, and (d) mean transit time.**

**Discussion**

The Steward Hamilton relationship is used to interpret the results of figure 4. Suppose that $X$ is amount of indicator is injected at $t = 0$, and that the concentration at time $t$, is $c(t)$. The flow rate $Q$ is assumed to be constant. During a time interval $\delta t$ an amount $Qc(t)\delta t$ of indicator will be wash out. Eventually all of the indication will leave the system thus,

$$X = Q\int_0^\infty c(t)dt\,. \qquad (3)$$

The imaged intensity is assumed to be linearly proportional to contrast agent concentration [7]. Thus the integral of concentration (Eq. 3) is equivalent to the area under the curve measured from time-intensity curves. The amount of indicator (contrast agent) injected remains constant during the experiment and thus $Q \propto 1/AUC$. The results shown in figure 4(a) qualitatively agree with Eq. (3), i.e., AUC is inversely proportional to flow rate. Similarly, the MTT and time to peak intensity are also found inversely proportional to flow rate as seen in figures 4(c)-(d). This confirms the relationship $V = Q * MTT$ [2]. The peak intensity appears to be largely unaffected by flow rate.

Another important finding is that when the volume of the bolus injection or the concentration the contrast agent is varied the relationships shown in figure 4 still hold. The MTT and time to peak intensity are reproducible with better than 10% variability and AUC and peak intensity vary linearly with the concentration of the injected bolus. When the concentration of contrast agent in the ROI is too high and causes signal saturation of the received acoustic signal the relationship of flow rate to the measured parameters seizes to be predictable.

In conclusion, indicator dilution methods [2, 3, 5] may be applied to DCE-US to allow for relative blood flow measurement. The variability of the measured hemodynamic parameters is less than 10%. Similar results have been obtained for flow of microbubbles in kidney dialysis cartridge which closer resembles microcirculation.

**References**


1. Averkiou M., Lampaskis M., Kyriakopoulou K., Skarlos D., Klouvas G., Strouthos C., Leen E., "Quantification of Tumor Microvascularity with Respiratory Gated Contrast Enhanced Ultrasound for Monitoring Therapy," Ultrasound in Med. & Biol. 36(1), 68-77, 2010.
2. Zierler K.,Indicator dilution methods for measuring blood flow, volume, and other properties of biological systems: A brief history and memoir, An . Biomed Eng., 28, 2000.
3. Mischi M., Jansen A. H. M., Korsten H. H. M., Identification of cardiovascular dilution systems by contrast ultrasound, UMB, 33, 439-451, 2007.
4. Ferrara K, Merritt C, Burns P, FS Foster, Mattrey RF, Wickline SA, Evaluation of tumor angiogenesis with us: Imaging, doppler, and contrast agents. Acad Radiol. 2000; 7:824 -839.
5. Qian H., Bassingthwaighte J. B., A class of flow bifurcation models with lognormal distribution and fractal dispersion, J. theor. Biol., 205, 261-268, 2000.
6. Lampaskis M., Averkiou M., "Investigation of the relationship of nonlinear backscattered ultrasound intensity with microbubble concentration at low MI" , Ultrasound in Med. & Biol. 36(2), 306-312, 2010

# High-speed fluorescence imaging of bubble-induced sonoporation

***Erik Gelderblom[1], Nico de Jong[1], Detlef Lohse[1], Michel Versluis[1], Floor Wolbers[2], Albert van den Berg[2]***

*[1]Physics of Fluids Group, University of Twente, Enschede, The Netherlands,*
*[2]BIOS Lab on a Chip group, University of Twente, Enschede, The Netherlands*

**Background**

Ultrasound contrast agents have proven to be able to enhance the endothelial cell permeability. A microbubble that vibrates near a cell can reversibly open the cell membrane, facilitating transfer of extracellular molecules into the cell. Van Wamel et al. [1] visualized the uptake of propidium iodide (PI) by endothelial cells surrounded by microbubbles after several seconds of ultrasound insonation at a mechanical index of 0.4. However, there is still a lack of detailed understanding of the physical mechanisms of sonoporation, particularly the time scales involved in ultrasound-induced uptake.

**Experimental setup**

Human umbilical vein endothelial cells (HUVEC) were grown in Opticells (Thermofisher, Denmark). Phospholipid-coated microbubbles with a perfluorobutane gas core were produced in-house (method described by Klibanov et al. [2]). The fluorescently labeled microbubbles were driven by ultrasound at a frequency of 1 MHz and at a pressure between 200 kPa and 1 MPa. A high-power CW laser was used as an excitation source for the fluorescent microbubbles as well as for the PI after penetrating the cell membrane. An acousto-optic modulator allowed for continuous and pulsed operation of the fluorescence excitation. High-speed recordings were made in color at 1000 frames per second using a Photron SA2 (San Diego, CA). A schematic overview of the setup is shown in figure 1.

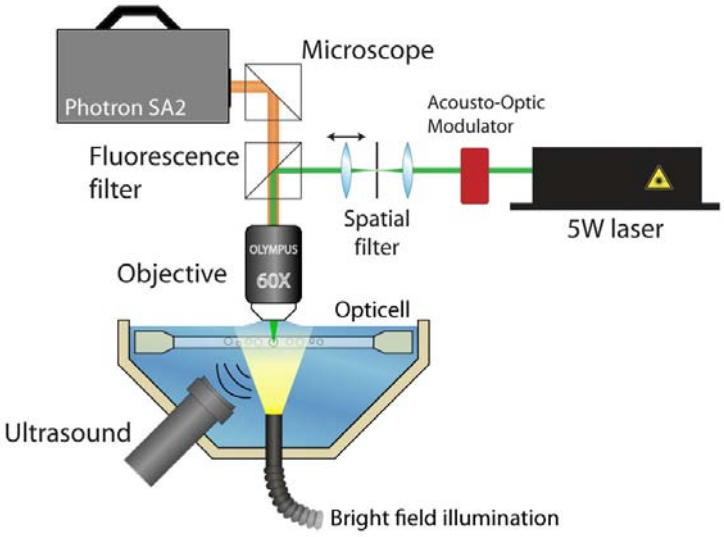


**Figure 1 – Schematic of the experimental setup**

**Results**

Figure 2 depicts a sequence of images taken with the high-speed camera, demonstrating the sonoporation process induced by microbubbles driven at 1 MPa. First, the laser is switched on, leading to green fluorescence of the microbubbles. The ultrasound excitation starts at t = 20 ms with 10 pulses of 20 cycles at a pulse repetition frequency of 500 Hz. Shortly after the insonation PI binding to nucleic acids inside the cytoplasm and nucleus is clearly marked by the red fluorescence.

After several minutes, the PI has fully penetrated into the cell nucleus. A strong signal is emitted by the PI binding to the DNA in the nucleus as well as the weaker signal from the PI binding to the RNA in the cytoplasm or the leaked DNA from the nucleus.

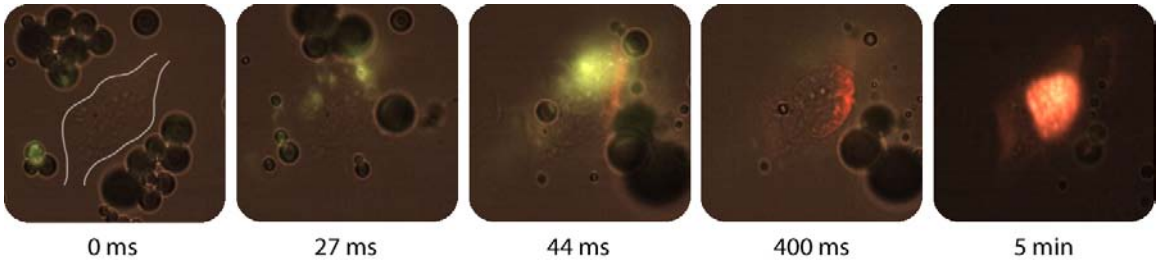


**Figure 2 – Combined bright-field and fluorescence recording of sonoporation. 0ms: fluorescent bubbles surround a HUVEC, 27ms: bubble oscillations, 44ms: red fluorescence from PI binding to nucleic acids in cytoplasm; 400ms: PI penetrating the cell nucleus, 5min: PI fully covering cell nucleus and cytoplasm**

**Outlook**

High-speed fluorescence recordings reveal the uptake of PI by endothelial cells as a result of microbubble oscillations. Detailed measurements at the time scale of bubble oscillations will be performed with the Brandaris 128 camera equipped for fluorescence imaging to fully capture and understand the process of bubble-induced sonoporation.

**References**

1. Wamel A van, Kooiman K, Harteveld M, et al. Vibrating microbubbles poking individual cells: drug transfer into cells via sonoporation. Journal of controlled release, 2006;112(2):149-55.
2. A.L. Klibanov, P.T. Rasche, M.S. Hughes, J.K. Wojdyla, K.P. Galen, J.H. Wible, and G.H. Brandenburger, Detection of Individual Microbubbles of Ultrasound Contrast Agents: Imaging of Free-Floating and Targeted Bubbles, Investigative Radiology, vol. 39, pp. 187-95 (2004).

# Vaporization of Fluorescently Labelled Perfluorocarbon Droplets

***Nikita Reznik[1], Minseok Seo[1,2], Ross Williams[2] and Peter N. Burns[1,2]***

*[1]University of Toronto, Toronto, Canada*
*[2]Sunnybrook Health Sciences Centre, Toronto, Canada*

Acoustically activated droplets of liquid perfluorocarbon (PFC) are currently being studied for both diagnostic and therapeutic applications. Acoustic activation is performed with applied ultrasound used to vaporize the droplet, converting it into a gas bubble. For diagnostic purposes, submicron droplets have the potential to serve as extravascular ultrasound contrast agents (Mattrey et al, 1982). Vaporized submicron droplets were shown to exhibit non-linear acoustic properties, applicable for detection with contrast specific imaging techniques (Reznik et al, 2009). Therapeutically, droplets are studied for their potential in HIFU therapy sensitization (Zhang and Porter, 2010), embolotherapy (Kripfgans et al, 2002) and drug delivery (Rapoport et al, 2007).

*In vitro* (Fabiilli et al, 2010; Fang et al, 2009) and *in vivo* (Rapoport et al, 2009) studies were performed to assess the efficacy of PFC droplets as vehicles for drug delivery. It was shown that the droplets have the ability to carry chemotherapeutic agents, and release them upon the droplets' acoustically induced vaporization into gas bubbles. However, further work is required in order to understand the mechanisms governing the process of droplet vaporization, or the release of an agent dispersed in liquid PFC. In this study we propose to use micron-sized fluorescently labelled PFC droplets as a model for studying the product of droplet phase-change and release of the fluorescent marker from the vaporized droplet.

**Methods**

Fluorescently labelled micron sized PFC droplets were prepared in the following manner. DiIC-18 lipophilic dye (Invitrogen, Burlington, ON) was dissolved in diethyl ether (Sigma Aldrich, Oakville, ON) at a concentration of 1 mg/mL. 225 μL of the ether solution was then mixed with 300 μL dodecalfuoropentane (DDFP, Synquest Labs, Alachua, FL), 150 μL perfluorohexane (PFH, Synquest Labs, Alachua, FL), 11 μL Krytox 157 FSL Oil (Miller Stephenson Chemical, Toronto, ON), used as surfactant to stabilize the droplets, and 10 mL of distilled water. The resulting solution was emulsified using a Vortex mixer (Mixer Genie-2, Scientific Industries Inc., Bohemia, NY) for 30 s to produce droplet suspensions in the micrometer size range. Sizing of the resultant emulsion was performed with Coulter Counter (Multisizer 3, Beckman Coulter, Mississauga, ON).

Single droplets were heated to 37 °C and vaporized in a 200 μm polyethylene tube (Advanced Polymers, Salem NH) using a single 50 cycle ultrasound pulse from a 7.5 MHz transducer (IL0706HP, Valpey-Fisher, Hopkinton MA ) at 1.8 MPa peak negative pressure. Optical observation of droplets was performed with an Olympus microscope (Olympus, Markham, ON) in either brightfield or fluorescence mode with a 60x microscope objective (NA = 1.0), providing spatial resolution of at least 500 nm. The microscope was coupled to a Fastcam APX-RS medium speed camera (Photron, San Diego, CA) and optical images for both brightfield and fluorescence modes were recorded at 1000 FPS, providing temporal resolution of 1 ms.

**Results**

Figure 1 shows a series of brightfield images of a vaporized 5 μm in diameter droplet in the first 100 ms after vaporization. Due to the phase change of liquid to gas, droplets experience an increase in diameter as a result of vaporization, and subsequent additional growth due to air diffusion into the bubble from the surrounding liquid.

Figure 2 depicts a similar vaporized droplet, of 8 μm in diameter, imaged in the fluorescence imaging mode. Prior to vaporization, the droplet is uniformly fluorescent (also confirmed by confocal microscopy). The droplets remain fluorescent for a period of at least 24 h, suggesting stable retention of fluorescent marker by the droplet. However, fluorescence is rapidly reduced after phase conversion. Within a few ms after vaporization, fluorescence signal is lost within the bulk of the newly formed bubble. Fluorescence signal from the edge of the bubble is gradually lost on a timescale from a few hundred milliseconds to a few seconds.

**Discussion and Conclusions**

We show here that it is possible to create micron sized fluorescently labelled PFC droplets that have the ability to undergo phase conversion when exposed to ultrasound. Although liquid droplets may not always provide high optical contrast with the surrounding liquid in brightfield images, observation of fluorescently labelled droplets can offer clear delineation of droplet boundaries.

While in the liquid phase, the droplet may sustain the dissolved fluorescent marker in its bulk. However, after vaporization, PFC gas can no longer contain the agent, which is rapidly expelled from the PFC bulk and towards the interface between the bubble and the surrounding liquid. The agent is then gradually dissolved out into the surrounding medium. Higher speed fluorescence photography may be able to shed some light on the process of vaporization and the role of the gas or shell, depending on the type of fluorescent labelling achieved.

These results show the difference in the interaction mechanisms between dissolved agents and PFC in liquid and gas form and present an attractive model for the study of the mechanism of phase-change induced drug release. Furthermore, the measure of fluorescence signal may provide a tool for differentiation between PFC liquid, PFC gas and surrounding medium. This may present a valuable tool, not only in the study of agent dissolution following vaporization, but also in the optical study of droplet vaporization mechanism on the microsecond scale.

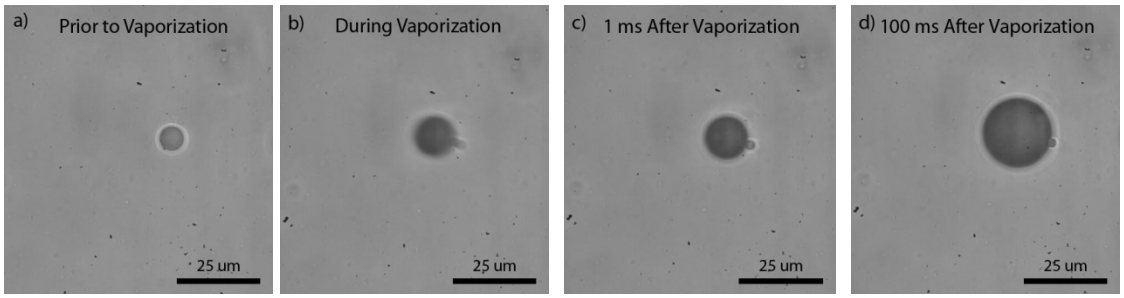


**Figure 1. Optical images of a 5 µm droplet (a) prior to vaporization, (b) during vaporization, (c) 1 ms after vaporization, (d) 100 ms after vaporization.**

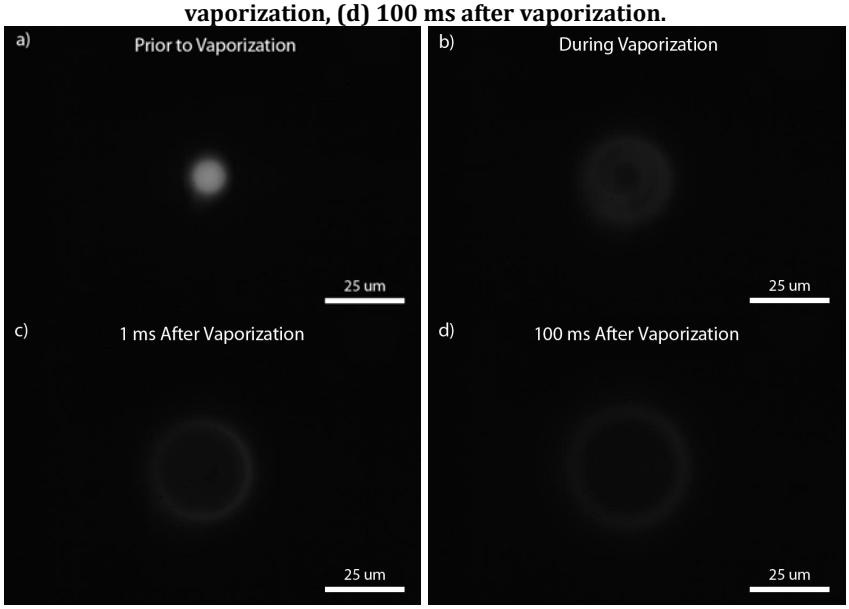


**Figure 2. Fluorescence images of an 8 µm droplet (a) prior to vaporization, (b) during vaporization, (c) 1 ms after vaporization, (d) 100 ms after vaporization.**

**References**


1. Fabiilli ML, Haworth KJ, Sebastian IE, Kripfgans OD, Carson PL, Fowlkes JB. Delivery of Chlorambucil using an acoustically-triggered perfluoropentane emulsion. Ultrasound in Med Biol 2010;36:1364-75.
2. Fang JY, Hung CF, Hua SC, Hwang TL. Acoustically active perfluorocarbon nanoemulsions as drug delivery carriers for camptothecin: Drug release and cytotoxicity against cancer cells. Ultrasonics 2009;49:39-46.
3. Kripfgans OD, Fowlkes JB, Woydt M, Eldevik OP, Carson PL. In vivo droplets vaporization for occlusion therapy and phase aberration correction. IEEE Trans Ultrason Ferroelectr Freq Control 2002;49:726-738.
4. Mattrey RF, Scheible FW, Gosink BB, Leopold GR, Long DM, Higgins CB. Perfluoroctylbromide: A liver/spleen-specific and tumor-imaging ultrasound contrast material. Radiology 1982;145:759-62.

5. Rapoport N, Gao Z, Kennedy A. Multifunctional nanoparticles for combining ultrasonic tumor imaging and targeted chemotherapy. J Natl Cancer Inst 2007;99:1095-106.
6. Rapoport NY, Kennedy AM, Shea JE, Scaife CL, Nam KH. Controlled and targeted tumor chemotherapy by ultrasound-activated nanoemulsions/microbubbles. J Control Release 2009;138:268-276
7. Reznik N, Williams R, Burns PN. "Optical and acoustic characterization of vapourized perfluorocarbon droplets as ultrasound contrast agents". Proc IEEE Ultrason Symp 2009;2778-81.
8. Zhang P, Porter T. An in vitro study of a phase-shift nanoemulsion: A potential nucleation agent for bubble-enhanced HIFU tumor ablation. Ultrasound Med Biol 2010;36:1856-66.

# The fate of microbubble spectral behaviour in the presence of a sequence of pulses

***D. H. Thomas,[1,a]), P. Looney[1], M Butler[1], N. Pelekasis[2], T. Anderson[1], and V. Sboros[1].***

*[1]Medical Physics, The University of Edinburgh, Edinburgh EH16 4SB, United Kingdom*
*[2]Department of Mechanical Engineering, University of Thessally, Volos 38834, Greece*

Consecutive ultrasound pulses have been shown to effectively enhance the contrast of the vascular bed in medical diagnostic ultrasound imaging applications. The oscillations of single Definity® microbubbles 2-6μm in radius have been measured using the Brandaris ultra high speed camera and separately using a calibrated microacoustic system.

Optical results show that microbubbles slowly reduce in size after ultrasound insonation, and that the subsequent amplitude of oscillation varies depending on size in relation to resonance. Ultrasound induced microbubble decay has also been identified from the evolution of the spectral content of scatter contained within consecutive acoustic emissions. The scattered echoes have been measured in response to two consecutive imaging pulses.

Changes in amplitude and nonlinearity of scatter have been observed which depend on the harmonic content of the initial response. Five different behaviours have been identified.

Based on comparisons with numerical simulations employing a modified Keller–Miksis equation, regions of scatter arising from fundamental and harmonic resonance match the experimental results, and explain the spectral differences in the fate of microbubble scatter. We suggest that diffusion alone cannot describe such microbubble decay, and the shedding of shell material may play an important role in the significant change of surface tension and size reduction of decaying microbubbles.

# Exploiting Subharmonic emission from Silica Nanoparticles for Dual mode Molecular Imaging

***Francesco Conversano[1], Andrea Ragusa[2], Antonio Greco[1], Sergio Casciaro[1]***

*[1]National Council of Research, Institute of Clinical Physiology, Lecce, Italy*
*[2]National Council of Research, Institute of Nanoscience, Lecce, Italy*

Contrast agents for ultrasound (US) imaging are currently used for several clinical applications, such as blood signal enhancement, myocardial perfusion imaging and characterization of liver lesions. During the last years, research in targeted microbubble contrast agents has opened new exciting perspectives in this field[1]: US molecular imaging (which relies on the detection of disease-targeted contrast particles), effective combination of echographic methods with other non-invasive imaging techniques to perform multimodal diagnostic studies, novel "theranostic" strategies based on the site-targeted delivery of drugs operated by smart contrast agents.

However, because microbubbles cannot leave the vascular compartment, they cannot reach cells located beyond the capillary vasculature, such as many cancer cells. Furthermore, vessels created by tumour angiogenesis have the tendency to be "leaky"[2] and to exhibit the so-called enhanced permeability and retention (EPR) effect, which results in exaggerated extravasation and retention of particles that are smaller than the pore size of tumour endothelium (typically between 380 and 780 nm)[3,4]. For these reasons, intensive investigations have been recently undertaken to develop nanoparticle-based cancer targeting agents for various imaging modalities, including ultrasound[5-9]. In this context, a very recent paper of our research group[5] demonstrated the feasibility of using solid silica nanoparticles (SiNPs) as US contrast agents in combination with broadband pulses at a common diagnostic frequency (7.5 MHz), showing also the possibility of an accurate automatic detection of nanoparticles through radiofrequency (RF) signal analysis.

In the present work we had a double aim: first, to demonstrate for the first time feasibility and usefulness of subharmonic imaging of SiNPs at diagnostic US frequencies, and, second, to investigate the acoustic effectiveness of a new class of multimodal nanocomposite contrast agents consisting of silica nanospheres covered by an outer shell of smaller magnetic nanoparticles, towards dual mode investigations combining US and magnetic resonance imaging (MRI).

In fact, nonlinear microbubble detection schemes have previously led to improved methods for segmenting flow signals from tissue at diagnostic ultrasound frequencies, subsequently leading to the development of nonlinear ultrasound imaging instrumentation[10]. Actually, microbubble harmonic imaging exploits the nonlinear oscillations of bubbles excited beyond a specific pressure threshold in order to identify the contrast agent presence through a selective filtration of the corresponding harmonic component in the signal (i.e. performing a tissue suppression). Harmonic imaging of solid nanoparticles exploits the harmonic distortion of an US signal propagating through a nanoparticle-containing tissue, in order to discriminate targeted tissues from non-targeted ones. Application of this detection strategy to nanoparticles small enough to extravasate from vascular compartment, and functionalized to selectively identify diseased tissue cells, has the potential to further increase the sensitivity of the nanoparticle-based methods for US molecular imaging that are currently under development.

In this study we employed silica nanospheres of three different diameters (160 nm, 330 nm and 660 nm) that were dispersed in variable volume concentrations (range 0.07-0.8%) in agarose gel samples contained into Petri dishes. Each prepared sample was imaged employing a digital ecograph (Megas GPX, Esaote Spa, Florence, Italy), equipped with a linear transducer and linked via optic fibre to a prototype platform for acquisition of unprocessed RF data (FEMMINA, ELEN Spa, Florence, Italy). The US probe was mounted on the motorized piston of an infusion pump (KDS 100, KD Scientific Inc., Holliston, MA, USA) and automatically scanned along the sample. The sample was immersed in distilled water and the transducer, in turn partially immersed in the water, was positioned perpendicular to the Petri dish bottom at such a distance that the transducer focus (set to 2 cm) was located half-way through gel depth. Each sample was scanned for 1 cm in its central part at a speed of 1 mm/min and 600 frames of RF data were each time acquired (frame-rate = 1 fps). Two different transducers were employed (LA532 and LA523, Esaote Spa), in order to obtain the effective generation of 10-cycle narrow-band US pulses at four different diagnostic frequencies (5 MHz, 6.6 MHz, 7.5 MHz, 10 MHz). For each frequency, mechanical index (MI) was varied between 0.2 and 0.6.

During the off-line analysis, for each acquired frame, a rectangular region of interest (ROI) composed of 100 echographic tracks with 200 points/track was positioned in the central zone of the imaged gel section, so that the corresponding backscatter values were not influenced by any boundary effect. The mean FFT curve of each frame was calculated as the average of the 100 FFT curves corresponding to the 100 track segments belonging to the ROI. The FFT curve associated to each sample was the average of the 600 curves resulting from the corresponding frame sequence. Resulting FFT curves were compensated to take into account the frequency band of the employed transducer, and the trends of the fundamental component peak and of the subharmonic component peak (detected in the frequency

interval corresponding to half of the fundamental component) were studied as a function of incident frequency, MI, nanoparticle size and concentration.

Samples containing nanoparticles at the constant volume concentration of 0.8% and insonified with narrow-band pulses of variable frequency having MI=0.2 were used to determine the effect of nanoparticle diameter and incident frequency on the mentioned FFT components. Obtained results show that the maximum of fundamental component intensity is associated to 330-nm SiNPs when insonifying at 7.5 MHz (confirming results recently obtained with broadband pulses centered at the same frequency), while, as expected, the employment of a lower US frequency shifts the peak towards bigger particles and vice versa. On the other hand, maximum intensity of subharmonic component was always associated with 330-nm SiNPs, independently on the incident US frequency. In particular, subharmonic intensity measured on samples containing 330-nm SiNPs was always about 20 dB higher than the corresponding intensity measured on "controls" (i.e., samples containing pure agarose gel). The highest subharmonic intensity was found when the insonifying frequency was 6.6 MHz: in this case 330-nm SiNPs produced an enhancement of 24 dB in subharmonic intensity with respect to the control.

Therefore, we employed 6.6-MHz pulses and 330-nm SiNPs to investigate the effect of nanoparticle concentration and MI on the FFT components, aiming in particular at determining the sensitivity of subharmonic intensity in the detection of SiNPs at very low concentrations (range 0.07-0.23%) and its relationship with MI, that was varied in the range 0.2-0.6. The corresponding results show that subharmonic intensity is highly sensitive to small variations of nanoparticle volume concentration, while significant increments in incident acoustic pressure produce limited effects on subharmonic enhancement. For instance, a two-fold increase in particle concentration from 0.07% to 0.14% produced an increment of 6.5 dB in the corresponding subharmonic intensity (MI=0.2), while a two-fold increase of the MI from 0.2 to 0.4 caused only an enhancement of 2.6 dB in the subharmonic intensity measured on the same sample. Furthermore, the combination of the lowest adopted MI value (0.2) and the lowest particle concentration (0.07%) produced a subharmonic intensity of 4.1 dB higher than that measured on a control insonified in the same way.

On the other hand, fundamental intensity showed a very low sensitivity to both particle concentration and MI increments, indicating that subharmonic intensity is particularly suited for the detection of small amounts of nanoparticles dispersed through a tissue with a "low power approach". Selective filtering of subharmonic component showed also a visible effect on the corresponding echographic images, in which only nanoparticle-containing areas were enhanced while all the other objects were suppressed.
In the final part of the study, the described experiments were repeated on new agarose gel samples, containing silica nanospheres covered by an outer shell of magnetic nanoparticles, made of either iron

oxide or hybrid FePt-iron oxide nanocrystals. SiNPs covered by iron oxide produced lower intensity enhancements with respect to the pure silica case, while SiNPs whose shell included FePt showed an acoustic behaviour qualitatively analogous to that of pure SiNPs of the same size, with a slightly less uniform image brightness. The main cause of the differences in acoustic behaviour between pure SiNPs and those covered by a magnetic shell could be observed on the corresponding TEM images: the addition of the smaller magnetic nanoparticles alters the particle surface morphology in a significant and complex manner, and this is likely to affect the related US backscatter phenomena.

In conclusion, this study demonstrated the feasibility of subharmonic imaging of SiNPs at diagnostic US frequencies. In all the investigated frequency range (5-10 MHz), the highest sensitivity of subharmonic intensity to particle concentration was found for 330-nm SiNPs, with this particle size resulting also very suitable for medical applications, since it potentially allows direct targeting of the most common tumors. Particle concentrations as low as 0.07% in volume can be effectively detected employing a low MI (0.2), therefore the method is particularly suited to accurately quantify the amount of nanoparticles that targeted a given tissue. Furthermore, the studied SiNPs maintained all these exciting properties even after a coverage by an outer shell of smaller magnetic nanoparticles, so representing a valuable candidate for tasks of dual mode molecular imaging.

**Acknowledgements**

This work was partially funded by the grant N° DM18604 – Bando Laboratori – DD MIUR 14.5.2005 n.602/Ric/2005 of the Italian Ministry of Instruction and Research.

**References**

1. Conversano F, Casciaro S. “Last advances in ultrasound molecular imaging”. In: Casciaro S. and Gersak B. (Eds.), “New technology frontiers in minimally invasive therapies”, Lupiensis Biomedical Publications, Lecce, 2007 (ISBN 978-88-902880-1-2); Chapter 18: 161-171.
2. Pasqualini R, Arap W, McDonald DM. Probing the structural and molecular diversity of tumor vasculature. Trend Molec Med 2002;8:563-571.
3. Hobbs SK, et al. Regulation of transport pathways in tumor vessels: role of tumor type and microenvironment. Proc Natl Acad Sci 1998;95:4607-4612.
4. Maeda H, Wu J, Sawa T, Matsunama Y, Hori K. Tumor vascular permeability and the EPR effect in macromolecular therapeutics: a review. J Control Release 2000;65:271-284.
5. Casciaro S, Conversano F, et al. Optimal enhancement configuration of silica nanoparticles for ultrasound imaging and automatic detection at conventional diagnostic frequencies. Invest Radiol 2010;45(11):715-724.
6. Liu J, et al. Nanoparticles as image enhancing agents for ultrasonography. Phys Med Biol 2006;51:2179-2189.
7. Wheatley MA, Forsberg F, Dube N, Patel M, Oeffinger BE. Surfacant-stabilized contrast agent on the nanoscale for diagnostic ultrasound imaging. Ultrasound Med Biol 2006;32:83-93.
8. Dayton PA, et al. Application of ultrasound to selectively localize nanodroplets for targeted imaging and therapy. Mol Imaging 2006;5:160-174.
9. Buchanan KD, Huang S, Kim H, MacDonald RC, McPherson DD. Echogenic liposome compositions for increased retention of ultrasound reflectivity at physiologic temperature. J Pharm Sci 2008;97:2242-2249.
10. Needles A, et al. High-frequency subharmonic pulsed-wave Doppler and color flow imaging of microbubble contrast agents. Ultrasound Med Biol 2008;34(7):1139-1151.

# In vitro sonothrombolysis of human blood clots with BR38 microbubbles

***B. Petit*** [1], ***F. Yan*** [2], ***D. Colevret*** [2], ***E. Gaud*** [2], ***M. Arditi*** [2], ***F. Tranquart*** [2], ***E. Allémann*** [1]

[1] *School of Pharmaceutical Sciences, University of Geneva, University of Lausanne, Geneva, Switzerland*
[2] *Bracco Suisse S.A, Plan-les-Ouates, Geneva, Switzerland*

**Introduction**

Ischemic stroke results from a cerebral vessel occlusion by a blood clot. Treatments are intended to restore the cerebral blood flow as soon as possible to avoid major brain damage. Intravenous administration of recombinant tissue plasminogen activator (rtPA) is currently the only thrombolytic drug approved for treatment of acute ischemic stroke [1].

*In vitro* and *in vivo* studies have shown that rtPA, in combination with ultrasound and microbubbles, can improve clot lysis [2, 3]. However, the exact mechanisms involved in this ultrasound-mediated thrombolytic process (termed as **sonothrombolysis**) remain unclear and the conditions for clot lysis are not yet optimized.

The aims of the present work were to set up a robust *in vitro* human clot model and to evaluate the extent of thrombolytic effects by the concomitant use of rtPA, ultrasound and microbubbles compared to rtPA alone.

**Methods and results**

***Clot preparation and characterization***

Fresh whole human blood clots were formed by incubation for six hours at 37 °C in glass capillaries with a cross-section of 3.4 mm through which a silk suture thread had been positioned beforehand. The dimensions of clots were measured by using a digital camera and automatic image processing code written in-house MatLab®. Clot structures were characterized by scanning electron microscopy (SEM) and immunostaining.

***In vitro clot lysis***

The clots were inserted in a transparent plastic tube connected to a peristaltic pump, filled with human plasma. The tube was then placed in a thermostated water bath at 37 °C and exposed to different experimental conditions: rtPA only, rtPA + ultrasound (1.6 MHz), microbubbles + ultrasound, and rtPA + microbubbles + ultrasound. Experimental microbubbles (BR38, Bracco Suisse SA, Switzerland) were used for sonothrombolysis experiments. The lysis of clots was performed during 60 minutes and

photographs were taken every 5 minutes to measure the diameter of the clot and its change in shape in its section exposed to ultrasound.

***Results and discussion***

The clots had initial diameters of 1.97 ± 0.12 mm (n=37, mean diameter ± sd). Scanning electron microscopy and immunostaining showed that the clots were formed by red blood cells, fibrin and platelets (Fig.1). The fibrin network and activated platelets were more present at the surface than inside the clot. *In vitro* thrombolysis showed that without rtPA, the exposure to ultrasound with microbubbles (BR38) and had only small effects on the reduction of the clot diameter (lysis rate ~ 1 µm/min, n=5). The lysis of the clot in the presence of rtPA alone depended on the concentration of the enzyme: 3.4 µm/min at 0.3 µg/mL and 6.1 µm/min at 3 µg/mL of rtPA, respectively. The combination of rtPA (0.3µg/mL) + ultrasound + BR38 induced the highest rate of clot lysis (7.3 µm/min).

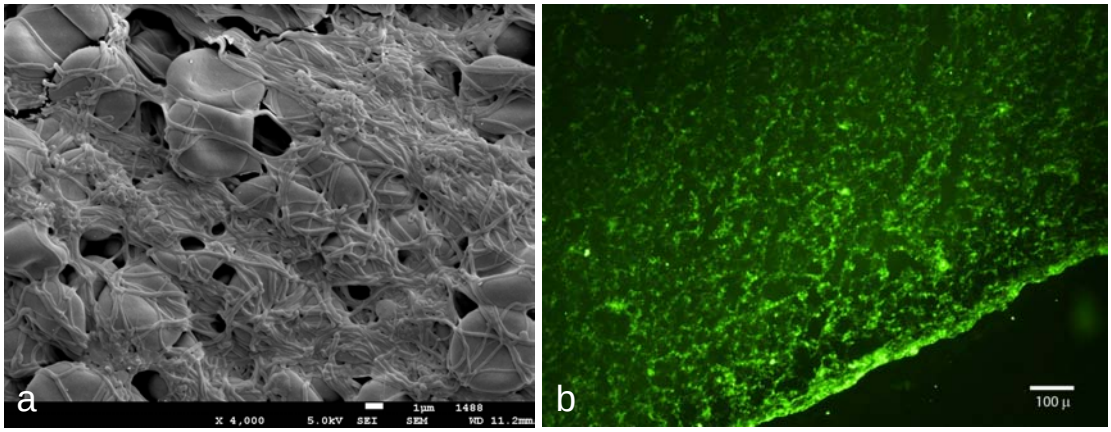


**Figure 1: (a) Scanning electron microscopy observation of the surface of the clot (magnification x4000); (b) Immunofluorescence staining of fibrin on the clot (magnification x100).**

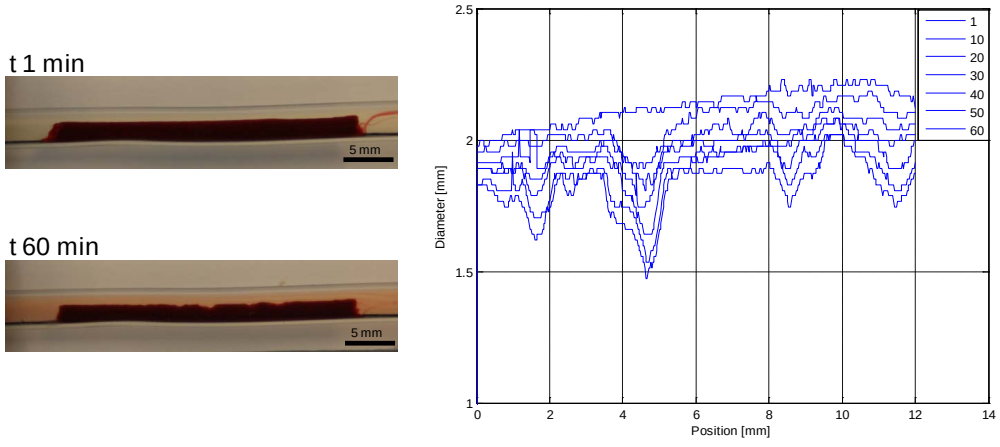


**Figure 2: Clot diameter (mm) profile as a function of the exposure time (min).**

**Conclusion**

Our preliminary experiments demonstrated that reproducible human blood clots can be obtained and characterized by SEM and immunostaining. Enhanced thrombolytic effects were observed with the combination of a low concentration of rtPA (0.3 µg/mL), ultrasound and BR38 microbubbles, compared to rtPA alone. The spatial distribution of sonothrombolysis as observed on the clots could be correlated to the actual local acoustic pressure profile of the ultrasound beam applied.

Optimization of sonothrombolysis settings and parameters is in progress and further studies will enable a thorough evaluation of the interactions and synergistic effects of microbubbles, ultrasound and rtPA on clot lysis.

**References**


1. Adams H P, Del Zoppo G, Alberts M J, Bhatt D L, Brass L, Furlan A, Grubb R L, Higashida R T, Jauch E C, Kidwell C, Lyden P D, Morgenstern L B, Qureshi A I, Rosenwasser R H, Scott P A, Wijdicks E F M. Guidelines for the Early Management of Adults With Ischemic Stroke. Stroke. 2007; 38: 1655–1711. doi:10.1161/STROKEAHA.107.181486
2. Meairs S, Culp W. Microbubbles for Thrombolysis of Acute Ischemic Stroke. Cerebrovasc Dis. 2009; 27(suppl 2): 55–65. doi:10.1159/000203127
3. Hitchcock Kathryn E. and Holland Christy K. Ultrasound-assisted thrombolysis for stroke therapy Better thrombus break-up with bubbles. Stroke. 2010;41 [suppl 1]:S50-S53. doi:10.1161/ STROKEAHA.110.595.348

# Bubbles and Angiogenesis: An update

***Peter N. Burns [1,4], John Hudson[1], Ross Williams[4], Brendan Lloyd[4], Mostfafa Atri[2], Greg Czarnota [3,4], Stuart Foster [1,4] and Georg Bjarnason [3,4]***

*Depts Medical Biophysics[1], Medical Imaging[2] and Oncology[3], University of Toronto, Canada*
*[4]Sunnybrook Health Sciences Centre, Toronto, Canada*

The importance of angiogenesis in cancer has been established for many years and the rationale for the development of targeted anti-angiogenic therapeutics well articulated (1). In the past decade, targeting of the vascular endothelial growth factor (VEGF) pathway has shown clinical benefit in patients with metastatic colorectal cancer, advanced non small cell lung cancer, hepatocellular carcinoma, metastatic breast cancer and renal cell carcinoma (2): several inhibitors are now available clinically. As anti-angiogenic therapies typically do not cause an immediate change in tumour volume, imaging of functional surrogates of therapeutic response has become an important method for assessing effectiveness of therapy. Current measures are based on dynamic contrast enhancement (DCE) characteristics of CT (3) and MRI (4), which have identified patients as early as 9 weeks into treatment who went on to show significant clinical benefit . Dynamic contrast-enhanced ultrasound (DCE-US) (5) is a relatively new approach to assess and quantify functional change in response to anti-angiogenic treatment which has been applied in several clinical studies (6). DCE-US is attractive for a number of reasons: ultrasound imaging is sufficiently fast to track enhancement kinetics with ease; the microbubble agent is purely intravascular and, unlike clinical CT and MR agents, is not complicated by interstitial extravasation; the bubbles' properties can be manipulated by the scanner itself to offer the unique tool of disruption-replenishment for flow measurement; and the modality is widely available and suited to bedside use in sick patients. Pre-clinical studies of anti-angiogenic treatments have correlated DCE-US with DCE-CT (7), DCE-US with DCE-MRI and DCE-US with FDG-PET measurements (8). Clinical correlations have been reported between changes in DCE-US parameters during the first two weeks of treatment with Sunitinib and overall survival (9), while revascularization of tumours following cessation of treatment with bevacizumab causes a drop in a DCE-US-derived perfusion index which correlates with histology in a murine tumour model (10). A number of large clinical trials are underway that are likely to further establish DCE-CEUS as a useful tool.

As far as the technology is concerned, one weakness of current US methods is the inability to acquire and analyse a tissue volume during the course of a single bolus. Because of the characteristic heterogeneity of the tumour circulation, this means that the practical inter-session reproducibility of DCE-CEUS is really quite low. One way of overcoming this problem is to slow down the contrast administration, using the disruption replenishment method in combination with a bubble infusion, thus

allowing enough time to acquire typically about 10 planes from a single contrast dose. Another method is to speed up the imaging acquisition, so that there is time to gather a volume of data throughout a single bolus. The new 2-D matrix array transducers allow this to be done for the first time, and are likely therefore likely to provide the first really strong application for '4D' contrast imaging outside the heart. Preliminary images will be shown.

In a disappointing - but all too familiar - development, it is meanwhile becoming apparent that the high expectations for anti-angiogenesis therapeutic agents for cancer are not being met in real life. In spite of very high cost and not inconsiderable toxic side-effects, the survival benefit that they confer is at best modest, and at present there is no way to predict who will respond favourably to the drugs. More alarming is the tendency for the vasculature to proliferate aggressively when the patient is off therapy (this is known as 'rebound'), an effect which in the majority of cases eventually becomes irreversible, amounting to acquired drug resistance. Worse still, evidence is emerging that anti-angiogenic therapy can actually enhance metastatic tumour spread (11). These observations highlight an urgent need to better understand the biological underpinnings of targeted therapeutics and to design better approaches to combine therapies in such a way as to minimize resistance. Few studies have been carried out which take advantage of a noninvasive biomarker of vascular response in either preclinical models of targeted therapy or in patients.

This creates some new and important opportunities for the development and validation of DCE-US as an imaging marker of tumour response. In an experimental setting, models of human cancer in small animals can be used to test entirely new treatment regimes, many of which combine anti-angiogenic drugs with chemotherapeutic agents or radiation. The new generation of high frequency arrays allow the same imaging methods used clinically to be scaled for use on small animals, with very impressive results (12). Ultrasound is alone in its ability, both in mice and in men, to be used repeatedly to follow the time course of response to therapy over the many months during which clinical resistance might develop. New studies are needed to compare the measurements it provides against biological markers of drug resistance. But the potential exists for it to offer a primary tool in the clinical translation of new therapeutic strategies for drug development and cancer treatment.

Finally, as always, microbubbles offer a surprise. It is well known that microbubbles under insonation at close association with cell membranes have the effect of permeabilising or porating, the cell. While this has been recognised as a way of enhancing drug uptake, it has not previously been considered in conjunction with exposure to ionising radiation. Radiotherapy is the most common treatment for cancer, and anti-angiogenic effects are also implicated in its tumour response. In practice, the application of radiotherapy is limited by its deleterious effect on normal tissue, so any agent that sensitizes target

tissue selectively to radiotherapy would be of particular value. To have such a sensitizer guided by a real time image would be especially useful. Probably by virtue of a synergistic effect with radiotherapy which itself results in an increase in cell membrane permeability, ultrasound and microbubbles have been shown to be capable not only of elucidating the effects of this treatment of cancer, but also of enhancing radiotherapy in a manner whose specificity is determined by the ultrasound beam itself. Some data pointing to biological mechanism of the effect will be described.

**References**


1. Kerbel R, Folkman J. Clinical translation of angiogenesis inhibitors. Nature Reviews Cancer 2002; 2:727-739.
2. Ellis LM, Hicklin DJ. VEGF-targeted therapy: mechanisms of anti-tumour activity. Nat Rev Cancer 2008; 8:579-591.
3. Choi H, Charnsangavej C, Faria SC, et al. Correlation of computed tomography and positron emission tomography in patients with metastatic gastrointestinal stromal tumor treated at a single institution with imatinib mesylate: proposal of new computed tomography response criteria. J Clin Oncol 2007; 25:1753-1759.
4. Hahn OM, Yang C, Medved M, et al. Dynamic contrast-enhanced magnetic resonance imaging pharmacodynamic biomarker study of sorafenib in metastatic renal carcinoma. J Clin Oncol 2008; 26:4572-4578.
5. Arditi M, Frinking PJ, Zhou X, Rognin NG. A new formalism for the quantification of tissue perfusion by the destruction-replenishment method in contrast ultrasound imaging. IEEE Trans Ultrason Ferroelectr Freq Control 2006; 53:1118-1129.
6. Lassau N, Lamuraglia M, Chami L, et al. Gastrointestinal stromal tumors treated with imatinib: monitoring response with contrast-enhanced sonography. Am J Roentgenol 2006; 187:1267-1273.
7. Pollard RE, Broumas AR, Wisner ER, Vekich SV, Ferrara KW. Quantitative contrast enhanced ultrasound and CT assessment of tumor response to antiangiogenic therapy in rats. Ultrasound Med Biol 2007; 33:235-245.
8. Niermann KJ, Fleischer AC, Huamani J, et al. Measuring tumor perfusion in control and treated murine tumors: correlation of microbubble contrast-enhanced sonography to dynamic contrast-enhanced magnetic resonance imaging and fluorodeoxyglucose positron emission tomography. J Ultrasound Med 2007; 26:749-756.
9. Lassau N, Koscielny S, Albiges L, et al. Metastatic renal cell carcinoma treated with sunitinib: early evaluation of treatment response using dynamic contrast-enhanced ultrasonography. Clin Cancer Res 2010; 16:1216-1225.
10. Guibal A, Taillade L, Mule S, et al. Noninvasive contrast-enhanced US quantitative assessment of tumor microcirculation in a murine model: effect of discontinuing anti-VEGF therapy. Radiology 2010; 254:420-429.
11. Ebos JM, Lee CR, Cruz-Munoz W, Bjarnason GA, Christensen JG, Kerbel RS. Accelerated metastasis after short-term treatment with a potent inhibitor of tumor angiogenesis. Cancer Cell 2009; 15:232-239.
12. Needles A, Arditi M, Rognin NG, et al. Nonlinear contrast imaging with an array-based micro-ultrasound system. Ultrasound Med Biol 2010; 36:2097-2106.

# Mechanisms of sonoporation

***Lentacker I.*, Geers B., De Smedt S.C.**

*Ghent Research Group on nanomedicines, Department of pharmaceutical sciences, Ghent University, Harelbekestraat 72, 9000 Gent, Belgium*

Ultrasound and microbubbles have gained much attention in the drug delivery field as targeted drug delivery system. Several research groups have shown that microbubbles can be used to promote the extravasation of drugs and selectively stimulate drug uptake in ultrasound treated areas, resulting in an enhanced efficacy of genetic drugs or anticancer drugs. This has been ascribed to ultrasound induced sonoporation. Sonoporation is a general term for different phenomena which result in the cellular uptake of drugs. The corresponding microstreaming gently affects cellular membranes and stimulates endocytosis. Another possibility is to implode microbubbles with higher ultrasound intensities and generate shock waves and microjets in the vicinity of cell membranes leading to the formation of cell membrane perforations. This presentation will give a short overview of the two main mechanisms that have been described to explain ultrasound induced sonoporation and will link them to different experimental set-ups.

**Acknowledgements**

Ine Lentacker is a post-doctoral fellow of the Fund for Scientific Research Flanders (FWO-Vlaanderen). The financial support of this institution is acknowledged with gratitude. The financial support of the European Union (via the FP7 projects Arise and Sonodrugs (NMP-4-LA-2008-213706)) is acknowledged.

**References**

1. Ultrasound exposure of lipoplex loaded microbubbles facilitates direct cytoplasmic entry of the lipoplexes. Lentacker I. et al. Molecular Pharmaceutics 2009, 6(2), 457-467.
2. Ultrasound and microbubble-targeted delivery of macromolecules is regulated by induction of endocytosis and pore formation. Meijering B.D. et al. Circulation Research 2009, 104(5), 579-86.

# Vascular Endoluminal Delivery of Mesenchymal Stem Cells Using Acoustic Radiation Force

***Catalin Toma, MD; Jianjun Wang, PhD; Xucai Chen, PhD; Flordeliza S. Villanueva, MD***

*University of Pittsburgh*
*Cardiovascular Institute*
*Center for Ultrasound Molecular Imaging and Therapeutics*
*Pittsburgh, Pennsylvania*

Restoration of functional endothelium is a requirement for preventing late stent thrombosis. We propose a novel method for targeted delivery of stem cells to a site of arterial injury using ultrasound-generated acoustic radiation force. Mesenchymal stem cells (MSCs) were surface-coated electrostatically with cationic gas-filled lipid microbubbles (mb-MSC). MSC coating with microbubbles was characterized microscopically and by flow cytometry. The effect of ultrasound (5 MHz) on directing mb-MSC movement toward the vessel wall under physiologic flow conditions was tested in vitro in a vessel phantom. In vivo testing of acoustic radiation force-mediated delivery of mb-MSCs to balloon-injured aorta was performed in rabbits using intravascular ultrasound (1.7 MHz) during intra-aortic infusion of mb-MSCs. Application of ultrasound led to marginalization and adhesion of mb-MSCs to the vessel phantom wall, while no effect was observed on mb-MSCs in the absence of ultrasound. The effect was maximal when there were 7±1 microbubbles/cell (n=6). In rabbits (n=6), adherent MSCs were observed in the ultrasound treated aortic segment 20 min following the injection (334±137 MSCs/cm2), while minimal adhesion was observed in control segments not exposed to ultrasound (2±1 MSCs/cm2, $p<0.05$). At 24 hours following mb-MSC injection and ultrasound treatment, the engrafted MSCs persisted and spread out on the luminal surface of the artery. The data demonstrate proof of principle that acoustic radiation force can target delivery of therapeutic cells to a specific endovascular treatment site. This approach may be used for endoluminal cellular paving and could provide a powerful tool for cell-based re-endothelialization of injured arterial segments.

# Use of Contrast Enhanced Ultrasound Imaging to Assess Tumor Response to Axitinib Treatment and Withdrawal.

***Terri A. Swanson[1], Theresa A. Tuthill[2], Kyle Kuszpit[3], Kenneth Zasadny[3] and Dana Hu-Lowe[4].***

*Worldwide Comparative Medicine, Molecular Medicine, BioImaging COE, Oncology Research, Pfizer Global Research and Development, Groton, CT 06340*

**Objective**

The goals of our studies were to use contrast enhanced ultrasound to examine impact on tumor growth and vascular flow, volume and tumor perfusion in non-small cell lung carcinoma cells (NSCLC) xenograft tumors in mice when (1) under treatment by axitinib (a selective VEGF receptor tyrosine kinase inhibitor); (2) after withdrawal of axitinib treatment. The results from the contrast ultrasound assessments will also be compared to those from FLT-PET imaging obtained under the same paradigm.

**Methods**

Studies were conducted under approval of the Institutional Animal Care and Use Committee (IACUC). Female nude mice were implanted with H460 non-small cell lung carcinoma cells on the flank. Tumor growth was monitored with caliper measurements and mice were randomized into three treatment groups: (1) vehicle, (2) continuous axitinib treatment (15 mg/kg, PO, BID), and (3) axitinib treatment for 10 days followed by a 2 day or 5 day break before resuming axitinib treatment. Mice were imaged at 0, 2, 9, 13, 16 and 21 days of after the initiation of dosing. Contrast ultrasound imaging was performed using the Vevo770 (VisualSonics, Toronto, ON) in 2D and 3D modes with Definity microbubble contrast agent (Lantheus, N. Billerica, MA). 3D Power Doppler, 3D contrast and 2D contrast uptake data sets were analyzed using the Vevo software and Matlab algorithms.

**Results**

Treatment with axitinib for 9 days caused decreased vascular volume and tumor perfusion when compared to vehicle treatment. Withdrawal of axitinib for 2 days showed a small increase in perfusion, which further increased after 5 days off drug period, and which was statistically significant from the signal obtained with continuous treatment regimen. Return to treatment after withdrawal resulted in a second decrease in perfusion. The kinetics and dynamic modulation of tumor perfusion measured by CEUS was similar to that of modulation of FLT-PET tracer uptake.

**Conclusions**

Contrast enhanced ultrasound may be an effective approach for monitoring changes in tumor perfusion in nonclinical tumor models. Furthermore, CEUS may be used to monitor tumor response to anti-angiogenic drugs before progression and to predict the optimal timing for combination therapy.

# Contrast Imaging of Breast Cancer Tumors – Work in progress

***Petter Østhus[1], Trine Holmen[2], Marianne Birgitte Brekke[3], Agnes Østlie[2], Thor Andreas Tangen[4], and Svein-Erik Måsøy[4]***

*[1]Department of Surgery, Section of breast and endocrine surgery, St. Olavs University Hospital, Trondheim, Norway*
*[2]Department of Radiology, Section of Mammography, St. Olavs University Hospital, Trondheim, Norway*
*[3]Department of Pathology and Medical Genetics, St. Olavs University Hospital, Trondheim, Norway*
*[4]Department of Circulation and Medical Imaging, Norwegian University of Science and Technology (NTNU), Trondheim Norway*

**Introduction**

Re-operation of breast cancer patients after the discovery of an insufficient resection margin is problematic both for the health care system and the patients. In a study by Jiang *et al.* [1], it was shown that contrast-enhanced ultrasound (CEUS) displayed a larger tumor than conventional BMode imaging in 62.8% of malign tumors. In total, 104 lesions were examined where 43 were malign, 60 benign, and 1 border case. Only one benign tumor appeared significantly larger on CEUS compared to BMode. The results were verified by histology.

The results of Jiang *et al.* formed the background for the hypothesis of the project presented here: *Can CEUS reduce the rate of re-operations in breast-conserving surgery?*

**Methods**

A small pilot study was initiated to obtain preliminary results. Fifteen patients scheduled for breast-conserving surgery are planned to be included into the study. The study has been approved by the local ethics committee, and the patients provide informed consent. All patients are also scheduled for a DCE-MRI examination to establish a "gold" standard.

The CEUS examination is performed by an experienced radiologist (TH).

The surgeon participates in the CEUS examination marking the image plane of the probe with a permanent marker pen. The patient is told to maintain the markings until the day of surgery, and the surgeon then marks the tumor so the pathologist may easily locate the plane of the ultrasound probe. This will minimize the problem of comparing the histology plane to the ultrasound imaging plane.

Standard histology is performed on the tumor, and additional CD31 or CD34 staining is performed to determine the amount of endothelial cells and thus the vascularization.

A Toshiba Applio XG V4.0 system with a PLT-805AT probe is used for the CEUS examination. A Bmode image is stored just prior to injection of the contrast bolus and the size of the tumor is measured. A bolus of 4.8 ml Sonovue is injected into the antecubital vein. Micro Flow Imaging (MFI) is activated in contrast mode and a 30 second recording is stored using a dual mode image showing both the BMode image and the MFI image. By activating MFI it is possible to visualize the areas of contrast agent activity. Based on descriptions from Jiang *et al.*, there is very little change in the MFI image after 30s, and this is also our experience.

After the MFI image has stabilized (15-30 seconds), the tumor is measured both in the BMode image and the MFI image.

**Results**

So far, three patients have been recruited. The results for these three show that the tumors appear larger using CEUS compared to BMode. There are also areas of the tumors that show little or no CEUS signal indicating low vascular or necrotic regions, but this has not yet been verified by histology. Figure 1 shows an example of a BMode image from one patient, and Figure 2 show the corresponding CEUS image.

Cineloops of the recordings and analysis of the results so far will be presented.

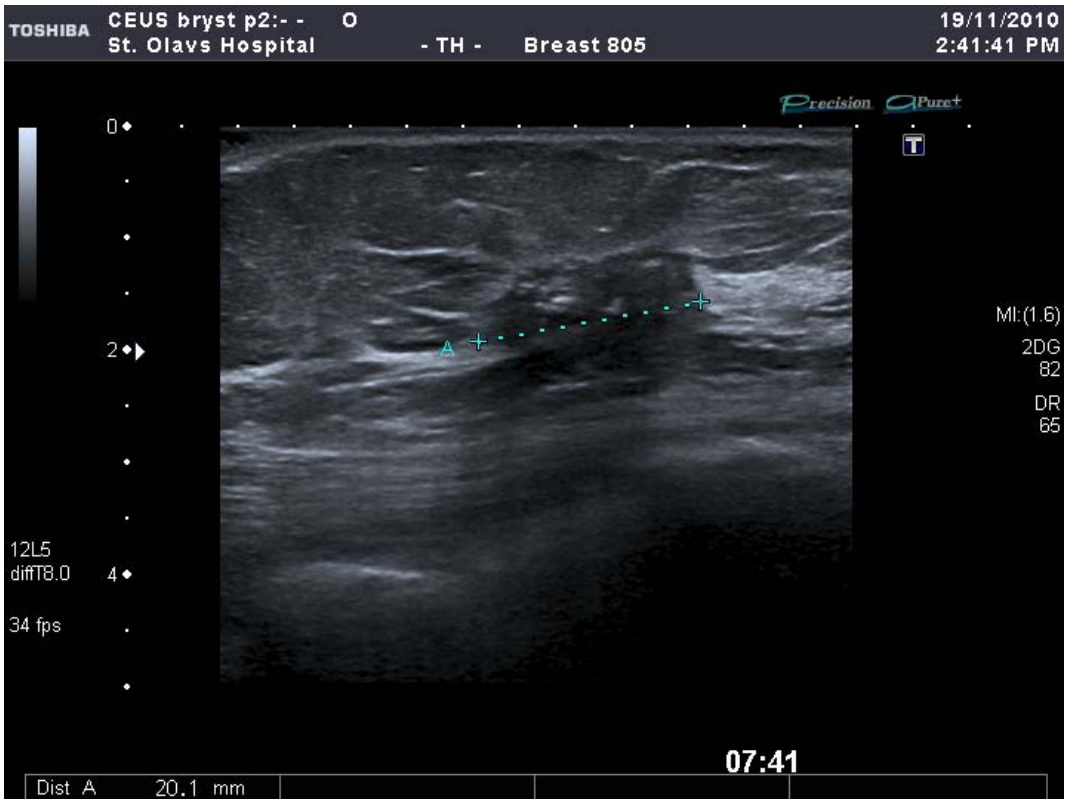


**Figure 1: BMode image of tumor.**

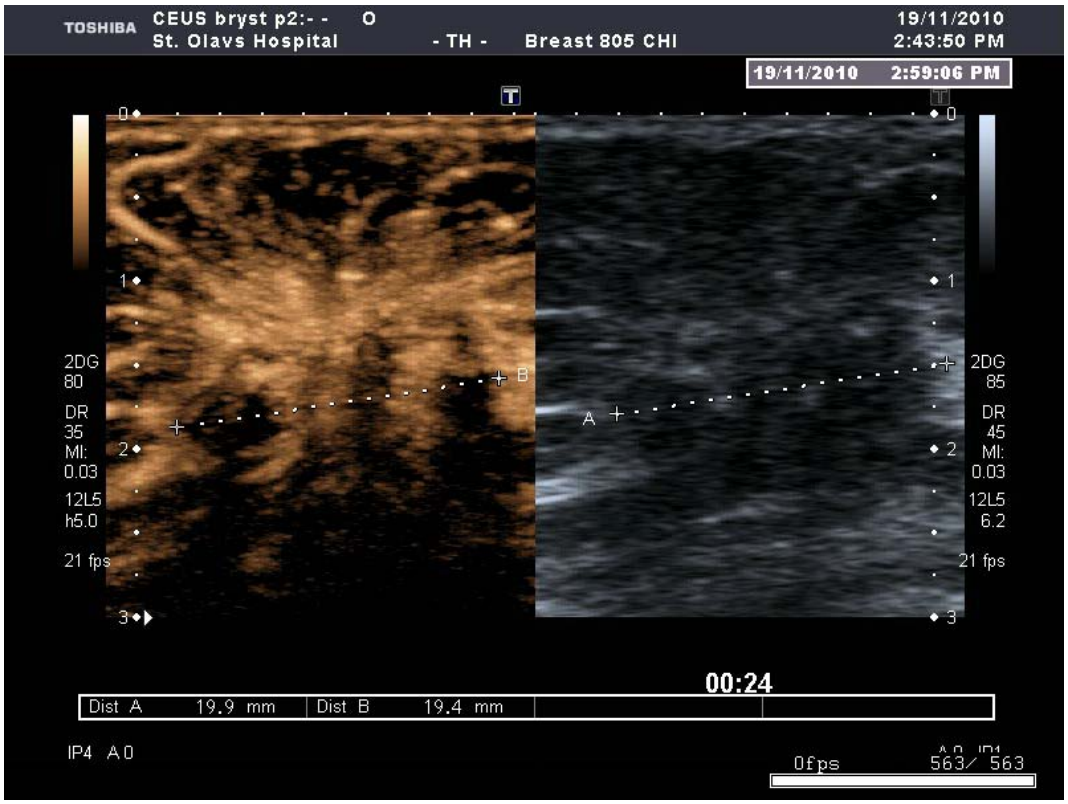


**Figure 2: CEUS image. To the left: MFI image, to the right: BMode image 24 seconds after injection of the bolus.**

**Reference**

Y.-X. Jiang, H. Lu, J.-B. Liu, Q.-L. Zhu, Q. Sung, and X.-Y. Chang, Breast tumor size assessment: Comparison of conventional ultrasound and contrast-enhanced ultrasound., Ultr. In Med. And Biol., Vol. 33, No. 12, pp.1873-1881, 2007.

# Drug and Gene-delivery in cardiovascular and tumor models

***Mareike Mühlmeister and Klaus Tiemann***

*Medical Clinic Cardiovascular Imaging,*
*University Hospital Münster*

Drug- and gene-delivery by targeted ultrasound might overcome crucial limitations of current therapeutic strategies in cardiovascular medicine and oncology. Optimizing therapeutic strategies in-vivo is somehow cumbersome, as readout usually requires harvesting the organs by sacrificing the animal. In addition, if new therapeutic particles or microbubbles are tested their biodistribution is also difficult to assess. We therefore tested the feasibility to assess biodistribution of therapeutic particles and microbubbles as well as success of delivery of particles by optical imaging. Optical imaging provides good temporal and sufficient spatial resolution to study biodistribution in variable organs (see figure 1).

We tested a new nanoparticle capable to carry drugs or genetically active material (p-DNA, siRNA) studied the biodistribution and the capability to deliver these particles by HIFU. We therefore co-injected perflutren filled microbubbles and nanoparticles (fluorescently labeled 150 nm human serum albumin nanoparticles or 70 kDa FITC-Dextran). In a U87MG dEGFR glioblastoma mouse-tumor model delivery into tumor tissue was assessed by optical imaging in-vivo and ex-vivo as well as by fluorescence microscopy. A dedicated HIFU system (Therapy and Imaging Probe System, Philips Research North America) was used (1.2 MHz, 2 MPa, 10.000 cycles, 0.2 Hz pulse repetition frequency), a matrix pattern with a step size of 0.5 mm (2.5 s waiting time between spots) was applied to cover the entire tumor volume. HIFU-delivery resulted in a 2-fold uptake of nanoparticles as compared to control animals without HIFU. For smaller particles (FITC-Dextran) delivery was much higher. In cell cultures about 40 % of a confluent layer of U87MG glioblastoma cells were FITC-positive by single short pulse using HIFU (see figure 2). These in-vitro results were comparable to in-vivo results in tumor and other tissues.

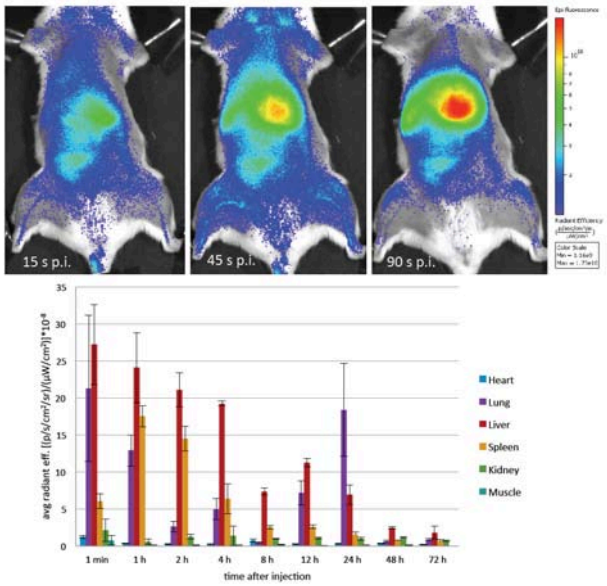


**Fig. 1: Optical imaging of 150 nm fluorescently labeled human serum albumin nanoparticles 15, 45 and 90 s after injection in-vivo and their biodistribution in ex-vivo organs at different time points after injection (n=3).**

In order to optimize delivery results, pre-treatment using HIFU was performed to modify cell-cell contacts as well as extracellular matrix/basal membrane. HIFU resulted in a significant modification of extracellular matrix by protease-activation (MMP-9), which could be demonstrated not only in tumor tissue but also in myocardial tissue. Pretreatment of myocardial tissue resulted in a significant reduction of e.g. laminin (matrix-protein). Using these pretreatment strategies delivery of naked p-DNA or other reporter particles to myocardial tissue was possible. Future strategies for drug- and gene-delivery should therefore take pre-treatment by HIFU into account.

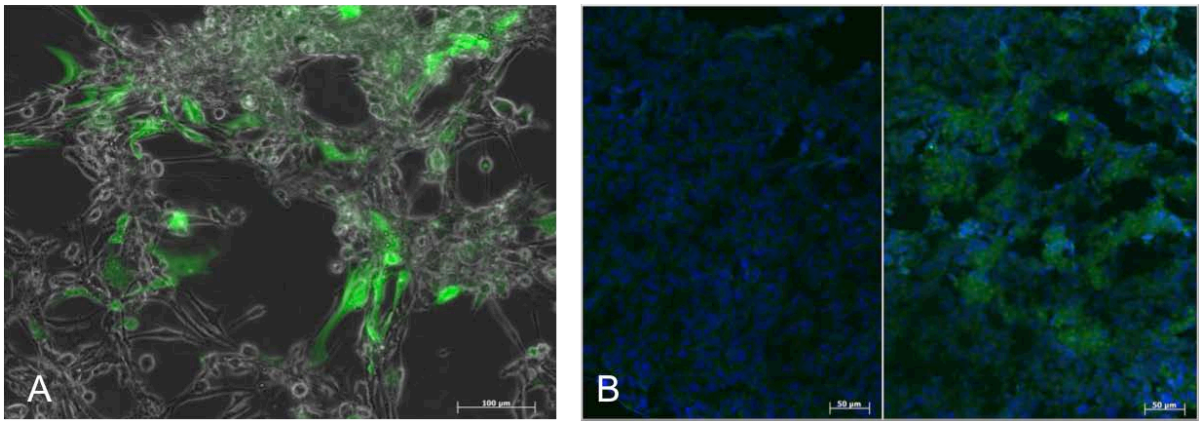


**Fig. 2: A. FITC-Dextran delivery in U87MG glioblastoma cells in-vitro with HIFU. B. Control (left) and HIFU treated U87MG dEGFR tumor (right) after co-injection of FITC-Dextran and microbubbles.**

# Acoustic Droplet Vaporization for Drug Delivery

***J. Brian Fowlkes, PhD***

*University of Michigan*
*Departments of Radiology and Biomedical Engineering*

Acoustic droplet vaporization (ADV) uses ultrasound to activate biocompatible microdroplets containing perfluorocarbon (PFC) liquid to undergo phase transition to form microbubbles. We have examined the use of the resulting microbubbles for a variety of potential medical applications[1] including to control of blood flow[2,3]. More recently, we have developed a controlled drug release approach[4,5] that provides encapsulation of lipid or water soluble drugs. As a demonstration of drug delivery, double emulsions with chlorambucil (CHL), a lipophilic chemotherapeutic, was tested by an incubation cellular assay in which the emulsion caused a 47% growth inhibition, whereas exposure of the emulsion to ultrasound at 6.3 MHz caused an 84% growth inhibition. This difference was statistically significant ($p < 0.01$) and indicates a potential to reduce systemic effects for drug administration. To further improve the drug retention, an alternative double emulsion was prepared in a two-step process using a perfluorocarbon surfactant to stabilize in internalized oil or water phase where the drug is contained. This provides for a diffusion restrictive layer of PFC liquid. Drug retention and release was evaluated in emulsions containing fluorescein in the interior water phase as a drug surrogate where an 8-fold increase in mass flux occurred following ADV. Additionally, double emulsions encapsulating thrombin are being developed to enhance the duration of ADV-generated embolization with the potential of bleeding control. In a standard blood coagulation assay, three out of five emulsion formulations resulted in a statistically significant ($p < 0.01$) decrease in clotting time with ADV released thrombin compared to emulsions not exposed to US. Therefore, there is a large range of potential applications for ADV activated drug release. This research is sponsored in part by NIH grant 5R01EB000281.

**References**

1. Kripfgans OD, et al., Ultrasound Med. Biol., 26 (7), 1177-1189, 2000.
2. Kripfgans OD, et al. IEEE Trans. Ultras. Ferroel. Frequency Control, 52, 1101-1110, 2005.
3. Zhang M, et al. Ultrasound Med Biol, 36(10): 1691-703, 2010.
4. Fabiilli ML et al., Ultrasound Med Biol, 36(8):1364-1375, 2010.
5. Fabiilli ML et al, Pharm Res, Published online 25 Sept 2010

# Biodegrable polymeric microcapsules for sequential ultrasound-triggered drug release.

***Dennis Lensen, Dennis M. Vriezema, Nico Verdonschot, Jan C. M. van Hest***

*Institute for Molecules and Materials, Radboud University Nijmegen, the Netherlands*
*Encapson B.V., Nijmegen, the Netherlands*
*Orthopaedic Research Laboratory, RUN Medical Centre, Nijmegen,the Netherlands*

***Erik C. Gelderblom, Nico de Jong, and Michel Versluis***

*Physics of Fluids Group, University of Twente, Enschede, The Netherlands*

Ultrasound-triggered release has become a attractive method of drug delivery since the release trigger can be applied locally. In addition, ultrasound can be used at lower pressures to monitor the arrival or presence of the microcapsules before activation in the release area, which could substantially improve therapeutic treatment. A next step forward would be realized if UCA drug delivery vehicles could be employed in triggered release or in sequential drug release. This could be achieved if a mixture of microcapsules is used which releases its encapsulated drugs at different ultrasound parameters, such as pressure, pulse repetition frequency or pulse length.

Here we describe the use of a series of biodegradable polymeric microcapsules with adjustable sensitivity toward ultrasound. Tuning of the shell thickness of a capsule made it possible to selectively trigger capsules using diagnostic ultrasound. We found a strong correlation between the activation pressure of the ultrasound, the pressure at which a capsule shell ruptures, and the shell thickness of similarly sized capsules.

The microcapsules were produced using an emulsion-evaporation technique. A mixture of perfluoroctanol-polylactic acid (PFO-PLLA) and dichloromethane and a non-volatile non-solvent (decane) was used. As the dichloromethane evaporated, small polymer-rich droplets were formed by phase separation within the emulsion droplets. By using different initial concentrations of polymer in the organic phase and by maintaining the same mechanical energy for droplet formation, four different capsules were prepared with increasing shell thickness.

The capsule dynamics was studied optically using the Brandaris 128 ultra high-speed camera during insonification of the capsules. A 15-cycle pressure pulse with a frequency of 1 MHz was applied at pressures ranging from low acoustic pressures (order 100 kPa), where no capsules were disrupted, to medium, where the thinnest capsules were disrupted, to high (1 MPa) where the thickest capsules were

destroyed. The Brandaris camera was operated at a frame rate of 5 Mfps, thus allowing for a highly detailed insight in the behavior of the microcapsules during the applied pressure wave.

Capsules with the thinnest shell were observed to display a buckling behavior at an acoustic pressure of 125 kPa, while above a certain acoustic pressure threshold near 400 kPa, the shell would yield, resulting in rupture of the shell and release of the gas content. The capsules with a higher shell thickness/diameter ratio did not show buckling behavior, apparently due to a shell thickness of these capsules that was too high to allow indentation. All capsules responded by rupturing when the acoustic pressure exceeded 1.2 MPa. These results are in agreement with the very recent theory of Marmottant et al. (JASA 2011, in print) on the buckling resistance of solid shelled microcapsules under ultrasound pressure, where they calculated that capsules with thin solid membranes can sustain in-plane compressions. They also stated that when the shell thickness increases, no buckling will be observed and the bubbles will only rupture and release their gas content.

The excellent control over the shell thickness of these capsules makes them ideally suited as vehicles for sequential drug delivery. Two different capsules types were mixed and the capsules with the thinner shell were fluorescently labeled with Nile Red. An overlayed image of fluorescence microscopy and bright-field imaging is shown in Figure 1. By applying a pressure pulse of 400 kPa the thin-shelled capsules are activated see Figure 1B. In multiple experiments it was observed that indeed all fluorescently labeled capsules, i.e. those with the same ratio of shell thickness/diameter, were activated. The other capsules showed a different morphology, although they were not violently disrupted. When applying a second pressure pulse of 1.2 MPa, also the thicker shelled microcapsules were disrupted, see Fig. 1C.

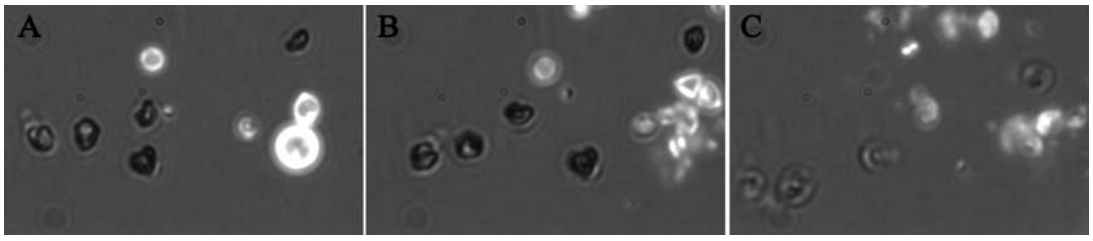


**Figure 1. Overlay microscope images of mixed microcapsules having different shell thicknesses, triggered by ultrasound. A. Image of the microcapsules when no pressure is applied. B. Image of the microcapsules when 400 kPa of pressure was applied. C. Image of the microcapsules when 1.2 MPa was applied.**

In conclusion, we have shown that capsules with different shell/diameter ratios can be triggered independently from each other. The strong correlation between shell/diameter ratio and ultrasonic pressure makes these capsules ideal for a pulsed drug release application and even sequential drug release from UCA delivery vehicles.

# Self-assemblED liposome-loaded microbubbles: the missing link for safe and efficient ultrasound triggered drug-delivery

***Geers Bart*[1], *Lentacker Ine*[1], *Sanders Niek*[2], *Demeester Joseph*[1], *Meairs Stephen*[3], *De Smedt Stefaan*[1]**

[1] *Ghent Research Group on Nanomedicines, Lab of General Biochemistry and Physical Pharmacy, Faculty of Pharmaceutical Sciences, Ghent University, Harelbekestraat 72, 9000 Gent, Belgium*
[2] *Laboratory of Gene Therapy, Faculty of Veterinary Medicine, Ghent University, Heidestraat 19, 9820 Merelbeke, Belgium*
[3]*Department of Neurology, Universitätsklinikum Mannheim, Heidelberg University, Theodor-Kutzer-Ufer 1-3, 66167 Mannheim, Germany*

**Introduction**

Liposome-loaded microbubbles have been recently introduced as a promising drug delivery platform for ultrasound guided drug delivery. We showed that in combination with ultrasound, such microbubbles strongly improved both doxorubicin (DOX) cytotoxicity (1) and pDNA (2) and siRNA (3) delivery to cells *in vitro*. However, the complex microbubble preparation method, the immunogenic nature of the avidin-biotin chemistry used to link the liposomes/lipoplexes to the microbubbles and the successive washing steps, made this material not ideal for easy clinical use. It is clear that the concept of liposome-/lipoplex-loaded microbubbles needs further development and improvement. In this work we faced the challenge to design DOX-liposome loaded lipid shelled microbubbles through the self-assembly of the involved compounds. Importantly, the method we propose involves just a single step and allows to make a sterile material. Hereby introducing a safe and efficient method that allows clinical translation of ultrasound induced drug delivery as illustrated in Figure 1.

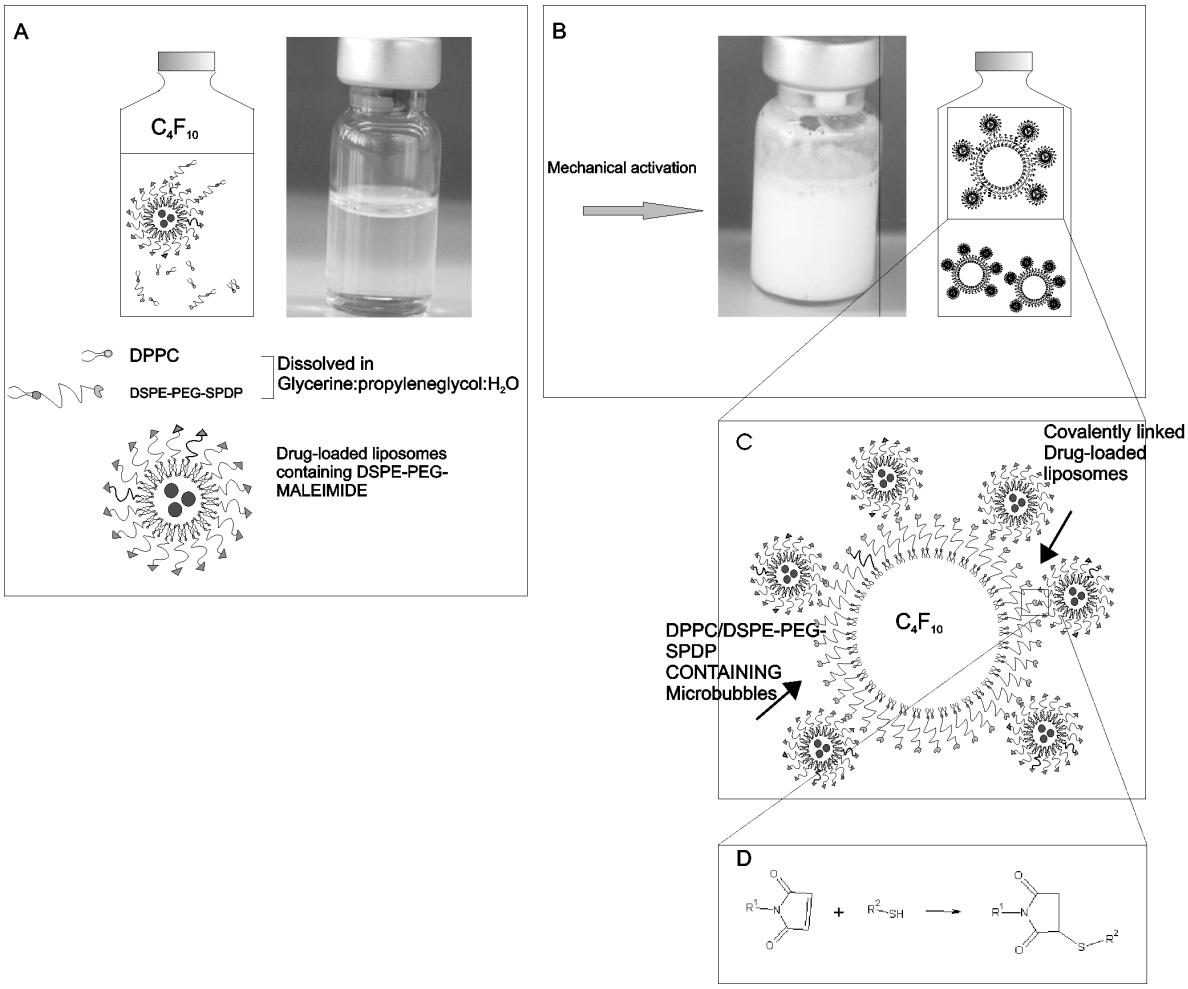


**Figure 1: Schematic depiction of the preparation of liposome-loaded through self-assembly of lipids in solution and functionalized liposomes. High speed shaking of vials, containing the phospholipids DPPC and DSPE-PEG-SPDP and drug loaded liposomes containing DSPE-PEG-MALEIMIDE (A), gives rise to lipid-shelled microbubbles (B) loaded with liposomes and with a $C^4F^{10}$ gas core (C). The liposomes become coupled to the microbubbles' surface through covalent thiol-maleimide linkages (D). Note that the microbubbles are a few microns in size while the liposomes are some hundreds of nanometers.**

## Methods and Materials:

Microbubbles were prepared using a solution of DSPE-PEG-SPDP and DPPC (Avanti polar lipids, Albaster, USA) in a propyleneglycol:glycerine:water mixture. 1.5ml of this solution was mixed with adequate amounts of DOX-liposomes and 50µl of a 10% dithiotreitol in water solution (Sigma-alldrich, Bornem, Belgium) which creates free thiol groups. After mixing in a 2 ml glass vial, $C_4F_{10}$ was added. A mechanical activation device (Capmix, 3M) was used to create gas filled microbubbles functionalized with thiol-groups. DOX-liposomes were prepared using a 15:85 DSPE-PEG-maleimide, DPPC mixture. After chloroform evaporation the lipid film was hydrated with a 250mM solution of $(NH_4)_2SO_4$ and extruded through a 100nm filter using a mini extruder (Avanti-polar lipids, Albaster, USA). Liposomes were dialyzed overnight to remove the excess of $(NH_4)_2SO_4$. Size measurements were performed using a Coulter Counter (Beckman Coulter, Brea, CA). Flow cytometry analysis was performed to evaluate

liposome-loading capacity using a BD FACScalibur flow cytometer (BD, Erembodegem, Belgium). Release of free Doxorubicin was evaluated fluorimetrically using a Perkin-elmer plate reader. Fluorimetry was performed at an excitation wavelength of 488nm and an emission wavelength of 580nm. Qualitative microscopy was performed using a Nikon-EZC1 confocal microscope using bodipy-loaded liposomes. Tumor cell killing efficiency was evaluated in vitro using the MTT cell proliferation assay on melanoma cells in opticell® plates. Ultrasound in vitro experiments were performed using a sonitron sonoporation device with an ultrasound frequency of 1MHz, a 30% duty cycle and an ultrasound intensity of $2W/cm^2$.

**Results**

Using confocal microscopy and coulter counter measurements we were able to show that the proposed method allows us to make liposome-loaded microbubbles (figure 2). Furthermore, we quantitatively characterized drug loading on the surface of the microbubble. Subsequently we evaluated whether these drug-loaded microbubbles would enable ultrasound induced drug release and activity using Doxorubicin as a model drug. Interestingly we show that these drug-loaded microbubbles generate cell killing even when amounts of drug are used which are non-toxic when applied without ultrasound.

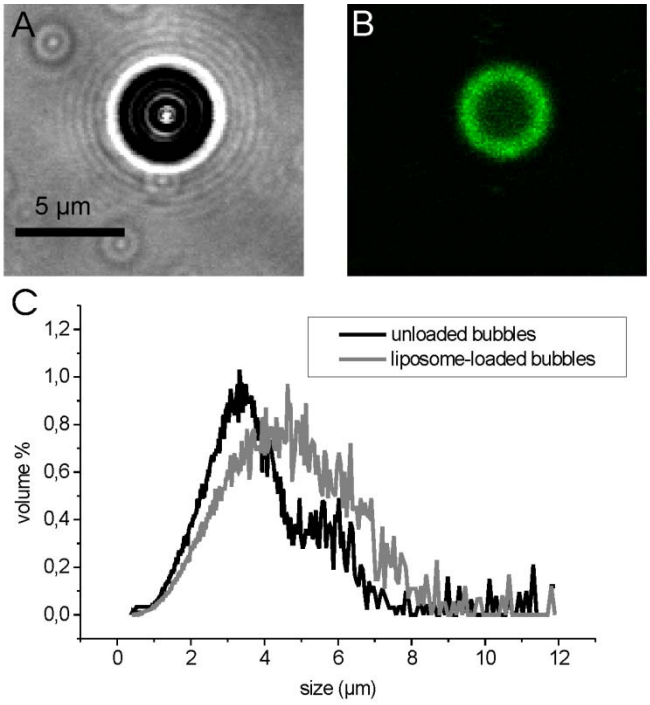


**Figure 2: Transmission image (A) and confocal image (B) of a (bodipy-labeled) liposome-loaded microbubble. Size distributions of unloaded and liposome loaded microbubbles as obtained by Coulter Counter measurements (C) show an increase in mean size when liposomes are bound to the microbubbles' surface.**

**Acknowledgements**

This work is part of the EU collaborative projects SONODRUGS (NMP-4-LA-2008-213706) and ARISE. Ine Lentacker is a post-doctoral fellow of the FWO flanders the financial support of this institute is thanked.

**References**

1. Lentacker I, Geers B, Demeester J, De Smedt SC, Sanders NN. Design and Evaluation of Doxorubicin-containing Microbubbles for Ultrasound-triggered Doxorubicin Delivery: Cytotoxicity and Mechanisms Involved. Mol Ther 2009 Jul 21.
2. Lentacker I, De Smedt SC, Demeester J, Van Marck V, Bracke M, Sanders NN. Lipoplex-loaded microbubbles for gene delivery: A Trojan horse controlled by ultrasound. Advanced Functional Materials 2007;17(12):1910-6.
3. Vandenbroucke RE, Lentacker I, Demeester J, De Smedt SC, Sanders NN. Ultrasound assisted siRNA delivery using PEG-siPlex loaded microbubbles. J Control Release 2008 Mar 20;126(3):265-73.

# Reduction of Restenosis by Dual-Ultrasound-Mediated Rapamycin Delivery from Microbubbles in a Rat Model of Vascular Injury

***Linsey C. Phillips[1], Ali H. Dhanaliwala, Alexander L. Klibanov, Brian R. Wamhoff, John A. Hossack***

*[1]Biomedical Engineering, University of Virginia*

**Introduction & Background**

In both humans undergoing percutaneous coronary angioplasty and animal models of balloon injury, smooth muscle cells in the arterial wall proliferate leading to neointima formation. This hyperproliferation of cells can lead to restenosis and blockage of the arteries. Consequently, there is a need for localized drug delivery at the site of vascular injury.

We have been investigating the use of ultrasound and microbubbles for targeted drug delivery. We have incorporated rapamycin, an anti-proliferative drug, into lipid-shelled microbubbles. The lipid microbubbles are similar to those approved by the FDA. We have previously shown that a focused ultrasound beam can be used to localize the rupture of the microbubbles and the subsequent drug delivery. We are currently investigating an *in vivo* rat model of balloon injury and drug delivery in an attempt to reduce smooth muscle cell proliferation and neointima formation in the lumen of rat carotid arteries. We sought to decrease neointima formation by using an acoustic radiation force pushing pulse to concentrate the microbubbles near the vessel wall, and high intensity burst pulses to deliver the therapeutic payload at the site of injury minutes after it has occurred.

**Methods**

Microbubbles were composed of base lipid components: phosphatidylcholine (2mg/ml) and polyethylene glycol stearate (2mg/ml). Rapamycin (0.4 mg/ml) was added to the base components to produce therapeutic microbubbles and a trace amount of the fluorescent dye DiI (Molecular Probes, Eugene, OR) was added to the base components to produce control microbubbles. The final amount of rapamycin in the microbubbles prior to injection was previously determined to be 29ng per million microbubbles.

Sprague-Dawley rats underwent carotid balloon injury by inserting a 3-French balloon catheter 1.5 cm past the bifurcation of the right common carotid. The balloon was inflated, pulled toward the bifurcation, deflated, and then moved back into the carotid a total of 3 times. Two ultrasound transducers were aligned with the injured vessel for image, pushing and bursting. A 15L8 transducer

connected to a Siemens Sequoia was aligned such that the injured artery was approximately 1 cm from the face of the transducer. This transducer was used to image the artery, in both B-mode and CPS mode, and to rupture the microbubbles. Bursting was accomplished with a 0dB (~1.5 MPa) pulse that was fired once a second for 3 seconds, paused for 2 seconds, then repeated for the duration of exposure. A second unfocused single element 1 MHz transducer was aligned at a 45 degree angle from the first transducer and perpendicular to the length of the artery. This transducer was used to push the microbubbles using a continuous wave 60 kPa 1MHz. Ultrasound pushing and bursting was initiated immediately following injury for a duration of 10 minutes. During this period, microbubbles were infused through a left jugular vein catheter over 8 minutes. Images were acquired periodically throughout the insonation. Control rats received either no microbubbles without ultrasound, or rapamycin-loaded microbubbles withoutultrasound. Animals which received DiI microbubbles were euthanized 1 hour after insonation, whereas animals which received drug-loaded rapamycin microbubbles were euthanized 2 weeks after insonation. Arteries were excised and processed for sectioning and histology. Statistical analysis between groups was performed with a student's t-test.

**Results**

DiI delivery was observed in the carotids of injured rats where ultrasound was applied. Delivery was observed following high intensity burst mode pulses only and was not significantly increased by the addition of the radiation force ultrasound. The neointima to media ratio (NI/M) of rats which underwent only balloon injury was found to be 1.54+/-0.25 (n=11) compared to 0.0 for uninjured controls (n=5). The NI/M of injured carotids treated with rapamycin microbubbles alone was 1.22 +/- 0.08 (n=3) as compared to 1.01 +/- 0.33 (n=7) for carotids treated with rapamycin microbubbles and ultrasound at the site of injury. Ultrasound mediated delivery of rapamycin from microbubbles at the site of vascular injury reduced neointima formation by 32%.

**Discussion and Conclusions**

Rats treated with rapamycin microbubbles had a reduction in neointima formation with and without ultrasound. With further optimization of the pushing and burst pulses it may be possible to increase delivery and enhance the therapeutic effect. These experiments demonstrate the feasibility of using rapamycin-microbubbles to reduce restenosis following balloon angioplasty.

# CEUS: Vasa Vasorum Update

***Steven Feinstein, MD, FACC, FESC***
***Professor of Medicine***

*Rush University Medical Center*
*Chicago, Illinois USA*

Today, there is an increased awareness and utilization of contrast enhanced ultrasound (CEUS) primarily due to the simplicity and safety of ultrasound imaging. Further, CEUS imaging does not utilize ionizing radiation, provides excellent spatial and temporal image resolution, and is cost-efficient.

While the initial clinical uses of CEUS focused on left ventricular chamber enhancement in echocardiography, the current expanded uses include vascular applications: (1) aortic vessels, (2) carotid arteries and (3) peripheral venous systems.

In 2004, Mattrey and Kono and Macioch et al., used CEUS as an alternative imaging modality for the assessment of carotid anatomy in patients. (1,2)Subsequently, numerous international investigators have corroborated the observations and described the clinical value of using CEUS for vascular imaging. (3-22)

Recent interest in CEUS for vascular imaging focuses on these specific topics: (a) Enhancement of the carotid artery lumen (plaque/ulcer), (b) Enhancement of the intima-media-thickness (IMT) and (c) Identification of adventitial/intra-plaque angiogenesis (vasa vasorum).

Perhaps the most intriguing application of CEUS in vascular imaging is centered on the identification of adventitial and intra-plaque angiogenesis (vasa vasorum) within the carotid vulnerable plaque.

From histologic studies, it is known that atherosclerotic plaques develop the nutrient blood supply from the adventitial arterial surfaces. These structures are readily identified following the use of CEUS. (23-25)

In the future, to accurately quantify the arterial vasa vasorum associated with atherosclerosis (adventitial and intra-plaque angiogenesis) a real-time, volumetric, analysis will be required. It is anticipated that ECG-gated 3-D/4-D ultrasound system will be developed to quantify intra-plaque vasa vasorum. And, perhaps in the not-to-distant future, the vasa vasorum vessels may serve as conduits to deliver therapy to the vulnerable plaque.

**References**


1. Kono Y, Pinnell SP, Sirlin CB, et al. Carotid arteries: contrast-enhanced US angiography--preliminary clinical experience. Radiology 2004;230:561-8.
2. Macioch JE, Katsamakis CD, Robin J, et al. Effect of contrast enhancement on measurement of carotid artery intimal medial thickness. Vasc Med 2004;9:7-12.
3. Alpern-Elran H, Morog N, Robert F, Hoover G, Kalant N, Brem S. Angiogenic activity of the atherosclerotic carotid artery plaque. J Neurosurg 1989;70:942-5.
4. Biedermann BC, Coll B, Adam D, Feinstein SB. Arterial microvessels: an early or late sign of atherosclerosis? J Am Coll Cardiol 2008;52:968; author reply 968-9.
5. Carlier S, Kakadiaris IA, Dib N, et al. Vasa vasorum imaging: a new window to the clinical detection of vulnerable atherosclerotic plaques. Curr Atheroscler Rep 2005;7:164-9.
6. Coli S, Magnoni M, Sangiorgi G, et al. Contrast-enhanced ultrasound imaging of intraplaque neovascularization in carotid arteries: correlation with histology and plaque echogenicity. J Am Coll Cardiol 2008;52:223-30.
7. Coll B, Feinstein SB. Carotid intima-media thickness measurements: techniques and clinical relevance. Curr Atheroscler Rep 2008;10:444-50.
8. Dunmore BJ, McCarthy MJ, Naylor AR, Brindle NP. Carotid plaque instability and ischemic symptoms are linked to immaturity of microvessels within plaques. J Vasc Surg 2007;45:155-9.
9. Feinstein SB. The powerful microbubble: from bench to bedside, from intravascular indicator to therapeutic delivery system, and beyond. Am J Physiol Heart Circ Physiol 2004;287:H450-7.
10. Feinstein SB. Contrast ultrasound imaging of the carotid artery vasa vasorum and atherosclerotic plaque neovascularization. J Am Coll Cardiol 2006;48:236-43.
11. Fleiner M, Kummer M, Mirlacher M, et al. Arterial neovascularization and inflammation in vulnerable patients: early and late signs of symptomatic atherosclerosis. Circulation 2004;110:2843-50.
12. Granada JF, Feinstein SB. Imaging of the vasa vasorum. Nat Clin Pract Cardiovasc Med 2008;5 Suppl 2:S18-25.
13. Kolodgie FD, Gold HK, Burke AP, et al. Intraplaque hemorrhage and progression of coronary atheroma. N Engl J Med 2003;349:2316-25.
14. Magnoni M, Coli S, Marrocco-Trischitta MM, et al. Contrast-enhanced ultrasound imaging of periadventitial vasa vasorum in human carotid arteries. Eur J Echocardiogr 2008.
15. McCarthy MJ, Loftus IM, Thompson MM, et al. Angiogenesis and the atherosclerotic carotid plaque: an association between symptomatology and plaque morphology. J Vasc Surg 1999;30:261-8.
16. Mofidi R, Crotty TB, McCarthy P, Sheehan SJ, Mehigan D, Keaveny TV. Association between plaque instability, angiogenesis and symptomatic carotid occlusive disease. Br J Surg 2001;88:945-50.
17. Schinkel AF, Krueger CG, Tellez A, et al. Contrast-enhanced ultrasound for imaging vasa vasorum: comparison with histopathology in a swine model of atherosclerosis. Eur J Echocardiogr 2010.
18. Shah F, Balan P, Weinberg M, et al. Contrast-enhanced ultrasound imaging of atherosclerotic carotid plaque neovascularization: a new surrogate marker of atherosclerosis? Vasc Med 2007;12:291-7.
19. Staub D, Patel MB, Tibrewala A, et al. Vasa vasorum and plaque neovascularization on contrast-enhanced carotid ultrasound imaging correlates with cardiovascular disease and past cardiovascular events. Stroke 2009;41:41-7.
20. Staub D, Schinkel AF, Coll B, et al. Contrast-enhanced ultrasound imaging of the vasa vasorum: from early atherosclerosis to the identification of unstable plaques. JACC Cardiovasc Imaging 2010;3:761-71.
21. Vavuranakis M, Kakadiaris IA, Papaioannou TG, et al. Contrast-enhanced intravascular ultrasound: combining morphology with activity-based assessment of plaque vulnerability. Expert Rev Cardiovasc Ther 2007;5:917-25.
22. Vicenzini E, Giannoni MF, Puccinelli F, et al. Detection of carotid adventitial vasa vasorum and plaque vascularization with ultrasound cadence contrast pulse sequencing technique and echo-contrast agent. Stroke 2007;38:2841-3.
23. Kumamoto M, Nakashima Y, Sueishi K. Intimal neovascularization in human coronary atherosclerosis: its origin and pathophysiological significance. Hum Pathol 1995;26:450-6.
24. Sluimer JC, Gasc JM, van Wanroij JL, et al. Hypoxia, hypoxia-inducible transcription factor, and macrophages in human atherosclerotic plaques are correlated with intraplaque angiogenesis. J Am Coll Cardiol 2008;51:1258-65.
25. Sluimer JC, Kolodgie FD, Bijnens AP, et al. Thin-walled microvessels in human coronary atherosclerotic plaques show incomplete endothelial junctions relevance of compromised structural integrity for intraplaque microvascular leakage. J Am Coll Cardiol 2009;53:1517-27.

# Imaging of the plaque neovascularization

***Arend Schinkel***

*Department of Cardiology, Erasmus MC*

Atherosclerosis is a progressive chronic inflammatory disease that may be complicated by cardiovascular events. Myocardial infarction, stroke, and peripheral vascular obstruction are generally caused by rupture or erosion of an unstable atherosclerotic plaque, resulting in acute arterial thrombosis. Atherosclerotic plaques with an increased risk to rupture, due to intraplaque hemorrhage or cap rupture, are considered vulnerable plaques. Identification of vulnerable plaques is needed to identify patients at risk and to develop treatment strategies for atherosclerosis and/or plaque stabilization. Recently, several non-invasive imaging techniques have become available for detecting these signs of atherosclerosis. Contrast-enhanced ultrasound imaging is the perhaps the most promising imaging modality, because of its high-spatial and -temporal resolution. Additionally, contrast-enhanced ultrasound is safe and the repeatability of recording, portability, and cost provide an incentive to develop approaches using this modality.

# Late-Phase Contrast Enhanced Ultrasound Reflects Biological Features of Instability in Human Carotid Atherosclerosis

***Joseph Shalhoub, Claudia Monaco, David RJ Owen, Thomas Gauthier, Ankur Thapar, Edward LS Leen, Alun H Davies***

*Imperial College London*

**Background**

The development of translational functional imaging modalities for risk stratification of atherosclerosis is sought for stroke prediction. Our group has developed late-phase contrast enhanced ultrasound (LP-CEUS) to quantify retention of microbubble contrast within carotid atherosclerosis, and have shown that it separates asymptomatic plaques from those responsible for recent cerebrovascular events (normalized signal cut-off at zero). We hypothesised that contrast is retained in areas of plaque inflammation. The aim of this study is to test whether the LP-CEUS signal reflects plaque biology.

**Methods & Results**

Subjects with carotid stenosis for endarterectomy (n=31) underwent axial LP-CEUS and diseased intimal segments were symmetrically divided in the long axis. Half-specimens underwent immunohistochemical analysis (n=29) for quantification of the macrophage marker CD68 and the endothelial marker CD31 (angiogenesis). Percentage area immunopositivity was significantly higher in subjects where normalized plaque late-phase intensity was ≥0 versus <0 (CD68 mean 11.80 vs 6.684, p=0.0037; CD31 mean 9.445 vs 4.819, p=0.0245). Half-specimens were processed for atheroma cell culture (n=21), supernatant collected at 24 hours and subjected to multi-analyte profiling by Luminex for 34 analytes. Interleukin (IL)-6, matrix metalloproteinase (MMP)-1 and MMP3 were significantly higher in the LP-CEUS ≥0 versus the <0 group (IL6 median 5797 vs 764.0, p=0.0302; MMP1 median 2173 vs 480.7, p=0.0428; MMP3 median 184.7 vs 16.05, p=0.0241).

**Conclusion**

LP-CEUS reflects biological features of inflammation, angiogenesis and matrix degradation, which are key features predisposing to plaque rupture. Further investigation of LP-CEUS as a tissue-specific marker of inflammation for risk stratification of carotid atherosclerosis is warranted.

# Quantification of the Plaque Neovascularization and the Hyperplastic Vasa-Vasorum Network with DCE-US

***Michalakis Averkiou, Christophoros Mannaris and Andrew Nicolaides***

*University of Cyprus, Nicosia, Cyprus*

**Introduction**

Cardiovascular disease is the number one killer in the world and stroke is the most common cause of disability. The lack of the proper tools that accurately identify vulnerable carotid plaques (the degree of internal carotid stenosis is the sole criterion for intervention) results in many asymptomatic patients having an unnecessary operation. Histological studies have recognized that plaque inflammation and the presence of plaque neovascularization are strong predictors of instability in atheromatous lesions and symptomatic carotid disease [1]. The ability to measure the hyperplastic network of vasa vasorum and the angiogenesis (new vessel growth) of the plaques may help the identification of asymptomatic patients with vulnerable plaques [2]. Doppler based techniques are unable to image the microcirculation. Ultrasound contrast agents open the way to microcirculation (perfusion) imaging. Thus, plaque perfusion studies can offer a new tools for the identification of vulnerable plaques and for therapy monitoring. The aim of this paper is to present the principles of microbubble imaging and its application to vascular ultrasound with quantification techniques for the study of carotid plaque neovascularization and the hyperplastic vasa vasorum network.

**Materials and Methods**

Fifteen patients with at least 50% carotid stenosis were imaged with Dynamic Contrast Enhanced Ultrasound (DCE-US) and bolus SonoVue injections of 1.2-2.4 ml. A Philips iU22 scanner was used and the images were acquired with the L9-3 and L12-5 linear arrays in a dual display mode (power modulation for depicting microbubbles and conventional B-mode, as shown in Fig. 1(a)-(b)) and low Mechanical Index (MI=0.06). The dynamic range was set to the maximum available, and the persistence was turned off to better accommodate the quantification of the images.

Indicator dilution techniques, injecting an indicator and making measurements during its transit, were used to quantify plaque neovascularization and the network of the vasa-vasorum. The indicator in our case is microbubble contrast agents. Use of the Stewart-Hamilton relations can lead to relative blood flow and blood volume measurements. Different indicator dilution models have been suggested for contrast ultrasound. Here we use the lognormal function. The quantification analysis consisted of forming time-intensity curves (TIC) and then fitting the data to the lognormal function and extracting hemodynamic-related parameters (wash-in time--WIT, mean transit time--MTT, area under the curve--AUC, peak intensity--$I_p$, etc.). Example TICs are shown in Fig. 1(c)-(d).

**Results**

Data from 22 carotids were collected and a total of 31 plaques were analyzed. Thirteen of those had some level of perfusion and neovascularization and 9 had active (thickened) vasa vasorum. The degree of stenosis was calculated according to the European Carotid Surgery Trial (ECST) criteria with both vascular contrast ultrasound and conventional ultrasound. In all cases studied, the degree of stenosis found with contrast was lower. It is not apparently clear why there is a discrepancy between the stenosis calculation found from contrast images and from velocity information.

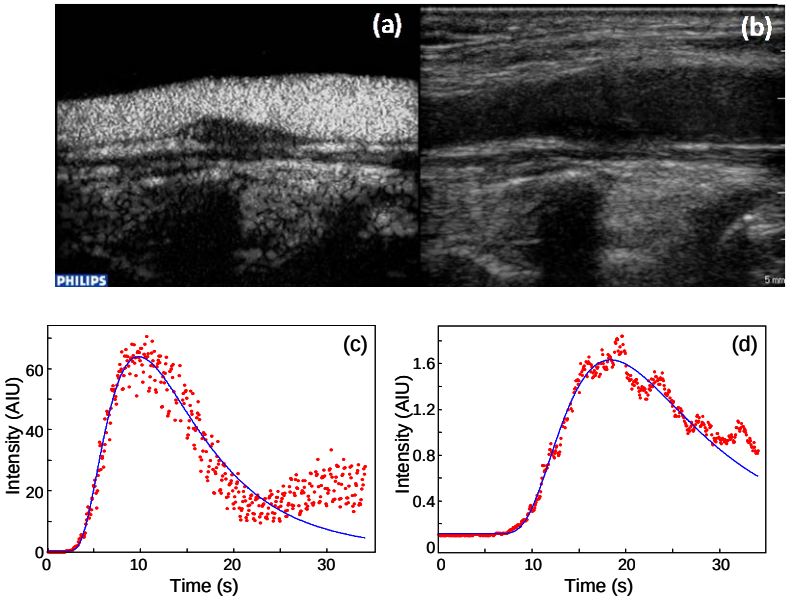


**Figure 1. Image of a carotid plaque. (a) Contrast image with PM technique at MI=0.06; (b) Conventional fundametal image also at MI=0.06. (c) A time intensity curve from a ROI in the lumen of the carotid and (d) from a ROI in a vascularized plaque. Red dots are the image data and the blue line is the best fit to the data with the lognormal function.**

The vessels feeding the plaque and the vasa vasorum are much smaller vessels than the carotid and there is a definite arrival delay between the two. The delay of arrival $\Delta t_a$ is measured from the time intensity curves. We have found that $\Delta t_a$ for plaques is 1.93 seconds (taken from 14 plaques) and 3.35 seconds for the vasa vasorum (taken from 7 enhancing vasa vasorum sections). These indicative times may also be used in deciding whether circulation in a region in the plaque or the vasa vasorum is real or caused by a nonlinear propagation artifact. It would be of interest to monitor this parameter in therapies aimed at plaque remodeling and reducing the cardiovascular risk.

The average WIT and MTT for the carotid is lower than those for the plaque microcirculation and the vasa vasorum. The increase of the WIT from the carotid to the microcirculation is almost 2-fold whereas the increase of MTT is about 10%. The WIT for plaques and vasa vasorum is about the same, whereas the MTT of the vasa vasorum is found to be about 20% greater. We propose as possible imaging biomarkers both the WIT and the MTT. All the results are summarized in Table 1.

**Discussion**

One issue often encountered in the quantification of the plaque neovascularization or vasa vasorum perfusion is an artifact where signal in the image is falsely registered in cases where the ROI (plaque or vasa vasorum) is at the distal wall. Pixels in the plaque are seen to increase their intensity as if microvessel blood flow is present. This is caused by the propagation of the ultrasound pulse in a very nonlinear (bubbly) medium [3] such as is the case of the blood in the carotid. The pulses used for nonlinear pulsing schemes are highly distorted during their passage in the carotid above the plaque or vasa vasorum of interest at the distal wall. This results in incomplete cancellation of the linear targets (the tissue) and their depiction as nonlinear, which is in turn interpreted as microbubbles or blood. The problem is reduced when lower bubble concentrations are used for the clinical exam, i.e., 1.2 ml instead of 2.4 ml of Sonovue. Even at this lower concentration, the artifact is not eliminated totally. Another option is to always study plaques and sections of the vasa vasorum that are at the proximal wall.

The intensity of the pixels in a ROI is proportional to the total blood volume in the area. However, the nature of diagnostic ultrasound is such that user settings may influence this value. By taking the ratio of the plaque (or the vasa vasorum) intensity over the carotid (lumen) the user influence on the settings is suppressed. It is hypothesized that plaques with more perfusion activity (higher signals in the ROI) may be more dangerous. The plaque/lumen intensity ratio shows that type 1 plaques that are pure cholesterol or necrotic material do not have any perfusion, as expected. Type 4 plaques have variable perfusion, but they are clinically safe, and are not associated with events. What is exciting is that in type 2 and 3 plaques some show high and some low perfusion. High perfusion is associated with macrophages and our hypothesis is that this finding may differentiate between subtypes of high risk and low risk plaques type 2 and 3. More research is needed in this area in the future.

| Quantification Parameter | Average Value | Quantification Parameter | Average Value |
|---|---|---|---|
| Carotid WIT (sec) | 5.36 | Plaque WIT (sec) | 9.94 |
| Carotid MTT (sec) | 18.42 | Plaque MTT (sec) | 20.63 |
| Carotid Recirculation (sec) | 18.45 | VV MTT (sec) | 24.66 |
| ΔT plaque-carotid (sec) | 1.93 | Intensity ratio plaque/lumen | 6.15 |
| ΔT VV-carotid (sec) | 3.35 | Intensity ratio VV/lumen | 5.94 |

Table 1: Average parameters for WIT, MTT, $\Delta T_{arrival}$, and intensity ratio for the carotid and the plaque neovascularization.

## Conclusions

Vascular contrast ultrasound is an emerging technique that adds clinical value and research information towards the identification of vulnerable plaques. It is quick to perform, inexpensive and less invasive compared with CT, MRI or PET imaging. In asymptomatic patients with carotid plaques, vascular contrast ultrasound is an adjunct tool to plaque morphology studies by providing valuable information on the degree of neovascularization and the extend of vasa vasorum activity.

**References**


1. McCarthy MJ, Loftus IM, Thompson MM, Jones L, London NJ, Bell PR, Naylor AR, Brindle NP. Angiogenesis and the atherosclerotic carotid plaque: an association between symptomatology and plaque morphology. J Vasc Surg 1999: 30(2):261-8.
2. Feinstein SB. Contrast ultrasound imaging of the carotid artery vasa vasorum and atherosclerotic plaque neovascularization. J Am Coll Cardiol 2006:48(2): 236-243.
3. Tang MX, Elson DS, Li R, Dunsby C, Eckersley RJ. Effects of nonlinear propagation in ultrasound contrast agent imaging. Ultrasound Med Biol 2010:36(3):459-66.

# Vascular recruitment in skeletal muscle during exercise and hyperinsulinemia assessed by contrast ultrasound in mice

***Etto C Eringa[1], Rick I Meijer[2], Caro-lynn A Alta[1], Lynda Juffermans[1], Erik H Serne[2], Yvo M Smulders[2], Victor WM van Hinsbergh[1] and Eugene J Barrett[2]***

*Departments of [1]Physiology and [2]Internal Medicine, VU University medical center, Amsterdam, the Netherlands; Department of [3]Endocrinology, University of Virginia, Charlottesville, USA*

The aim of this study was to noninvasively quantify the effects of exercise and insulin on capillary blood volume and red blood cell velocity in skeletal muscle in mice in vivo with the use of contrast-enhanced ultrasound.

**Methods**

Male Black/6 mice (22±1 grams) were subjected to isometric muscle contraction (1 Hz, 1-5 minutes) or a hyperinsulinemic, euglycemic clamp (3 mU/min/kg, 30 and 60 minutes). Red blood cell velocity ($V_{RBC}$) and microvascular blood volume (MBV) were calculated from the relation between pulsing interval and video intensity during destructive imaging, and from microbubble wash-in during non-destructive imaging.

**Results**

Microbubble replenishment could be visualized and quantified using both destructive and non-destructive imaging. The relationship between pulsing interval and Acoustic Intensity (AI) could be described by an exponential association curve (AI=A*(1-exp(-b*t)), where MBV can be calculated from A and $V_{RBC}$ from b (fig 1). Both exercise and insulin induced a two-fold increase in MBV, without detectable changes in $V_{RBC}$. The effect of exercise on MBV was maximal after 1 minute, and stayed constant thereafter. The effect of insulin was detectable after 30 minutes of insulin exposure and was similar at 60 minutes.

**Conclusions**

Exercise and insulin both increase microvascular blood in mice, which can be measured noninvasively by contrast-enhanced ultrasound. Our findings enable studies of the genes and tissues that regulate microvascular function, which will result in novel insight into the pathogenesis of diabetes, hypertension and cardiovascular disease.

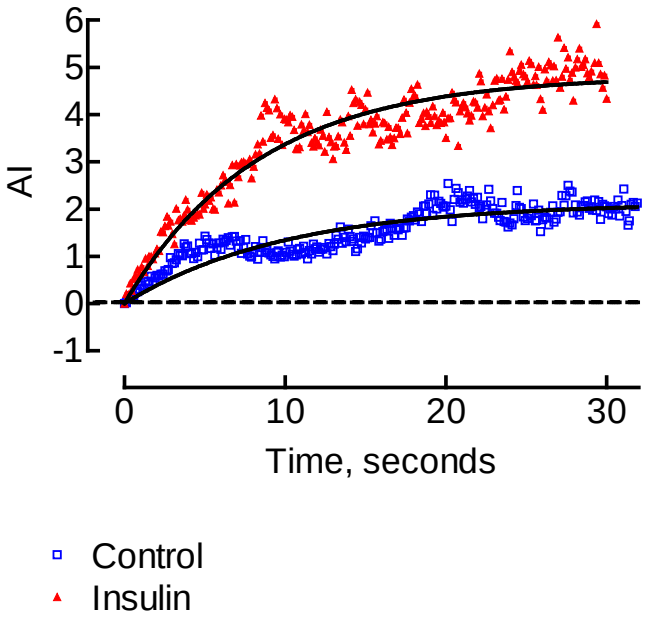


**Fig 1. Effect of insulin on muscle perfusion in the mouse hindlimb, assessed by contrast-enhanced ultrasound.**

# The 16th European Symposium on Ultrasound Contrast Imaging Rotterdam is sponsored by:

**GE Healthcare**
Mrs. Julie Woodland
Senior Brand Manager
MR and Ultrasound
Medical Diagnostics
Amersham Place
Little Chalfont Bucks HP7 9NA - UK

**SIEMENS AG - Ultrasound Division**
Mr. Richard Medley, Product Manager
H WS ES US CRM Operations
Sir William Siemens Square
Newton House
Frimley, Camberley, SY GU16 8QD - UK

**PHILIPS Medizin Systeme GmbH**
Mr. Janusz Bielczynski
CV Ultrasound Marketing Manager
Hewlett Packard Str.2
D-71034 Boeblingen - Germany

**ZonMw**
Mr. H.J. Smid
Research and Innovation
Postbus 93245
2509 AE Den Haag
The Netherlands

**Oldelft BV**
Mr. R. 't Hoen
Elektronicaweg 10
2628 XG Delft
The Netherlands

**Hitachi Medical Systems**
Ellison Bibby
European Marketing
Sumpfstrasse 24
6300 Zug - Switzerland

**Nederlandse Hartstichting**
Mw. Dr.ir. K. Eizema
Manager Research Department
P.O. Box 300
2501 CH Den Haag
The Netherlands

**BRACCO International BV**
Mr. Marco Graf, Congress Manager
GCO Global Strategic Marketing
Centro Galleria 2
Via Cantonale
CH-6928 Manno
Switzerland

**KNAW**
Dr. R.J.H. Trienes
Manager International Research Grants
P.O. Box 19121
1000 GC Amsterdam
The Netherlands

**Erasmus Trustfonds**
Drs. R. Rijntjes
Eendrachtsweg 41
3012 LD Rotterdam
The Netherlands

**Visualsonics**
Mr. Anil K K Amlani
Acting President and CEO
3080 Yonge Street
Toronto, Ontario
M4N 3N1 - Canada

**Zonare Medical Systems, INC.**
Mr. Casey R. Lunt
International Clinical Marketing Manager
Sumatrakade 1393
1019 RP Amsterdam - The Netherlands

**Philips Research**
Ralf Seip
Director Ultrasound
345 Scarborough Road
Briarcliff Manor - NY 10510, USA

**Coeur**
Mr. J.W. Deckers
Erasmus MC - Thoraxcenter
Dr. Molewaterplein 50
3015 GE Rotterdam
The Netherlands

# FIRST ANNOUNCEMENT 2012

# 17th EUROPEAN SYMPOSIUM ON ULTRASOUND CONTRAST IMAGING

# 19-20 JANUARY 2012

# ROTTERDAM, THE NETHERLANDS

**Course Directors:** **Folkert ten Cate**
**Nico de Jong**
**Edward Leen**

**Information:** **on the 17th EUROPEAN SYMPOSIUM ON ULTRASOUND CONTRAST IMAGING:**

**Mieke Pruijsten , m.pruijsten@erasmusmc.nl**

Erasmus MC
Universitair Medisch Centrum Rotterdam

# The 16th European Symposium of Ultrasound Contrast Imaging, Rotterdam is sponsored by: